Chapter 2
Buckling and Post-buckling of Beams

Abstract This chapter presents buckling and post-buckling analysis of straight beams under thermal and mechanical loads. The Euler and Timoshenko beam theories are considered and buckling and postbuckling behaviors are discussed. The buckling analysis of beams with piezoelectric layers is presented and the effect of piezo-control on the beam stability is analyzed. The vibration of thermo-electrically excited beams in the state of buckling and post-buckling is discussed and the chapter concludes with the thermal dynamic analysis of beams. The beam material in this chapter is assumed to be functionally graded, where the presented formulations may be simply reduced to the beams with isotropic/homogeneous material.

2.1 Introduction

Beams are the basic elements of many structural systems and design problems. Under mechanical forces or thermal stresses, beams may become structurally unstable. The mechanical or thermal stresses may be induced by the static or dynamic loads, providing a static or dynamic stability problem. The buckling and post-buckling behavior of beams should be essentially known for a structural design problem. This chapter presents the basic governing equations for the stability analysis of beams. Static and dynamic buckling and post-buckling problems of beams of functionally graded materials, piezo-control of buckling and post-buckling, beams on elastic foundation, and dynamic buckling of beams are discussed in detail (Fig. 2.1).

2.2 Kinematic Relations

The strain-displacement relations for straight beams under loading conditions that produce axial or lateral deflections are derived in this section. Different types of beam theories, from the Euler beam theory to the more sophisticated higher order beam

M.R. Eslami, *Buckling and Postbuckling of Beams, Plates, and Shells*,
Structural Integrity 1, https://doi.org/10.1007/978-3-319-62368-9_2

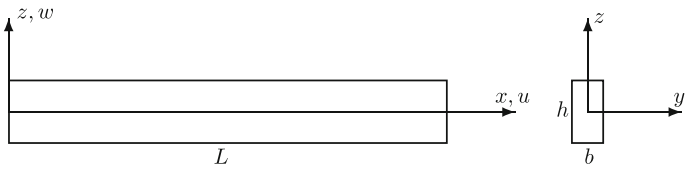

Fig. 2.1 The geometry and coordinate system of a beam

theory may be considered for the analysis of beams. In this section, the analysis of beams may be based on the first order shear deformation theory using the Timoshenko assumptions. According to this theory, the displacement field of the beam is assumed to be [1]

$$\begin{aligned} \bar{u}(x,z) &= u + z\varphi \\ \bar{w}(x,z) &= w \end{aligned} \tag{2.2.1}$$

where $\bar{u}(x,z)$ and $\bar{w}(x,z)$ are displacements of an arbitrary point of the beam along the x and z-directions, respectively. Here, u and w are the displacement components of middle surface and φ is the rotation of the beam cross-section, which is function of x only. The strain-displacement relations for the beam are given in the form

$$\begin{aligned} \varepsilon_{xx} &= \frac{\partial \bar{u}}{\partial x} + \frac{1}{2}\left(\frac{\partial \bar{w}}{\partial x}\right)^2 \\ \gamma_{xz} &= \frac{\partial \bar{u}}{\partial z} + \frac{\partial \bar{w}}{\partial x} \end{aligned} \tag{2.2.2}$$

where ε_{xx} and γ_{xz} are the axial and shear strains. Substituting Eq. (2.2.1) into (2.2.2) give

$$\begin{aligned} \varepsilon_{xx} &= \frac{du}{dx} + \frac{1}{2}\left(\frac{dw}{dx}\right)^2 + z\frac{d\varphi}{dx} \\ \gamma_{xz} &= \varphi + \frac{dw}{dx} \end{aligned} \tag{2.2.3}$$

The constitutive law for a material, using the linear thermoelasticity assumption, is given by [3]

$$\begin{aligned} \sigma_{xx} &= E\left[\varepsilon_{xx} - \alpha(T - T_0)\right] \\ \sigma_{xz} &= \frac{E}{2(1+\nu)}\gamma_{xz} \end{aligned} \tag{2.2.4}$$

In Eq. (2.2.4), σ_{xx} and σ_{xz} are the axial and shear stresses, T_0 is the reference temperature, and T is the absolute temperature distribution through the beam. Equations (2.2.2) and (2.2.4) are combined to give the axial and shear stresses in the beam in terms of the middle surface displacements as

$$\begin{aligned}\sigma_{xx} &= E\left(\frac{du}{dx}+\frac{1}{2}\left(\frac{dw}{dx}\right)^2+z\frac{d\varphi}{dx}-\alpha\left(T-T_0\right)\right)\\ \sigma_{xz} &= \frac{E}{2(1+\nu)}\left(\varphi+\frac{dw}{dx}\right)\end{aligned} \tag{2.2.5}$$

The stress resultants of the beam expressed in terms of the stresses through the thickness, according to the first order theory, are

$$\begin{aligned}N_x &= \int_{-\frac{h}{2}}^{\frac{h}{2}}\sigma_{xx}dz\\ M_x &= \int_{-\frac{h}{2}}^{\frac{h}{2}}z\sigma_{xx}dz\\ Q_{xz} &= K_s\int_{-\frac{h}{2}}^{\frac{h}{2}}\sigma_{xz}dz\end{aligned} \tag{2.2.6}$$

where K_s is the shear correction factor. The values of 5/6 or $\pi^2/12$ may be used as an approximate value for the composite and FGM beams with rectangular cross section. The shear correction factor is taken as $K_s = \pi^2/12$ for the FGM beam in this section.

We assume that the beam material is made of functionally graded materials (FGMs). For an FGM that is made of two constituent materials, ceramic and metal may be assumed as the constituent materials. If the volume fraction of ceramic is V_c and that of metal is V_m, then a power law distribution of the constituents across the beam thickness may be assumed of the form [3]

$$V_c + V_m = 1, \quad V_c = \left(\frac{1}{2}+\frac{z}{h}\right)^k \tag{2.2.7}$$

where h is total height of beam's cross section and z is the coordinate measured from the middle surface of the beam ($-h/2 \le z \le h/2$), k is the power law index which has the value equal or greater than zero. Variation of V_c with k and z/h is shown in Fig. 2.2. The value of k equal to zero represents a fully ceramic beam ($V_c = 1$) and k equal to infinity represents a fully metallic beam ($V_c = 0$). We assume that the mechanical and thermal properties of the FGM beam are distributed based on Voigt's rule [4]. Thus, the property variation of a functionally graded material using Eq. (2.2.7) is given by

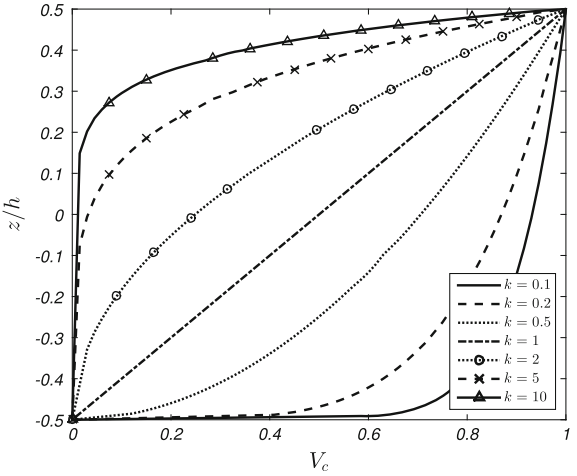

Fig. 2.2 Variation of ceramic volume fraction with power law index and thickness coordinate

$$P(z) = P_m + P_{cm}\left(\frac{1}{2} + \frac{z}{h}\right)^k \tag{2.2.8}$$

where $P_{cm} = P_c - P_m$, and P_m and P_c are the corresponding properties of the metal and ceramic, respectively. In this analysis the material properties, such as Young's modulus $E(z)$, coefficient of thermal expansion $\alpha(z)$, and the thermal conductivity $K(z)$ may be expressed by Eq. (2.2.8), where Poisson's ratio ν is assumed to be constant across the beam thickness due to its small variations for the constituent materials [3].

Using Eqs. (2.2.5), (2.2.6), and (2.2.8) and noting that u, w, and φ are only functions of x, the expressions for N_x, M_x, and Q_{xz} are obtained as

$$\begin{aligned} N_x &= E_1\left(\frac{du}{dx} + \frac{1}{2}\left(\frac{dw}{dx}\right)^2\right) + E_2\frac{d\varphi}{dx} - N^T \\ M_x &= E_2\left(\frac{du}{dx} + \frac{1}{2}\left(\frac{dw}{dx}\right)^2\right) + E_3\frac{d\varphi}{dx} - M^T \\ Q_{xz} &= \frac{E_1 K_s}{2(1+\nu)}\left(\varphi + \frac{dw}{dx}\right) \end{aligned} \tag{2.2.9}$$

where E_1, E_2, and E_3 are constants and N^T and M^T are thermal force and thermal moment resultants, which are calculated using the following relations

$$\begin{aligned} E_1 &= \int_{-\frac{h}{2}}^{\frac{h}{2}} E(z)dz = h\left(E_m + \frac{E_{cm}}{k+1}\right) \\ E_2 &= \int_{-\frac{h}{2}}^{\frac{h}{2}} zE(z)dz = h^2 E_{cm}\left(\frac{1}{k+2} - \frac{1}{2k+2}\right) \end{aligned}$$

$$E_3 = \int_{-\frac{h}{2}}^{\frac{h}{2}} z^2 E(z) dz = h^3 \left(\frac{1}{12} E_m + E_{cm} \left(\frac{1}{k+3} - \frac{1}{k+2} + \frac{1}{4k+4} \right) \right)$$
$$N^T = \int_{-\frac{h}{2}}^{\frac{h}{2}} E(z)\alpha(z)(T - T_0) dz$$
$$M^T = \int_{-\frac{h}{2}}^{\frac{h}{2}} zE(z)\alpha(z)(T - T_0) dz \tag{2.2.10}$$

Note that to find the thermal force and moment resultants, the temperature distribution through the beam should be known.

2.3 Equilibrium Equations

Equilibrium equations of an FGM beam under thermal loads may be obtained through the static version of virtual displacement principle. According to this principle, assuming that the external load is absent, an equilibrium position occurs when the first variation of strain energy function vanishes. Thus, one may write

$$\delta U = \int_0^L \int_{-\frac{b}{2}}^{\frac{b}{2}} \int_{-\frac{h}{2}}^{\frac{h}{2}} \left[\sigma_{xx} \delta\varepsilon_{xx} + K_s \sigma_{xz} \delta\gamma_{xz} \right] dz dy dx = 0 \tag{2.3.1}$$

With the aid of definitions for stress resultants given by Eq. (2.2.6), and performing the integration by part technique to relieve the displacement gradients, the following system of equilibrium equations are obtained

$$\begin{aligned} \frac{dN_x}{dx} &= 0 \\ \frac{dM_x}{dx} - Q_{xz} &= 0 \\ \frac{dQ_{xz}}{dx} + N_x \frac{d^2 w}{dx^2} &= 0 \end{aligned} \tag{2.3.2}$$

The boundary conditions for each side of the beam may be set by the force type or kinematical type, as

$$\begin{aligned} N_x \quad &\text{or} \quad u \\ M_x \quad &\text{or} \quad \varphi \\ Q_{xz} + N_x \frac{dw}{dx} \quad &\text{or} \quad w \end{aligned} \tag{2.3.3}$$

In each set, the first condition is the natural boundary condition and the second one stands as the essential type of boundary condition. Based on the above boundary

conditions, following cases are possible in thermal stability analysis of a beam

$$\begin{aligned} \text{Clamped (C)} &: u = w = \varphi = 0 \\ \text{Simply-Supported (S)} &: u = w = M_x = 0 \\ \text{Roller (R)} &: u = \varphi = Q_{xz} + N_x \frac{dw}{dx} = 0 \end{aligned} \tag{2.3.4}$$

2.4 Stability Equations

To derive the stability equations, the adjacent-equilibrium criterion is used. Assume that the equilibrium state of a functionally graded beam is defined in terms of the displacement components u_0, w_0, and φ_0. The displacement components of a neighboring stable state differ by u_1, w_1, and φ_1 with respect to the equilibrium position. Thus, the total displacements of a neighboring state are [1]

$$\begin{aligned} u &= u_0 + u_1 \\ w &= w_0 + w_1 \\ \varphi &= \varphi_0 + \varphi_1 \end{aligned} \tag{2.4.1}$$

Similar to the displacements, the force and moment resultants of a neighboring state may be related to the state of equilibrium as

$$\begin{aligned} N_x &= N_{x0} + N_{x1} \\ M_x &= M_{x0} + M_{x1} \\ Q_{xz} &= Q_{xz0} + Q_{xz1} \end{aligned} \tag{2.4.2}$$

Here, stress resultants with subscript 1 represent the linear parts of the force and moment resultant increments corresponding to u_1, φ_1, and w_1. The stability equations may be obtained by substituting Eqs. (2.4.1) and (2.4.2) into (2.3.2). Upon substitution, the terms in the resulting equations with subscript 0 satisfy the equilibrium conditions and therefore drop out of the equations. Also, the nonlinear terms with subscript 1 are ignored because they are small compared to the linear terms. The remaining terms form the stability equations as

$$\begin{aligned} E_1 \frac{d^2 u_1}{dx^2} + E_2 \frac{d^2 \varphi_1}{dx^2} &= 0 \\ E_2 \frac{d^2 u_1}{dx^2} + E_3 \frac{d^2 \varphi_1}{dx^2} - \frac{E_1 K_s}{2(1+\nu)} \left(\varphi_1 + \frac{dw_1}{dx} \right) &= 0 \\ \frac{E_1 K_s}{2(1+\nu)} \left(\frac{d\varphi_1}{dx} + \frac{d^2 w_1}{dx^2} \right) + N_{x0} \frac{d^2 w_1}{dx^2} &= 0 \end{aligned} \tag{2.4.3}$$

Combining Eq. (2.4.3) by eliminating u_1 and φ_1 provides an ordinary differential equation in terms of w_1, which is the stability equation of an FGM beam under transverse thermal loadings

$$\frac{d^4 w_1}{dx^4} + \mu^2 \frac{d^2 w_1}{dx^2} = 0 \tag{2.4.4}$$

with

$$\mu^2 = \frac{E_1 N_x^T}{(E_1 E_3 - E_2^2)\left(1 - 2N^T \frac{1+\nu}{E_1 K_s}\right)} \tag{2.4.5}$$

The stress resultants with subscript 1 are linear parts of resultants that correspond to the neighboring state. Using Eqs. (2.2.9) and (2.4.3), the expressions for Q_{xz1}, N_{x1}, and M_{x1} become

$$\begin{aligned} N_{x1} &= E_1 \frac{du_1}{dx} + E_2 \frac{d\varphi_1}{dx} \\ M_{x1} &= E_2 \frac{du_1}{dx} + E_3 \frac{d\varphi_1}{dx} \\ Q_{xz1} &= \frac{E_1 K_s}{2(1+\nu)} \left(\varphi_1 + \frac{dw_1}{dx}\right) \end{aligned} \tag{2.4.6}$$

2.5 Thermal Buckling of FGM Beams

2.5.1 Introduction

The mechanical and thermal buckling of beams, as a major solid structural component, have been the topic of many researches for a long period of time. Development of the new materials, such as the functionally graded materials (FGMs), have necessitated more researches in this area. Huang and Li [5] obtained an exact solution for mechanical buckling of FGM columns subjected to uniform axial load based on various beam theories. Zhao et al. [6] studied the post-buckling of simply supported rod made of functionally graded materials under uniform thermal load and nonlinear temperature distribution across the beam thickness using the numerical shooting method. They found that under the same temperature condition, the deformation of immovably simply supported FGM rod is smaller than those of the two homogeneous material rods. Also end constrained force of FGM rod is smaller than the corresponding values of the two homogeneous material rods with small deformation. Accordingly, the stability of FGM rod is higher than those of two homogeneous material rods when there is a temperature difference. Li et al. [7] presented the post-buckling behavior of fixed-fixed FGM beams based on the Timoshenko beam theory

under nonlinear temperature loading. They found the effect of transverse shear deformation on the critical buckling temperature of beams and used the shooting method to predict the post-buckling behavior of beams. It is found that the non-dimensional thermal axial force increases along with the increase of the power law index, as the increment of metal constituent can produce more thermal expansion of the beam under the same value of thermal load. Kiani and Eslami [8] discussed the buckling of functionally graded material beams under three types of thermal loadings through the thickness. A semi inverse method to study the instability and vibration of FGM beams is carried out by Aydogdu [9]. Ke et al. [10] presented the post-buckling of a cracked FGM beam for hinged-hinged and clamped-hinged edge conditions based on the Timoshenko beam theory. Also, Ke et al. [11] presented the free vibration and mechanical buckling of cracked FGM beams using the first order shear deformation beam theory for three types of boundary conditions. They found that the FGM beams with a smaller slenderness ratio and a lower Young's modulus ratio are much more sensitive to the edge crack. Ma and Lee [12] discussed the nonlinear behavior of FGM beams under in-plane thermal loading by means of first order shear deformation theory of beams. Derivation of the equations is based on the concept of neutral surface and numerical shooting method is used to solve the coupled nonlinear equations. Their study concluded that when a clamped-clamped FGM beam is subjected to uniform thermal loading it follows the bifurcation-type buckling, while the simply-supported beams do not. Most recently, post-buckling path of an Euler–Bernoulli beam under the action of in-plane thermal loading is investigated in [13] using the energy-based Ritz method. A full analytical method is presented in [14], which accurately predicts the temperature-deflection path of clamped-clamped and hinged-hinged FGM beams.

In this section, buckling analysis of FGM beams subjected to thermal loading is analyzed based on the Timoshenko beam theory [8]. Five possible types of boundary conditions are assumed and the existence of bifurcation type buckling is examined for each case. Based on the static version of virtual displacements, three coupled differential equations are obtained as equilibrium equations. The beam is assumed under three types of thermal loads and closed form approximate solutions are obtained to evaluate the critical buckling temperatures.

2.5.2 Functionally Graded Timoshenko Beams

Consider a beam made of FGMs with rectangular cross section [8]. It is assumed that length of the beam is L, width is b, and the height is h. Rectangular Cartesian coordinates is used such that the x axis is at the left side of the beam on its middle surface and along the length and z is measured from the middle surface and is positive upward, as shown in Fig. 2.1. The analysis of beam is based on the first order shear deformation beam theory using the Timoshenko assumptions. The kinematic relations, equilibrium equations, and the stability equations for the first order shear

deformation theory of beams were established in the previous sections. We first examine the condition where the beam should follow the bifurcation path.

2.5.3 Existence of Bifurcation Type Buckling

Consider a beam made of FGMs subjected to transverse temperature distribution. When axial deformation is prevented in the beam, an applied thermal load may produce an axial load. Only perfectly flat pre-buckling configurations are considered in the present case, which lead to bifurcation type buckling. Now, based on Eq. (2.3.2) and in the prebuckling state, when beam is completely undeformed, the generated pre-buckling force through the beam is equal to

$$N_{x0} = -N^T \tag{2.5.1}$$

Here, a subscript 0 is adopted to indicate the pre-buckling state. Also, according to Eq. (2.3.2), an extra moment is produced through the beam which is equal to

$$M_{x0} = -M^T \tag{2.5.2}$$

In general, this extra moment may cause deformation through the beam, except when it is vanished for some especial types of thermal loading or when boundary conditions are capable of handling the extra moments. The clamped and roller boundary conditions are capable of supplying the extra moments on the boundaries, while the simply-supported edge does not. Therefore, the $C-C$ and $C-R$ FGM Timoshenko beams remain un-deformed prior to buckling, while the other types of beams with at least one simply supported edge, commence to deflect. Also, an isotropic homogeneous beam under simply supported boundary conditions remains un-deformed when it is subjected to uniform temperature rise, because thermal moment vanishes through the beam. Therefore, bifurcation type buckling exists for the $C-C$ and $C-R$ FGM beams subjected to arbitrary transverse thermal loading. The same is true for the isotropic homogeneous beams subjected to uniform temperature rise.

2.5.4 Thermal Buckling

When temperature distribution through the beam is along the thickness direction only, the parameter μ of Eq. (2.4.5) is constant. In this case, the analytical solution of Eq. (2.4.3) is [8]

$$w_1(x) = C_1 \sin(\mu x) + C_2 \cos(\mu x) + C_3 x + C_4 \tag{2.5.3}$$

Table 2.1 Boundary conditions for the FGM Timoshenko beams. Here, C indicates clamped, S shows simply-supported, and R is used for roller edge [8]

Edge supports	B.Cs at $x = 0$	B.Cs at $x = L$
$C - C$	$u_1 = w_1 = \varphi_1 = 0$	$u_1 = w_1 = \varphi_1 = 0$
$S - S$	$w_1 = u_1 = M_{x1} = 0$	$w_1 = u_1 = M_{x1} = 0$
$C - S$	$u_1 = w_1 = \varphi_1 = 0$	$w_1 = u_1 = M_{x1} = 0$
$C - R$	$u_1 = w_1 = \varphi_1 = 0$	$u_1 = \varphi_1 = Q_{xz1} + N_{x0}\frac{dw_1}{dx} = 0$
$S - R$	$w_1 = u_1 = M_{x1} = 0$	$u_1 = \varphi_1 = Q_{xz1} + N_{x0}\frac{dw_1}{dx} = 0$

Using Eqs. (2.4.3), (2.4.6), and (2.5.3) the expressions for u_1, φ_1, N_{x1}, M_{x1}, and Q_{xz1} become

$$\begin{aligned}
\varphi_1(x) &= -S(\mu)(C_1\cos(\mu x) - C_2\sin(\mu x)) - C_3\\
u_1(x) &= \frac{E_2}{E_1}S(\mu)(C_1\cos(\mu x) - C_2\sin(\mu x)) + C_5 x + C_6\\
M_{x1}(x) &= \mu S(\mu)\frac{(E_1E_3 - E_2^2)}{E_1}(C_1\sin(\mu x) + C_2\cos(\mu x)) + E_2C_5\\
Q_{xz1}(x) &= \frac{E_1K_s}{2(1+\nu)}(\mu - S(\mu))(C_1\cos(\mu x) - C_2\sin(\mu x))\\
N_{x1}(x) &= E_1C_5
\end{aligned} \tag{2.5.4}$$

with

$$S(\mu) = \frac{\mu}{1 + 2(1+\nu)\mu^2\frac{(E_1E_3 - E_2^2)}{E_1^2K_s}} \tag{2.5.5}$$

The constants of integration C_1 to C_6 are obtained using the boundary conditions of the beam. Also, the parameter μ must be minimized to find the minimum value of N_x^T associated with the thermal buckling load. Five types of boundary conditions are assumed for the FGM beam with combination of the roller, simply supported, and clamped edges. Boundary conditions in each case are listed in Table 2.1. Let us consider a beam with both edges clamped. Using Eqs. (2.5.3) and (2.5.4), the constants C_1 to C_6 must satisfy the system of equations

$$\begin{bmatrix}
0 & 1 & 0 & 1 & 0 & 0\\
\sin(\mu L) & \cos(\mu L) & L & 1 & 0 & 0\\
-S(\mu) & 0 & -1 & 0 & 0 & 0\\
-S(\mu)\cos(\mu L) & S(\mu)\sin(\mu L) & -1 & 0 & 0 & 0\\
\frac{E_2}{E_1}S(\mu) & 0 & 0 & 0 & 0 & 1\\
\frac{E_2}{E_1}S(\mu)\cos(\mu L) & -\frac{E_2}{E_1}S(\mu)\sin(\mu L) & 0 & 0 & L & 1
\end{bmatrix}
\begin{bmatrix} C_1\\ C_2\\ C_3\\ C_4\\ C_5\\ C_6 \end{bmatrix} =
\begin{bmatrix} 0\\ 0\\ 0\\ 0\\ 0\\ 0 \end{bmatrix} \tag{2.5.6}$$

Table 2.2 Constants of formula (2.5.8) which are related to boundary conditions [8]

Parameter	$C-C$	$S-S$	$C-S$	$S-R$	$C-R$
p	39.47842	9.86960	20.19077	2.46740	9.86960
q	78.95684	19.73920	44.41969	4.93480	19.73920

To have a nontrivial solution, the determinant of coefficient matrix must be set to zero, which yields

$$S(\mu)L(2-2\cos(\mu L)-LS(\mu)\sin(\mu L))=0 \tag{2.5.7}$$

The smallest positive value of μ which satisfies Eq. (2.5.7) is $\mu_{min}=\frac{6.28319}{L}$. It can be seen that for the other types of boundary conditions, except $C-S$ case, the nontrivial solution leads to an exact parameter for μ. Using an approximate solution given in [15] for the critical axial force of $C-S$ beams, the critical thermal force for an FGM Timoshenko beam with arbitrary boundary conditions can be expressed as

$$N_{cr}^{T}=\frac{\frac{p}{L^2}\left(E_3-\frac{E_2^2}{E_1}\right)}{1+q\frac{1+\nu}{K_sL^2}\left(\frac{E_3}{E_1}-(\frac{E_2}{E_1})^2\right)} \tag{2.5.8}$$

where p and q are constants depending upon the boundary conditions and are listed in Table 2.2. The critical thermal buckling force for an FGM beam based on the classical beam theory may be derived by omitting the shear term in Eq. (2.5.8).

For an isotropic homogeneous beam, setting $k=0$ in Eq. (2.5.8), the critical buckling force is

$$N_{cr}^{T}=\frac{pEh^3}{12L^2+qh^2\frac{1+\nu}{K_s}} \tag{2.5.9}$$

which is a well-known relation for the critical axial buckling load of the Timoshenko beam given in [15].

2.5.5 Types of Thermal Loads

Uniform Temperature Rise (UTR)

Consider a beam which is at reference temperature T_0. When the axial displacement is prevented, the uniform temperature may be raised to $T_0+\Delta T$ such that the beam buckles. Substituting $T=T_0+\Delta T$ into Eq. (2.2.10) gives [8]

$$N^T = \Delta T h \left(E_m \alpha_m + \frac{E_{cm}\alpha_m + E_m \alpha_{cm}}{k+1} + \frac{E_{cm}\alpha_{cm}}{2k+1} \right) \tag{2.5.10}$$

Using Eq. (2.5.8), the critical buckling temperature difference ΔT_{cr}^{Uni} is expressed in the form

$$\Delta T_{cr}^{Uni} = \frac{\frac{p}{\alpha_m}\left(\frac{h}{L}\right)^2 F(k,\xi)}{G(k,\xi,\zeta)\left[1 + q\frac{1+\nu}{K_s}\left(\frac{h}{L}\right)^2 E(k,\xi)\right]} \tag{2.5.11}$$

where $\xi = \frac{E_{cm}}{E_m}$ and $\zeta = \frac{\alpha_{cm}}{\alpha_m}$. Also, the functions $E(k,\xi)$, $F(k,\xi)$, and $G(k,\xi,\zeta)$ are defined as

$$\begin{aligned} F(k,\xi) &= \frac{1}{12} + \frac{\xi(k^2+k+2)}{4(k+1)(k+2)(k+3)} - \frac{\xi^2 k^2}{4(k+1)(k+2)^2(k+1+\xi)} \\ E(k,\xi) &= \frac{k+1}{12(k+1+\xi)} + \frac{\xi(k^2+k+2)}{4(k+2)(k+3)(k+1+\xi)} \\ &\quad - \frac{\xi^2 k^2}{4(k+2)^2(k+1+\xi)^2} \\ G(k,\xi,\zeta) &= 1 + \frac{\xi+\zeta}{k+1} + \frac{\xi\zeta}{2k+1} \end{aligned} \tag{2.5.12}$$

Linear Temperature Through the Thickness (LTD)

Consider a thin FGM beam which the temperature in ceramic-rich and metal-rich surfaces are T_c and T_m, respectively. The temperature distribution for the given boundary conditions is obtained by solving the heat conduction equation across the beam thickness. If the beam thickness is thin enough, the temperature distribution is approximated linear through the thickness. So the temperature as a function of thickness coordinate z can be written in the form [8]

$$T = T_m + (T_c - T_m)\left(\frac{1}{2} + \frac{z}{h}\right) \tag{2.5.13}$$

Substituting Eq. (2.5.13) into (2.2.10) gives the thermal force as

$$\begin{aligned} N^T &= h(T_m - T_0)\left(E_m \alpha_m + \frac{E_{cm}\alpha_m + E_m\alpha_{cm}}{k+1} + \frac{E_{cm}\alpha_{cm}}{2k+1} \right) \\ &\quad + h\Delta T\left(\frac{E_m\alpha_m}{2} + \frac{E_{cm}\alpha_m + E_m\alpha_{cm}}{k+2} + \frac{E_{cm}\alpha_{cm}}{2k+2} \right) \end{aligned} \tag{2.5.14}$$

where $\Delta T = T_c - T_m$. Combining Eqs. (2.5.8) and (2.5.14) gives the final form of the critical buckling temperature difference through the thickness as

$$\Delta T_{cr}^{Linear} = \frac{\frac{p}{\alpha_m}\left(\frac{h}{L}\right)^2 F(k,\xi)}{H(k,\xi,\zeta)\left(1+q\frac{1+\nu}{K_s}\left(\frac{h}{L}\right)^2 E(k,\xi)\right)} - (T_m - T_0)\frac{G(k,\xi,\zeta)}{H(k,\xi,\zeta)} \tag{2.5.15}$$

Here, the functions $E(k,\xi)$, $F(k,\xi)$, and $G(k,\xi,\zeta)$ are defined in Eq. (2.5.12) and function $H(k,\xi,\zeta)$ is defined as given below

$$H(k,\xi,\zeta) = \frac{1}{2} + \frac{\xi+\zeta}{k+2} + \frac{\xi\zeta}{2k+2} \tag{2.5.16}$$

Nonlinear Temperature Through the Thickness (NLTD)

Assume an FGM beam where the temperature in ceramic-rich and metal-rich surfaces are T_c and T_m, respectively. The governing equation for the steady-state one-dimensional heat conduction equation, in the absence of heat generation, becomes [8]

$$\begin{aligned} \frac{d}{dz}\left(K(z)\frac{dT}{dz}\right) &= 0 \\ T\left(+\frac{h}{2}\right) &= T_c \\ T\left(-\frac{h}{2}\right) &= T_m \end{aligned} \tag{2.5.17}$$

where $K(z)$ is given by Eq. (2.2.8). Solving this equation via polynomial series and taking the sufficient terms to assure the convergence, yields the temperature distribution across the beam thickness as

$$T = T_m + \frac{(T_c - T_m)}{D}\left\{\sum_{i=0}^{N}\frac{(-1)^i}{ik+1}\left(\frac{K_{cm}}{K_m}\right)^i\left(\frac{1}{2}+\frac{z}{h}\right)^{ik+1}\right\} \tag{2.5.18}$$

with

$$D = \sum_{i=0}^{N}\frac{(-1)^i}{ik+1}\left(\frac{K_{cm}}{K_m}\right)^i \tag{2.5.19}$$

Evaluating N_x^T and solving for ΔT gives the critical buckling value of the temperature difference as

Table 2.3 Temperature dependent coefficients for $SUS304$ and Si_3N_4 [16]

Material	Properties	P_{-1}	P_0	P_1	P_2	P_3
$SUS304$	$\alpha[\mathrm{K}^{-1}]$	0	$12.33e-6$	$8.086e-4$	0	0
	$E[\mathrm{Pa}]$	0	$201.04e+9$	$3.079e-4$	$-6.534e-7$	0
	$K[\mathrm{Wm}^{-1}\mathrm{K}^{-1}]$	0	15.379	$-1.264e-3$	$-2.092e-6$	$-7.223e-10$
	ν	0	0.28	0	0	0
	$\rho[\mathrm{kgm}^{-3}]$	0	2170	0	0	0
Si_3N_4	$\alpha[\mathrm{K}^{-1}]$	0	$5.8723e-6$	$9.095e-4$	0	0
	$E[\mathrm{Pa}]$	0	$348.43e+9$	$-3.07e-4$	$2.16e-7$	$-8.946e-11$
	$K[\mathrm{Wm}^{-1}\mathrm{K}^{-1}]$	0	13.723	$-1.032e-3$	$5.466e-7$	$-7.876e-11$
	ν	0	0.28	0	0	0
	$\rho[\mathrm{kgm}^{-3}]$	0	8166	0	0	0

$$\Delta T_{cr}^{NLTD} = \frac{\frac{p}{\alpha_m}\left(\frac{h}{L}\right)^2 F(k,\xi)}{I(k,\xi,\zeta,\gamma)\left(1+q\frac{1+\nu}{K_s}\left(\frac{h}{L}\right)^2 E(k,\xi)\right)} - (T_m - T_0)\frac{G(k,\xi,\zeta)}{I(k,\xi,\zeta,\gamma)} \tag{2.5.20}$$

In this relation $\gamma = \frac{K_{cm}}{K_m}$ and the function $I(k,\xi,\zeta,\gamma)$ is defined as

$$I(k,\xi,\zeta,\gamma) = \frac{1}{D}\sum_{i=0}^{N}\frac{(-1)^i}{ik+1}\left\{\frac{1}{ik+2} + \frac{\zeta+\eta}{ik+k+2} + \frac{\zeta\eta}{ik+2k+2}\right\} \tag{2.5.21}$$

2.5.6 Results and Discussion

Consider a ceramic-metal functionally graded beam [8]. The combination of materials consist of Silicon-Nitride as ceramic and stainless steel as metal. The elasticity modulus, the thermal expansion coefficient, and the thermal conductivity coefficient for these constituents are highly dependent to the temperature. The temperature dependency of the material properties are assumed to follow the Touloukian model as [16]

$$P = P_0\left(P_{-1}T^{-1} + 1 + P_1T + P_2T^2 + P_3T^3\right) \tag{2.5.22}$$

where P_{-1}, P_0, P_1, P_2, and P_3 are constants and unique to each constituent. For the constituents of this study, these constants are given in Table 2.3. The temperature independent case (TID) describes the condition where properties are evaluated at reference temperature $T_0 = 300\,\mathrm{K}$. The case TD, on the other hand, represents the conditions where properties are calculated at current temperature based on the Touloukian model described by Eq. (2.5.22).

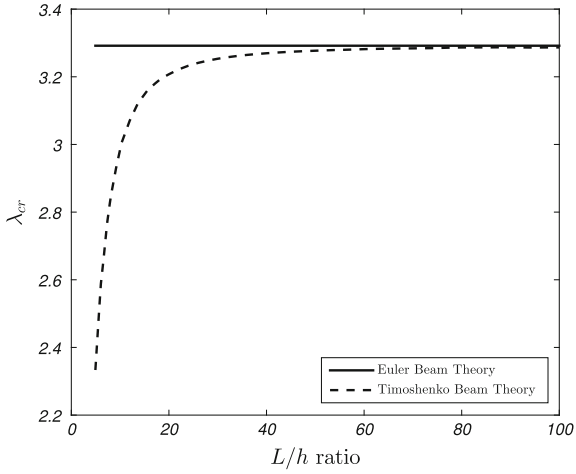

Fig. 2.3 Influence of shear deformations on critical buckling temperature difference

To validate the formulation of this section, the effect of transverse shear deformation on critical buckling temperature difference of a homogeneous beam is plotted in Fig. 2.3. For this purpose, the results are compared between the Euler and Timoshenko beam theories. The beam is under the uniform temperature rise. Nondimensional critical buckling temperature is defined by $\lambda_{cr} = \alpha \Delta T_{cr}^{Uni} (L/h)^2$. It is apparent that the critical buckling temperature difference for beams with L/h ratio more than 50 is identical between the two theories. But, for L/h ratio less than 50, the difference between the two theories become larger and it will become more different for L/h values less than 20. The same graph is reported in [7] based on the numerical shooting method.

In Fig. 2.4, the critical buckling temperature difference of an FGM beam under the uniform temperature rise loading is depicted [8]. Both edges are clamped. The *TD* case indicates that properties are temperature dependent, whereas the *TID* indicates that properties are evaluated at reference temperature. As seen, when the power law index increases, the critical buckling temperature decreases permanently. When it is compared to the *TD* case, the *TID* case overestimates the buckling temperatures. Difference between the *TID* and *TD* cases is more pronounced at higher temperatures. As seen for the constituents of this study, an increase in the power law index results in less critical buckling temperature difference.

In Fig. 2.5, two other cases of thermal loadings are compared with respect to each other. As seen, in both of these cases an increase in the power law index results in lower buckling temperature. The *LTD* case, as an approximate solution for the *NLTD* case, underestimates the critical buckling temperatures except for the case of reduction of an FGM beam to the associated homogeneous case. This is expected, as in this case the analytical solution of the heat conduction equation is also linear.

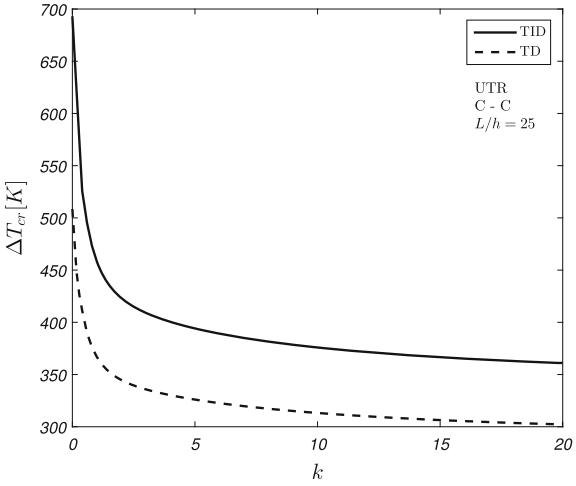

Fig. 2.4 Effect of temperature dependency of the constituents on ΔT_{cr}

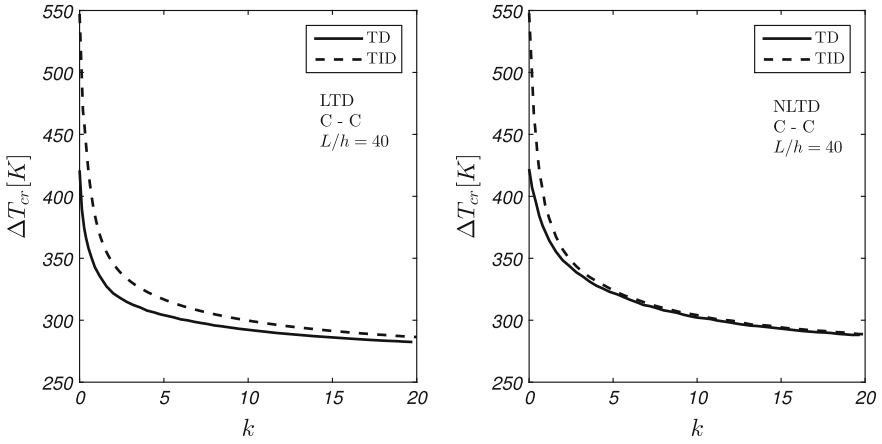

Fig. 2.5 Effect of temperature dependency of the constituents on ΔT_{cr} subjected to linear and nonlinear heat conduction across the thickness

The influence of boundary conditions on buckling temperature difference is plotted in Fig. 2.6. The uniform temperature rise case of loading is assumed and properties are assumed to be *TD*. The case of a homogeneous beam is chosen. As expected, the higher buckling temperature belongs to a beam with both edges clamped and the lower one is associated with a beam with one side simply supported and the other one roller. The critical buckling temperature of the S-S and C-R cases are the same.

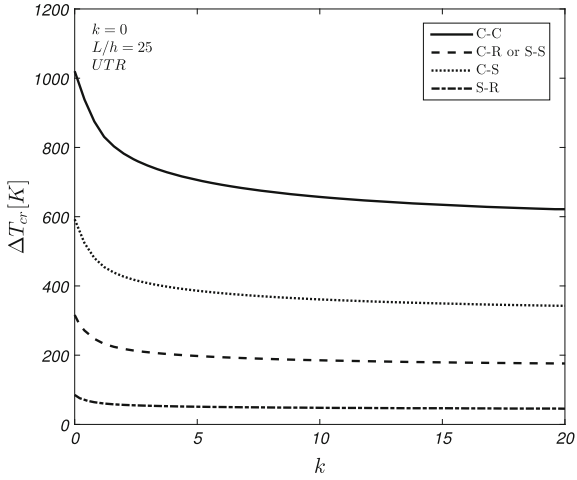

Fig. 2.6 The influence of boundary conditions on ΔT_{cr}

2.6 Thermo-Electrical Buckling of Beams

2.6.1 Introduction

Smart materials belongs to a class of advanced materials which are used widely in structural engineering. As a branch of smart materials, the piezoelectric materials are used extensively due to their applications in controlling the deformation, vibration, and instability of solid structures. Many studies are reported on behavior of structures integrated with the piezoelectric layers. Kapuria et al. [17] developed an efficient coupled zigzag theory for electro-thermal stress analysis of hybrid piezoelectric beams. Control and stability analysis of a composite beam with piezoelectric layers subjected to axial periodic compressive loads is reported by Chen et al. [18]. In their study, by employing the Euler beam theory and nonlinear strain-displacement, Hamilton's principle is used to obtain the dynamic equation of the beams integrated with the piezoelectric layers.

Piezoelectric FGM structures have the advantages of functionally graded materials and piezoelectric materials linked together. Bian et al. [19] presented an exact solution based on the state space formulation to study the functionally graded beams integrated with surface bounded piezoelectric actuators and sensors. Alibeigloo [20] reported an analytical solution for thermoelasticity analysis of the FGM beams integrated with piezoelectric layers. By assuming the simply-supported edge conditions, he used the state space method in conjunction with the Fourier series in longitudinal direction to obtain an analytical solution. An analytical method for deflection control of the FGM beams containing two piezoelectric layers is reported by Gharib et al. [21]. Following the Timoshenko beam theory and the power law form of material property distribution, three coupled ordinary differential equations are derived as equilibrium equations of an FGM beam integrated with orthotropic piezoelectric

layers. Vibration of thermally post-buckled functionally graded material beams with surface-bonded piezoelectric layers subjected to both thermal and electrical loads is carried out by Li et al. [22]. Buckling and postbuckling analysis of the FGM beams with general boundary conditions is reported by Kiani et al. [23, 24] and [25] based on the Euler and Timoshenko beam theories.

The instability problem of piezoelectric FGM beams subjected to thermal load and applied constant voltage is discussed in this section [24]. Three types of thermal loads and five types of boundary conditions are assumed for the beam. Based on the Timoshenko beam theory and power law assumption for property distribution, the equilibrium and stability equations for the beam are derived and the eigenvalue solution is carried out to obtain the critical buckling temperature.

2.6.2 Piezoelectric FGM Beam

Consider a beam with rectangular cross section made of an FGM substrate of thickness h, width b, length L, and piezoelectric films of thickness h_a that are perfectly bonded on its top and bottom surfaces as actuators. No adhesive layer is assumed to exist between the smart layers and the FGM media. Due to the asymmetrically mid-plane configuration of the FGM beam, total structure acts as an asymmetrical three-layered media.

2.6.3 Governing Equations

Material properties of the FGM substrate are distributed based on a power law form function described by Eq. (2.2.8). The rectangular Cartesian coordinates is used such that the x axis is along the length of the beam on its middle surface and z is measured from the middle surface and is positive upward, as shown in Fig. 2.7. Analysis of the beam is developed based on Timoshenko's beam theory [24]. Axial and lateral components of displacement field through the beam are given in Eq. (2.2.1).

If the applied voltage V_p to the piezoelectric layers is across the thickness, then the electrical field is generated only in the $z-$direction and is denoted by E_z, which is equal to [26–29]

$$E_z = \frac{V_p}{h_p} \tag{2.6.1}$$

It should be pointed out that, since the electrical field is equal to the negative gradient of electrical potential, the electric potential at the top surface of the top smart layer $z = +h/2 + h_p$ and bottom surface of the bottom layer $z = -h/2 - h_p$ are equal to $-V_p$ and V_p, respectively. Within the framework of linear thermoelasticity of a medium, stress-strain relations are

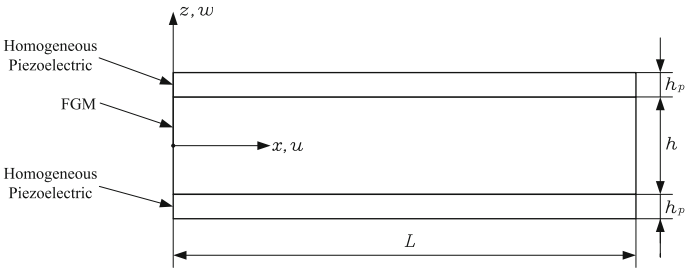

Fig. 2.7 Schematic and geometry of a FGM beam integrated with piezoelectric layers

$$\begin{aligned}\sigma_{xx} &= E\left[\varepsilon_{xx} - \alpha(T - T_0)\right]\\ \sigma_{xz} &= \frac{E}{2(1+\nu)}\gamma_{xz}\end{aligned} \tag{2.6.2}$$

and for the piezoelectric layers [26]

$$\begin{aligned}\sigma^p_{xx} &= E_a\left[\varepsilon_{xx} - \alpha_p(T - T_0) - d_{31}E_z\right]\\ \sigma^p_{xz} &= \frac{E_p}{2(1+\nu_p)}\gamma_{xz}\\ D_z &= E_p d_{31}\varepsilon_{xx} + k_{33}E_z + p_3(T - T_0)\end{aligned} \tag{2.6.3}$$

In the above equations, σ_{xx} and σ_{xz} are the axial and shear stresses through the FGM layer and σ^p_{xx} and σ^p_{xz} are the axial and shear stresses through the piezoelectric layers. Also, ν and ν_p are Poisson's ratios for the FGM beam and piezoelectric layers, respectively. Here, T_0 is the reference temperature and T is the temperature distribution through the beam. Also, E_p, D_z, d_{31}, and k_{33} are the elasticity modules, electric displacement, piezoelectric constant, pyroelectric constant, and the dielectric permittivity coefficient for the piezoelectric layers, respectively. Equations (2.2.1), (2.6.2), and (2.6.3) are combined to give the axial and shear stresses in terms of the middle surface displacements as

$$\begin{aligned}\sigma_{xx} &= E\left(\frac{du}{dx} + \frac{1}{2}\left(\frac{dw}{dx}\right)^2 + z\frac{d\varphi}{dx} - \alpha\left(T - T_0\right)\right)\\ \sigma^p_{xx} &= E_p\left(\frac{du}{dx} + \frac{1}{2}\left(\frac{dw}{dx}\right)^2 + z\frac{d\varphi}{dx} - \alpha_p\left(T - T_0\right) - \frac{V_p}{h_p}d_{31}\right)\\ \sigma_{xz} &= \frac{E}{2(1+\nu)}\left(\varphi + \frac{dw}{dx}\right)\\ \sigma^p_{xz} &= \frac{E_p}{2(1+\nu_p)}\left(\varphi + \frac{dw}{dx}\right)\end{aligned} \tag{2.6.4}$$

The force and moment resultants in the beam expressed in terms of the stresses through the thickness, according to the Timoshenko beam theory, are

$$\begin{aligned} N_x &= \int_{-\frac{h}{2}}^{\frac{h}{2}} \sigma_{xx} dz + \int_{\frac{h}{2}}^{\frac{h}{2}+h_p} \sigma_{xx}^p dz + \int_{-\frac{h}{2}-h_p}^{-\frac{h}{2}} \sigma_{xx}^p dz \\ M_x &= \int_{-\frac{h}{2}}^{\frac{h}{2}} z\sigma_{xx} dz + \int_{\frac{h}{2}}^{\frac{h}{2}+h_p} z\sigma_{xx}^p dz + \int_{-\frac{h}{2}-h_p}^{-\frac{h}{2}} z\sigma_{xx}^p dz \\ Q_{xz} &= K_s \left(\int_{-\frac{h}{2}}^{\frac{h}{2}} \sigma_{xz} dz + \int_{\frac{h}{2}}^{\frac{h}{2}+h_p} \sigma_{xz}^p dz + \int_{-\frac{h}{2}-h_p}^{-\frac{h}{2}} \sigma_{xz}^p dz \right) \end{aligned} \tag{2.6.5}$$

Here, K_s is the shear correction factor which is chosen as $K_s = 5/6$.

Using Eqs. (2.6.4) and (2.6.5) and noting that u and w are functions of x only, N_x, M_x, and Q_{xz} are obtained as

$$\begin{aligned} N_x &= (E_1 + 2h_p E_p)\left(\frac{du}{dx} + \frac{1}{2}\left(\frac{dw}{dx} \right)^2 \right) + E_2 \frac{d\varphi}{dx} - N^T - 2V_p E_p d_{31} \\ M_x &= E_2 \left(\frac{du}{dx} + \frac{1}{2}\left(\frac{dw}{dx} \right)^2 \right) + (E_3 + HE_p)\frac{d\varphi}{dx} - M^T \\ Q_{xz} &= K_s \left(\frac{E_1}{2(1+\nu)} + \frac{h_p E_p}{1+\nu_p} \right)\left(\varphi + \frac{dw}{dx} \right) \end{aligned} \tag{2.6.6}$$

Constants E_i are defined in Eq. (2.2.10). Besides, N^T and M^T are thermal force and thermal moment resultants through the piezo-FGM beam and are

$$\begin{aligned} H &= \frac{2}{3}\left(h_p^3 + \frac{3}{2}h_p^2 h + \frac{3}{4}h_p h^2 \right) \\ N^T &= \int_{-\frac{h}{2}-h_p}^{\frac{h}{2}+h_p} E(z)\alpha(z)(T - T_0) dz \\ M^T &= \int_{-\frac{h}{2}-h_p}^{\frac{h}{2}+h_p} zE(z)\alpha(z)(T - T_0) dz \end{aligned} \tag{2.6.7}$$

The total potential energy U for a piezoelectric FGM beam under thermal loads is defined as the sum of total potential energies for piezoelectric layers U_p and the potential energy of the FGM beam U_b as

$$\begin{aligned} U_b &= \frac{1}{2}\int_x \int_y \int_z \left(\sigma_{xx}\left(\varepsilon_{xx} - \alpha(T - T_0) \right) + K_s \sigma_{xz} \varepsilon_{xz} \right) dz dy dx + \\ U_p &= \frac{1}{2}\int_x \int_y \int_z \left(\sigma_{xx}^p \left(\varepsilon_{xx} - \alpha_p(T - T_0) \right) K_s \sigma_{xz}^p \varepsilon_{xz} - E_z D_z \right) dz dy dx \end{aligned} \tag{2.6.8}$$

where in definition of U_b, $z \in [-\frac{h}{2}, \frac{h}{2}]$, and in definition of U_p, $z \in [-\frac{h}{2} - h_p, -\frac{h}{2}] \cup [\frac{h}{2}, h_p + \frac{h}{2}]$. Deriving the first variation of total potential energy function and performing the integration by part to relieve the displacement gradients, yields the equilibrium equations and associated boundary conditions given by Eqs. (2.3.2) and (2.3.3).

2.6.4 Existence of Bifurcation Type Buckling

Consider a beam made of FGMs with piezoelectric layers subjected to the transverse temperature distribution and applied actuator voltage. When the axial deformation is prevented in the beam, an applied thermal load and external voltage may produce an axial load. Only perfectly flat pre-buckling configurations are considered in the present work, which lead to bifurcation type buckling. Now, based on Eq. (2.6.6) and in the prebuckling state, when beam is completely undeformed and axial elongation is prevented at boundaries, the generated pre-buckling force through the beam is equal to [24]

$$N_{x0} = -N^T - 2V_p E_p d_{31} \tag{2.6.9}$$

Here, a subscript 0 is adopted to indicate the pre-buckling state deformation. Also, according to Eq. (2.6.6), an extra moment is produced through the beam which is equal to

$$M_{x0} = -M^T \tag{2.6.10}$$

In general, this extra moment may cause deformation through the beam, except when it is vanished for some especial types of thermal loading or when boundary conditions are capable of handling the extra moments. The clamped and roller boundary conditions are capable of supplying the extra moments on the boundaries, while the simply-supported edge does not. Therefore, the $C-C$ and $C-R$ piezoelectric FGM Timoshenko beams remain undeformed prior to buckling, while for the other types of beams with at least one simply supported edge, beam commence to deflect. Also, symmetrically mid-plane beam remains undeformed when it is subjected to uniform temperature rise, because thermal moment vanishes through the beam. Therefore, bifurcation type buckling exists for the $C-C$ and $C-R$ piezoelectric FGM beams subjected to arbitrary transverse thermal loading and constant voltage. The same is true for the beams with isotropic homogeneous core and simply supported boundary conditions subjected to the combined action of uniform temperature rise and constant voltage.

2.6.5 Stability Equations

To derive the stability equations, the adjacent-equilibrium criterion is used. Assume that the equilibrium state of a beam is defined in terms of the displacement components u_0, w_0, and φ_0. The displacement components of a neighboring stable state differ by u_1, w_1, and φ_1 with respect to the equilibrium position. The incremental stress resultants are obtained using Eq. (2.4.2). Since thermal resultant and in-plane electrical force are constant, Eq. (2.4.4) describes the stability equation of the beam, where a new definition for parameter μ is needed as follows [24]

$$\mu^2 = \frac{(E_1 + 2h_pE_p)(N^T + 2V_pE_pd_{31})}{\left((E_3 + HE_p)(E_1 + 2h_pE_p) - E_2^2\right)\left(1 - \frac{N^T + 2V_pE_pd_{31}}{K_s\left(\frac{E_1}{2(1+\nu)} + \frac{h_pE_p}{1+\nu_p}\right)}\right)} \tag{2.6.11}$$

Besides, definition of perturbed displacements and stress resultants are given as

$$\begin{aligned}
w_1(x) &= C_1\sin(\mu x) + C_2\cos(\mu x) + C_3x + C_4\\
\varphi_1(x) &= -S(\mu)(C_1\cos(\mu x) - C_2\sin(\mu x)) - C_3\\
u_1(x) &= \frac{E_2}{E_1 + 2h_pE_p}S(\mu)(C_1\cos(\mu x) - C_2\sin(\mu x)) + C_5x + C_6\\
M_{x1}(x) &= \mu S(\mu)\frac{((E_3 + HE_p)(E_1 + 2h_pE_p) - E_2^2)}{E_1 + 2h_pE_p}(C_1\sin(\mu x)\\
&\quad + C_2\cos(\mu x)) + E_2C_5\\
Q_{xz1}(x) &= K_s\left(\frac{E_1}{2(1+\nu)} + \frac{h_pE_p}{1+\nu_p}\right)(\mu - S(\mu))(C_1\cos(\mu x) - C_2\sin(\mu x))\\
N_{x1}(x) &= (E_1 + 2h_pE_p)C_5
\end{aligned} \tag{2.6.12}$$

with

$$S(\mu) = \frac{\mu}{1 + \mu^2\frac{(E_3+HE_p)(E_1+2h_pE_p)-E_2^2}{K_s(E_1+2h_pE_p)\left(\frac{E_1}{2(1+\nu)} + \frac{h_pE_p}{1+\nu_p}\right)}} \tag{2.6.13}$$

The constants of integration C_1 to C_6 are obtained using the boundary conditions of the beam. The parameter μ has to be minimized to find the minimum value of N^T associated with the thermal buckling load. Five types of boundary conditions are considered for the ends of the beam. Mathematical expression of edge conditions are given in Table 2.1. Similar to the process developed in the previous section, the critical thermal force through the beam is obtained as

$$N_{cr}^T = \frac{p\left((E_3 + HE_p)(E_1 + 2h_pE_p) - E_2^2\right)}{L^2\left\{(E_1 + 2h_pE_p) + \frac{q\left((E_3+HE_p)(E_1+2h_pE_p)-E_2^2\right)}{K_s\left(\frac{E_1}{1+\nu} + \frac{2h_pE_p}{1+\nu_p}\right)L^2}\right\}} - 2V_pE_pd_{31} \tag{2.6.14}$$

Neglecting the term produced by shear deformation, gives the critical thermal load of piezoelectric FGM beams based on the Euler–Bernoulli beam theory as

$$N_{cr}^{T} = \frac{p}{L^2}\left(E_3 + HE_p - \frac{E_2^2}{E_1 + 2h_pE_p}\right) - 2V_pE_pd_{31} \tag{2.6.15}$$

Also, Eq. (2.6.14) may be reduced to thermal buckling force of an FGM beam without piezoelectric layers, when both h_p and V_p tend to zero. In this case, N_{cr}^{T} becomes

$$N_{cr}^{T} = \frac{\frac{p}{L^2}\left(E_3 - \frac{E_2^2}{E_1}\right)}{1 + q\frac{1+\nu}{K_sL^2}\left(\frac{E_3}{E_1} - (\frac{E_2}{E_1})^2\right)} \tag{2.6.16}$$

2.6.6 Types of Thermal Loads

Uniform Temperature Rise (UTR)

Consider a beam at reference temperature T_0. In such a case, the uniform temperature may be raised to $T_0 + \Delta T$ such that the beam buckles. Evaluating the thermal force resultant for the case of uniform temperature rise loading, using Eq. (2.6.7), reaches us to [24]

$$\Delta T_{cr} = \frac{p\left((E_3 + HE_p)(E_1 + 2h_pE_p) - E_2^2\right)}{L^2Q_1\left\{(E_1 + 2h_pE_p) + \frac{q\left((E_3+HE_p)(E_1+2h_pE_p)-E_2^2\right)}{K_sL^2\left(\frac{E_1}{1+\nu}+\frac{2h_pE_p}{1+\nu_p}\right)}\right\}} - \frac{2V_pE_pd_{31}}{Q_1} \tag{2.6.17}$$

with

$$Q_1 = h\left(\alpha_mE_m + \frac{\alpha_mE_{cm} + \alpha_{cm}E_m}{n+1} + \frac{\alpha_{cm}E_{cm}}{2n+1}\right) + 2h_p\alpha_pE_p \tag{2.6.18}$$

Nonlinear Temperature Through the Thickness (NLTD)

To calculate the critical buckling temperature for the case of gradient through the thickness of beam, the one-dimensional equation of heat conduction in the z direction must be solved. In the FGM media, heat conduction equation for the steady state one-dimensional case, in the absence of heat generation, becomes [24]

$$\frac{d}{dz}\left(K(z)\frac{dT}{dz}\right) = 0 \tag{2.6.19}$$

with the boundary conditions

$$T\left(+\frac{h}{2}\right)=T_c \quad T\left(-\frac{h}{2}\right)=T_m \tag{2.6.20}$$

The solution of heat conduction equation along with the thermal boundary conditions is obtained via the power-series solution as

$$T(z)=T_m+(T_c-T_m)\frac{\sum_{i=0}^{N}\frac{1}{ik+1}(-\frac{K_{cm}}{K_m})^i\left(\frac{1}{2}+\frac{z}{h}\right)^{ik+1}}{\sum_{i=0}^{N}\frac{1}{ik+1}(-\frac{K_{cm}}{K_m})^i}, \qquad z\in[-\frac{h}{2},+\frac{h}{2}] \tag{2.6.21}$$

where N is the number of expanded terms and should be chosen appropriately to assure convergence of the solution.

Considering temperature T_t at top surface of the beam and T_b at bottom surface of the beam, the temperature boundary conditions become

$$T\left(\frac{h+h_p}{2}\right)=T_t, \quad T\left(-\frac{h+h_p}{2}\right)=T_b \tag{2.6.22}$$

and the temperature distribution through each of the piezoelectric layers is

$$\begin{aligned} T(z)&=\frac{2}{h_p}\left(T_t(z-\frac{h}{2})-T_c(z-\frac{h+h_p}{2})\right), \qquad z\in\left[+\frac{h}{2},+\frac{h+h_p}{2}\right]\\ T(z)&=\frac{2}{h_p}\left(-T_b(z+\frac{h}{2})+T_m(z+\frac{h+h_p}{2})\right), \qquad z\in\left[-\frac{h+h_p}{2},-\frac{h}{2}\right] \end{aligned} \tag{2.6.23}$$

Here, T_c and T_m are obtained in terms of T_t and T_b when continuity conditions of temperature and thermal charge are applied to the bonded surfaces of piezoelectric layers and FGM media as

$$\begin{aligned} T_m&=\frac{T_b+(T_t+T_b)\frac{h_pK_m}{2Q_2hK_p}}{1+\frac{h_pK_m}{Q_2hK_p}}\\ T_c&=\frac{T_t+(T_t+T_b)\frac{h_pK_m}{2Q_2hK_p}}{1+\frac{h_pK_m}{Q_2hK_p}} \end{aligned} \tag{2.6.24}$$

in which

$$Q_2=\sum_{i=0}^{N}\frac{1}{ik+1}\left(-\frac{K_{cm}}{K_m}\right)^i \tag{2.6.25}$$

Evaluating the thermal force resultant through three layers and solving for $\Delta T_{cr}=T_t-T_b$ reaches us to

$$\Delta T_{cr} = \left(1 + \frac{h_p K_m}{Q_2 h K_p}\right) \left\{ \frac{N_{cr}^T - (T_b - T_0) Q_1}{Q_3 + \frac{h_p K_m}{2 Q_2 h K_p} Q_4 + \frac{h_p E_p \alpha_p}{2}(1 + \frac{h_p K_m}{Q_2 h K_p})} \right\} \tag{2.6.26}$$

where

$$\begin{aligned} Q_3 &= \frac{h}{Q_2} \left\{ E_m \alpha_m \sum_{i=0}^{N} \frac{(-\frac{K_{cm}}{K_m})^i}{(ik+1)(ik+2)} \right. \\ &+ (E_{cm}\alpha_m + E_m \alpha_{cm}) \sum_{i=0}^{N} \frac{(-\frac{K_{cm}}{K_m})^i}{(ik+1)(ik+k+2)} \\ &\left. + E_{cm}\alpha_{cm} \sum_{i=0}^{N} \frac{(-\frac{K_{cm}}{K_m})^i}{(ik+1)(ik+2k+2)} \right\} \\ Q_4 &= h \left(\alpha_m E_m + \frac{\alpha_m E_{cm} + \alpha_{cm} E_m}{k+1} + \frac{\alpha_{cm} E_{cm}}{2k+1} \right) \end{aligned} \tag{2.6.27}$$

For the case when middle layer is homogeneous, the temperature distribution is linear through-the-thickness. In this case Eq. (2.6.26) simplifies to

$$\Delta T_{cr} = 2 \frac{N_{cr}^T}{Q_1^{Hom}} - 2(T_b - T_0) \tag{2.6.28}$$

2.6.7 Results and Discussion

Consider a piezoelectric FGM beam. The combination of materials consists of aluminum and alumina for the FGM substrate and PZT-5A for piezoelectric layers. The actuator layer thickness, unless otherwise stated, is $h_p = 0.001\,\text{m}$. Young's modules, coefficient of thermal expansion, and conductivity for aluminum are $E_m = 70\,\text{GPa}$, $\alpha_m = 23 \times 10^{-6}/^\circ C$ and $K_m = 204\,\text{W/mK}$, and for alumina are $E_c = 380\,\text{GPa}, \alpha_c = 7.4 \times 10^{-6}/^\circ C$ and $K_c = 10.4\,\text{W/mK}$, respectively. The PZT-5A properties are $E_p = 63\,\text{GPa}$, $\nu_p = 0.3$ and $d_{31} = 2.54 \times 10^{-10}\,\text{m/V}$ [23, 24, 26].

Figure 2.8 depicts the critical buckling temperature difference versus h for a piezoelectric/ceramic/piezoelectric beam for various types of boundary conditions subjected to the uniform temperature rise, when power law index is chosen $k = 0$ [24]. It is apparent that by increasing h, ΔT_{cr} becomes larger. Also, the critical buckling temperature for the $S - S$ and $C - R$ types of boundary conditions are identical and lower than the $C - C$ and $C - S$ beams, but larger than the value related to the $S - R$ beams.

The influence of beam geometry on ΔT_{cr}, for various power law indices, when the applying voltage is $V_p = +200\,\text{V}$, is illustrated in Fig. 2.9 for the uniform temperature

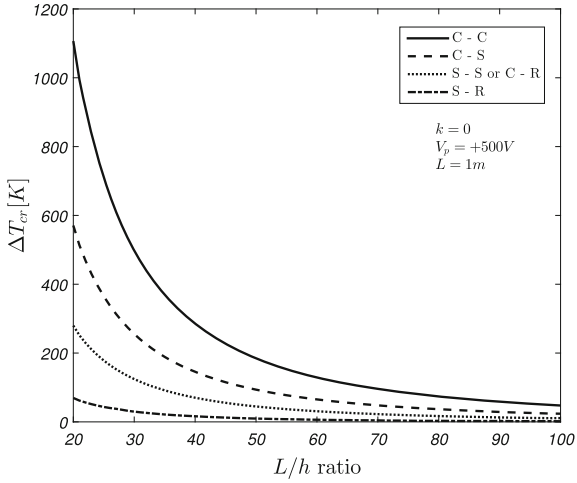

Fig. 2.8 Boundary conditions effect on ΔT_{cr}

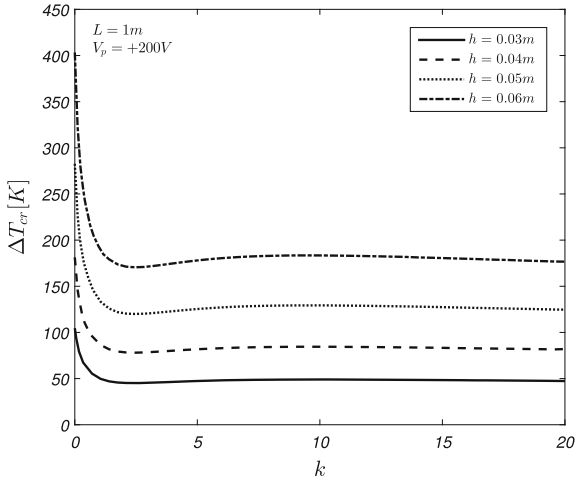

Fig. 2.9 Influence of power law index on critical buckling temperature difference of piezo-FGM beams

rise and the $C - R$ boundary conditions. As the thickness increases, the critical buckling temperature increases. Also it may be concluded that the critical temperature for the given constituents decreases for $k < 2$, then increases for $2 < k < 10$ and finally decreases for $k > 10$.

The buckling temperature difference ΔT_{cr} for a $C - C$ piezoelectric FGM beam ($L = 0.25$ m, $h = 0.01$ m) that is subjected to uniform temperature rise and constant voltage is calculated and presented in Table 2.4. Five cases of electrical loadings are considered $V_p = 0, \pm 200V, \pm 500$ V. Here, $V_p = 0$ V denotes a grounding condition. The results show that for this type of piezoelectric layer, the critical buckling temperature difference decreases with the increase of the applied voltage. The changes are, however, small. It should be mentioned that increasing or decreasing the critical

Table 2.4 Effect of applied voltage on buckling temperature difference of the $C-C$ piezo-FGM beams subjected to uniform temperature rise ($L = 0.25\,\text{m}$, $h = 0.01\,\text{m}$) [24]

$V_p(V)$	Theory	$k=0$	$k=0.5$	$k=1$	$k=2$	$k=5$
+500	Euler	796.606	478.876	413.243	389.489	420.050
	Timoshenko	782.473	470.930	406.483	382.738	411.168
+200	Euler	796.948	479.174	413.561	389.851	420.491
	Timoshenko	782.814	471.229	406.801	383.100	411.609
0	Euler	797.175	479.373	413.773	390.092	420.785
	Timoshenko	783.042	471.428	407.013	383.341	411.903
–200	Euler	797.403	479.572	413.985	390.333	421.079
	Timoshenko	783.270	471.627	407.225	383.582	412.197
–500	Euler	797.704	479.870	414.303	390.695	421.520
	Timoshenko	783.611	471.925	407.544	383.944	412.638
Without layers	Euler	711.323	403.017	330.461	292.974	302.254
	Timoshenko	699.680	397.133	325.896	288.874	297.174

temperature difference by applying voltage in comparison with the grounding condition depends on both sign of the applied voltage and the sign of piezoelectric constant. For the piezoelectric layers used in this study, the piezoelectric constant d_{31} is positive and it can be seen that the critical buckling temperature decreases by increasing the voltage. For a piezoelectric material, when the piezoelectric constant is negative (such as PZT-4 or PZT-5H), when voltage increases the critical buckling temperature difference becomes larger.

2.7 Postbuckling of Piezo-FGM Timoshenko Beams

2.7.1 Introduction

The post-buckling analysis of beams subjected to either mechanical or thermal loads is a complex nonlinear problem. Buckling and post-buckling behavior of elastic rods subjected to thermal load is presented by Li et al. [30]. They achieved the results by solving the nonlinear equilibrium equations of the slender pinned-fixed Euler–Bernoulli beams via the shooting method. Librescu et al. [31] studied the behavior of thin walled beams made of FGMs that operate at high temperatures. The study includes the vibration and instability analysis with the effects of the volume fraction and temperature gradients. Employing the finite element method, Bhangale and Ganesan [32] investigated the thermoelastic buckling and vibration behavior of an FGM sandwich beam. Literature on the analytical solution for the post-buckling of FGM beams under thermal loads is limited to a few published articles [14, 33].

This section presents an analytical solution for the post-buckling response of the FGM Timoshenko beam with and without layers of piezoelectric actuator using the mid-plane based concept [34]. The governing equations for the static behavior of FGM beam with two piezoelectric layers under thermo-electrical load are derived. The three nonlinear equilibrium equations are reduced to a fourth order uncoupled equation in terms of the lateral deflection. With the analytical solution of this equation, any type of boundary condition may be considered to be used. It is seen that considering the clamped-clamped boundary condition leads to an eigenvalue problem. For the simply supported-simply supported edge conditions, however, the boundary conditions are non-homogeneous and the response of the beam is of the nonlinear bending type. Numerical results are presented for a beam made of $SUS304$ as metal constituent and Si_3N_4 as ceramic constituent.

2.7.2 Governing Equations

Assume a beam made of FGMs with rectangular cross section $b \times h$ and length L bonded with two identical piezoelectric layers at the top and bottom surfaces of the beam. Thickness of each piezoelectric layer is h_p. The schematic and coordinate system of the beam are shown in Fig. 2.7.

Thermo-mechanical properties are graded across the thickness, where their patterns may be expressed by any arbitrary mathematical function. Since the volume fraction of each phase gradually varies in the gradation direction, the mechanical properties of FGMs vary across this direction. Here, we assume a continuous alteration of the volume fraction of ceramic from ceramic-rich surface to the metal-rich surface. The gradation profile is assumed of the form given by Eqs. (2.2.7) and (2.2.8).

For the piezoelectric layers, the stress-strain relation is updated to account for the electrical effects such that

$$\sigma_x = E_p \left[\varepsilon_x - \alpha_p (T - T_0) - d_p E_z\right]$$

$$\sigma_{xz} = G_p \gamma_{xz} \tag{2.7.1}$$

In the above equations, σ_x and σ_{xz} are the axial and transversal components of the stress tensor, E and G are the elasticity and shear modulus, and E_z and d are the electric field and piezoelectric constant, respectively. Besides, a subscript p indicates that characteristics belong to the piezoelectric layers.

For the case when piezoelectric layers are thin enough, applying the electrical voltage to the top and bottom surfaces induces the electrical field where only the through-the-thickness one may be assumed to be dominant. When only the reverse effect of piezoelectric layers is considered, we may write [22–24, 33]

$$E_z = \frac{V_p}{h_p} \tag{2.7.2}$$

Since the electrical field is negative gradient of the electrical potential, the applied actuator voltage to the top of the top piezoelectric layer ($z = h/2 + h_p$) and to the bottom of the bottom piezoelectric layer ($z = -h/2 - h_p$) are $-V_p$ and $+V_p$, respectively.

Relations between stress components and stress resultants, within the framework of the Timoshenko beam theory, are [24, 35]

$$\begin{aligned} N_x &= \int_{-\frac{h}{2}-h_p}^{\frac{h}{2}+h_p} \sigma_x dz \\ M_x &= \int_{-\frac{h}{2}-h_p}^{\frac{h}{2}+h_p} z\sigma_x dz \\ Q_{xz} &= \int_{-\frac{h}{2}-h_p}^{\frac{h}{2}+h_p} K_s \sigma_{xz} dz \end{aligned} \tag{2.7.3}$$

where K_s is called the shear correction factor and it depends upon the geometry, boundary conditions, and loading type. Determination of the shear coefficient is not straightforward. Normally $K_s = 5/6$ is used for a rectangular section. Substituting σ_x and σ_{xz} into Eq. (2.7.3) and integrating with respect to the z coordinate, result in

$$\begin{aligned} N_x &= (E_1 + 2E_p h_p)\left\{\frac{du_0}{dx} + \frac{1}{2}\left(\frac{dw_0}{dx}\right)^2\right\} + E_2\frac{d\varphi}{dx} - N^T - N^E \\ M_x &= E_2\left\{\frac{du_0}{dx} + \frac{1}{2}\left(\frac{dw_0}{dx}\right)^2\right\} + (E_3 + H_3 E_p)\frac{d\varphi}{dx} - M^T \\ Q_{xz} &= K_s(G_1 + 2G_p h_p)\left(\varphi + \frac{dw_0}{dx}\right) \end{aligned} \tag{2.7.4}$$

where M^T, N^T, and N^E are the thermal moment, thermal force, and electrical force resultants, respectively. It is worth mentioning that no electrical moment is induced in the structure since the electrical loading and electrical properties are symmetrical with respect to the mid-plane. Besides, E_1, E_2, and E_3 are stretching, coupling stretching-bending, and the bending stiffnesses, respectively, and are obtained as

$$\begin{aligned} E_1 &= \int_{-\frac{h}{2}}^{\frac{h}{2}} E(z)dz = h\left(E_c + \frac{E_{mc}}{k+1}\right) \\ E_2 &= \int_{-\frac{h}{2}}^{\frac{h}{2}} zE(z)dz = h^2 E_{mc}\left(\frac{1}{2k+2} - \frac{1}{k+2}\right) \end{aligned}$$

$$
\begin{aligned}
E_3 &= \int_{-\frac{h}{2}}^{\frac{h}{2}} z^2 E(z) dz = h^3 \left\{ \frac{E_c}{12} + E_{mc} \left(\frac{0.25}{k+1} - \frac{1}{k+2} + \frac{1}{k+3} \right) \right\} \\
H_3 &= 2 \int_{\frac{h}{2}}^{h_p + \frac{h}{2}} z^2 E_p dz = \frac{2}{3} \left(h_p^3 + \frac{3}{2} h_p^2 h + \frac{3}{4} h_p h^2 \right) \\
N^T &= \int_{-\frac{h}{2}}^{\frac{h}{2}} E(z) \alpha(z) (T - T_0) dz + 2 h_p E_p \alpha_p (T - T_0) \\
N^E &= 2 E_p d_p V_p \\
M^T &= \int_{-\frac{h}{2}}^{\frac{h}{2}} z E(z) \alpha(z) (T - T_0) dz
\end{aligned} \tag{2.7.5}
$$

With the absence of external applied loads, the total virtual potential energy of the beam is equal to the virtual strain energy of the beam under thermal and electrical loads, which is equal to

$$
\delta U = \int_0^L \int_{-\frac{h}{2} - h_p}^{\frac{h}{2} + h_p} \int_0^b \left(\sigma_x \delta \varepsilon_x + K_s \sigma_{xz} \delta \gamma_{xz} - D_z \delta E_z \right) dy dz dx \tag{2.7.6}
$$

The equilibrium equations of FGM Timoshenko beam with piezoelectric layers are obtained according to the virtual work principle [35]. Integrating Eq. (2.7.6) by part, with the consideration of Eqs. (2.7.4) and (2.7.5), result in the followings nonlinear equilibrium equations [34]

$$
\begin{aligned}
\delta u_0 &: \frac{dN_x}{dx} = 0 \\
\delta w_0 &: \frac{dQ_{xz}}{dx} + \frac{d}{dx} \left(N_x \frac{dw_0}{dx} \right) = 0 \\
\delta \varphi &: Q_{xz} - \frac{dM_x}{dx} = 0
\end{aligned} \tag{2.7.7}
$$

Due to this integration process, natural and essential boundary conditions are obtained as

$$
\begin{gathered}
N_x = 0 \ \text{ or } \ u_0 = \text{known} \\
Q_{xz} + N_x \frac{dw_0}{dx} = 0 \ \text{ or } \ w_0 = \text{known} \\
M_x = 0 \ \text{ or } \ \varphi = \text{known}
\end{gathered} \tag{2.7.8}
$$

For the sake of simplicity and generality, the following non-dimensional variables are introduced and are used in the rest of this work

$$\xi = \frac{x}{L}, \quad U^* = \frac{u}{L}, \quad W^* = \frac{w}{h}, \quad \delta = \frac{h}{L}, \quad \mu = \frac{h_p}{h}$$

$$f_1 = \frac{E_1 + 2E_p h_p}{E_m h}, \quad f_2 = \frac{E_2}{E_m h L}, \quad f_3 = \frac{E_3 + H_3 E_p}{E_m h L^2}$$

$$g_1 = \frac{K_s(G_1 + 2G_p h_p)}{E_m h}$$

$$N^{T*} = \frac{N^T}{E_m h}, \quad N^{E*} = \frac{N^E}{E_m h} \quad M^{T*} = \frac{M^T}{E_m h L} \tag{2.7.9}$$

where E_m is the elasticity modulus of metal constituent. Substitution of the above non-dimensional parameters into Eq. (2.7.7) and utilizing Eq. (2.7.4) give the governing equations of the beam in dimensionless forms as [34]

$$f_1 \frac{d^2U^*}{d\xi^2} + f_1\delta^2 \frac{dW^*}{d\xi}\frac{d^2W^*}{d\xi^2} + f_2 \frac{d^2\varphi}{d\xi^2} = 0 \tag{2.7.10a}$$

$$\left\{ f_1 \left(\frac{dU^*}{d\xi} + \frac{1}{2}\delta^2 \left(\frac{dW^*}{d\xi} \right)^2 \right) + f_2 \frac{d\varphi}{d\xi} - N^{T*} - N^{E*} \right\} \delta \frac{d^2W^*}{d\xi^2} + g_1 \left(\frac{d\varphi}{d\xi} + \delta \frac{d^2W^*}{d\xi^2} \right) = 0 \tag{2.7.10b}$$

$$g_1 \left(\varphi + \delta \frac{dW^*}{d\xi} \right) - f_2 \left(\frac{d^2U^*}{d\xi^2} + \delta^2 \frac{dW^*}{d\xi}\frac{d^2W^*}{d\xi^2} \right) - f_3 \frac{d^2\varphi}{d\xi^2} = 0 \tag{2.7.10c}$$

Solution

At the first glance it seems to be difficult to solve Eq. (2.7.10) analytically due to the strong non-linearity and the included coupling in the ordinary differential equations. To obtain an analytical solution, first these equations are uncoupled. Based on the first equilibrium equations (2.7.7), the axial force resultant is constant through the span at each temperature. Since N^{T*} and N^{E*} are both constants, we may write [34]

$$f_1 \left(\frac{dU^*}{d\xi} + \frac{1}{2}\delta^2 \left(\frac{dW^*}{d\xi} \right)^2 \right) + f_2 \frac{d\varphi}{d\xi} = -N^{M*} \tag{2.7.11}$$

where N^{M*} is constant along the span but varies at each load step. Substitution of Eq. (2.7.11) into (2.7.10b) leads to

$$g_1 \left(\frac{d\varphi}{d\xi} + \delta \frac{d^2W^*}{d\xi^2} \right) + \left(-N^{M*} - N^{T*} - N^{E*} \right) \delta \frac{d^2W^*}{d\xi^2} = 0 \tag{2.7.12}$$

and by substituting Eq. (2.7.10a) into (2.7.10c) we have

$$\left(\frac{f_3 f_1 - f_2^2}{f_1}\right)\frac{d^2\varphi}{d\xi^2} - g_1\left(\varphi + \delta\frac{dW^*}{d\xi}\right) = 0 \tag{2.7.13}$$

By differentiating Eq. (2.7.12) and using Eq. (2.7.13), the following equations are obtained

$$\left(\frac{P_1 F - P_1 P_2}{P_2}\right)\delta\,\frac{d^3 W^*}{d\xi^3} - P_2\delta\,\frac{dW^*}{d\xi} = P_2\varphi \tag{2.7.14a}$$

$$\left(\frac{P_1 F - P_1 P_2}{P_2}\right)\delta\,\frac{d^4 W^*}{d\xi^4} - F\delta\,\frac{d^2 W^*}{d\xi^2} = 0 \tag{2.7.14b}$$

Here, we have set

$$P_1 = \frac{f_3 f_1 - f_2^2}{f_1}, \quad P_2 = g_1, \quad F = N^{M*} + N^{T*} + N^{E*} \tag{2.7.15}$$

As seen, Eq. (2.7.10) are changed to new decoupled equations. Since $F - P_2$ is negative and both P_1 and F are positive, the solution of Eq. (2.7.14b) may be written as

$$W^* = C_1\sin(a\xi) + C_2\cos(a\xi) + C_3\xi + C_4 \tag{2.7.16}$$

in which we have set

$$a = \sqrt{\frac{F P_2}{P_1 P_2 - P_1 F}} \tag{2.7.17}$$

and C_1, C_2, C_3, and C_4 are constants that depends on the boundary conditions on both sides. Based on Eq. (2.7.14a), we have the following closed-form solution for φ

$$\varphi = -\delta a C_1\left(1 - \frac{F}{P_2}\right)\cos(a\xi) + \delta a C_2\left(1 - \frac{F}{P_2}\right)\sin(a\xi) - \delta C_3 \tag{2.7.18}$$

We may now considers two types of boundary conditions; simply-supported-simply-supported ($S-S$) and clamped-clamped ($C-C$). Mathematical expressions for these classes of edge supports are

$$\text{Clamped(C)}: \quad U^* = W^* = \varphi = 0$$

$$\text{Simply-supported(S)}: \quad U^* = W^* = M_x^* = 0$$

where

$$M_x^* = f_2\left(\frac{dU^*}{d\xi} + \frac{1}{2}\delta^2\left(\frac{dW^*}{d\xi}\right)^2\right) + f_3\frac{d\varphi}{d\xi} - M^{T*} \tag{2.7.19}$$

2.7.3 Clamped–Clamped Boundary Conditions

For the case of a beam with both edges clamped, both slopes and deflections vanish at both edges of the beam. Recalling Eqs. (2.7.16) and (2.7.18), we have the following system of homogeneous equations [34]

$$\begin{aligned} C_2 + C_4 &= 0 \\ -\delta a\left(1-\frac{F}{P_2}\right)C_1 - \delta C_3 &= 0 \\ \sin(a)C_1 + \cos(a)C_2 + C_3 + C_4 &= 0 \\ -\delta a\left(1-\frac{F}{P_2}\right)\cos(a)C_1 + \delta a\left(1-\frac{F}{P_2}\right)\sin(a)C_2 - \delta C_3 &= 0 \end{aligned} \tag{2.7.20}$$

which result in

$$\begin{aligned} C_1 &= \left(\frac{\cos(a)-1}{a\,(P_2-F)-P_2\sin(a)}\right)P_2 C \\ C_2 &= C \\ C_3 &= -a(1-\frac{F}{P_2})\left(\frac{\cos(a)-1}{a\,(P_2-F)-P_2\sin(a)}\right)P_2 C \\ C_4 &= -C \end{aligned} \tag{2.7.21}$$

Notice that due to the homogeneous boundary conditions for the $C-C$ edge supports, solution of the equations is obtained as an eigen-value problem. When the constants $C_i, i = 1, 2, 3, 4$ are inserted into the last of Eq. (2.7.20), one may reach to the following transcendental equation

$$\sin(a) - \frac{(1-\cos(a))^2 P_2}{(P_2-F)\,a - P_2\sin(a)} = 0 \tag{2.7.22}$$

Equation (2.7.22) has to be solved with respect to the parameter a. For the buckling mode, which is associated with the minimum positive root of the above equation, we have

$$a = 2\pi \tag{2.7.23}$$

Recalling Eq. (2.7.15) along with the substitution of Eq. (2.7.23) into (2.7.17), and considering the fact that in the prebuckling state $N^{M*} = 0$, the critical thermal force of the beam is obtained as

$$N_{cr}^{T*} = \frac{4\pi^2 P_1 P_2}{4\pi^2 P_1 + P_2} - N^{E*} \tag{2.7.24}$$

To trace the post-buckling equilibrium path of the beam, dependency of the lateral deflection to the temperature rise should be extracted. For the first buckling mode,

$C_1 = C_3 = 0$ and therefore the post-buckling deflection of the beam simplifies to

$$W^*(\xi) = C\,[\cos(2\pi\xi) - 1] \tag{2.7.25}$$

where C is a constant and has to be obtained considering the immovability conditions on both edges.

Substitution of Eq. (2.7.25) into (2.7.11) and integrating with respect to ξ along the beam length, we arrive at

$$f_1 \int_0^1 \frac{dU^*}{d\xi} d\xi + f_1 \frac{\delta^2}{2} \int_0^1 \left(\frac{dW^*}{d\xi}\right)^2 d\xi + f_2 \int_0^1 \frac{d\varphi}{d\xi} d\xi = -\int_0^1 N^{M*} d\xi \tag{2.7.26}$$

Here, the first integral in the left-hand side vanishes, because of the immovable condition on both sides. The third one also vanishes due to the clamping condition, which does not accept any rotation at the edge. Substituting Eq. (2.7.25) into (2.7.26) and using Eq. (2.7.17) and considering the boundary conditions, the following equation for C is obtained

$$C = \sqrt{\frac{N^{T*} + N^{E*} - \dfrac{4\pi^2 P_1 P_2}{4\pi^2 P_1 + P_2}}{f_1 \delta^2 \pi^2}} \tag{2.7.27}$$

It should be emphasized that parameter C is associated with deflection of the beam. Substituting $\xi = 1/2$ into Eq. (2.7.25) reaches us to

$$C = -\frac{1}{2} W^*(1/2) \tag{2.7.28}$$

Therefore, Eq. (2.7.27) presents the temperature-deflection path of the beam. In order to find the axial force N_x^* as a temperature rise function, definition of C from Eq. (2.7.27) is substituted into the result of Eq. (2.7.26) which gives us

$$N^{M*} = -f_1 \pi^2 \delta^2 C^2 \tag{2.7.29}$$

It is seen that in the pre-buckling regime, which is free of lateral deflection, $N^{M*} = 0$. Recalling Eq. (2.7.15), along with the substitution of Eq. (2.7.27) into (2.7.29), result in the total axial force resultants as

$$\begin{aligned} N_x^* &= -N^{T*} - N^{E*} \quad \text{in prebuckling regime} \\ N_x^* &= -\frac{4\pi^2 P_1 P_2}{4\pi^2 P_1 + P_2} \quad \text{in postbuckling regime} \end{aligned} \tag{2.7.30}$$

As seen from the above equations, in both pre- and post-buckling regimes, the axial force is independent of beam position. Besides, in pre-buckling state the axial force

varies linearly with respect to temperature rise while in post-buckling regime it is independent of temperature rise parameter.

2.7.4 Simply Supported-Simply Supported Boundary Conditions

For a beam which is simply-supported at both edges, deflection and bending moment should be vanished at both ends. Therefore, the following system of equations is obtained in this case [34]

$$\begin{aligned} C_2 + C_4 &= 0 \\ \sin(a)C_1 + \cos(a)C_2 + C_3 + C_4 &= 0 \\ \delta F C_2 &= M^{T*} + \frac{f_2}{f_1} N^{M*} \\ \delta F\left(\sin(a)C_1 + \cos(a)C_2\right) &= M^{T*} + \frac{f_2}{f_1} N^{M*} \end{aligned} \tag{2.7.31}$$

The above equations are solved for the coefficients and written in terms of a constant C

$$\begin{aligned} C_1 &= \tan\left(\frac{a}{2}\right) C \\ C_2 &= C \\ C_3 &= 0 \\ C_4 &= -C \end{aligned} \tag{2.7.32}$$

where

$$C = \frac{M^{T*} + \dfrac{f_2}{f_1} N^{M*}}{\delta F} \tag{2.7.33}$$

The relation between C and a from Eqs. (2.7.15), (2.7.17), and (2.7.33) can be derived as

$$C = \frac{a^2 P_1 + P_2}{\delta a^2 P_1 P_2}\left(M^{T*} - \frac{f_2}{f_1}\left(N^{T*} + N^{E*}\right)\right) + \frac{f_2}{\delta f_1} \tag{2.7.34}$$

With the aid of Eqs. (2.7.16) and (2.7.32), substituting them into Eq. (2.7.11) and integrating with respect to ξ, we have

$$f_1 \int_0^1 \frac{dU^*}{d\xi} d\xi + f_1 \frac{\delta^2}{2} \int_0^1 \left(\frac{dW^*}{d\xi}\right)^2 d\xi + f_2 \int_0^1 \frac{d\varphi}{d\xi} d\xi = -\int_0^1 N^{M*} d\xi \tag{2.7.35}$$

Because of the immovable boundary conditions for U^*, the first integral in Eq. (2.7.35) vanishes. The second and third integrals may be derived as

$$\int_0^1 \left(\frac{dW^*}{d\xi}\right)^2 d\xi = C^2\left(\frac{a^2 - a\sin(a)}{1+\cos(a)}\right)$$
$$\int_0^1 \frac{d\varphi}{d\xi}d\xi = \frac{2aC\delta}{1+\dfrac{P_1}{P_2}a^2}\left(\frac{1-\cos(a)}{\sin(a)}\right) \tag{2.7.36}$$

Substitution of Eqs. (2.7.36) into (2.7.35), performing the proper simplifications on the right-hand side integral of Eq. (2.7.35) according to Eqs. (2.7.33) and (2.7.34) along with defining the parameter B as

$$B = \frac{\left(M^{T*} - \dfrac{f_2}{f_1}\left(N^{T*} + N^{E*}\right)\right)\left(1+\dfrac{P_1}{P_2}a^2\right)}{\delta a^2 P_1} + \frac{f_2}{\delta f_1} \tag{2.7.37}$$

transforms Eq. (2.7.35) into the form

$$-a^3\frac{N^{T*}+N^{E*}}{P_1}\left(1+\frac{P_1}{P_2}a^2\right)(1+\cos(a)) + \frac{f_1B^2}{2P_2}\left(1+\frac{P_1}{P_2}a^2\right)^3(a-\sin(a))$$
$$+\frac{f_2^2}{2f_1P_2}a^4\left(1+\frac{P_1}{P_2}a^2\right)(a-\sin(a)) + \frac{f_2B}{P_2}a^2\left(1+\frac{P_1}{P_2}a^2\right)(a-\sin(a))$$
$$+\frac{2f_2B}{P_2}a^2\left(1+\frac{P_1}{P_2}\right)\sin(a) + \frac{2f_2^2}{f_1P_2}a^4\sin(a) + a^5(1+\cos(a)) = 0 \tag{2.7.38}$$

Equation (2.7.38) exhibits the relation between load parameters and a in which $a \neq 0, 2(m-1)\pi$ and $m = 1, 2, \ldots$. It is seen that depending on the load level, a may take on multiple values for a given load. Furthermore, unlike the case of an FGM beam with both ends clamped, in which the load-deflection is presented in a closed-form solution, here the deflection of the beam at each load step should be extracted from a transcendental equation.

Notice that for the especial cases of homogeneity, i.e. when power law index is equal to zero or infinity, both stretching-bending coupling stiffness and thermal moment vanish. In this case the response of the beam is obtained from an eigen-value problem, since the system of equations (2.7.31) reduces to a homogeneous one. Same as the process developed for the case of an FGM beam with both edges clamped, it is seen that the characteristic equation of the beam is equal to

$$\sin(a) = 0 \tag{2.7.39}$$

which has the minimum value $a = \pi$. In such case, all constants C_2, C_3, and C_4 are equal to zero and the deflection equation of the beam is obtained as

$$W^*(\xi) = C \sin(\pi\xi) \tag{2.7.40}$$

Similar to the process used for the $C - C$ type of edge supports, the constant C as a function of load parameter is obtained as

$$C = \sqrt{\frac{N^{T*} + N^{E*} - \dfrac{\pi^2 P_1 P_2}{\pi^2 P_1 + P_2}}{0.25 f_1 \delta^2 \pi^2}} \tag{2.7.41}$$

in which based on Eq. (2.7.40) we have

$$C = W^*(1/2) \tag{2.7.42}$$

and the total axial load, as a function of temperature parameter, is equal to

$$\begin{aligned} N_x^* &= -N^{T*} - N^{E*} \qquad \text{in prebuckling regime} \\ N_x^* &= -\frac{\pi^2 P_1 P_2}{\pi^2 P_1 + P_2} \qquad \text{in postbuckling regime} \end{aligned} \tag{2.7.43}$$

Since the bifurcation point is the junction of primary and secondary equilibrium paths, the critical buckling thermal load is obtained when N_x^* is removed between Eq. (2.7.43)

$$N_{cr}^{T*} = \frac{\pi^2 P_1 P_2}{P_1 \pi^2 + P_2} - N^{E*} \tag{2.7.44}$$

2.7.5 *Results and Discussion*

In this part, a functionally graded material beam made of $SUS304$ as metal constituent and Si_3N_4 as ceramic constituent along with $G1195N$ as piezoelectric layers are considered. Beam is under uniform temperature rise loading. The material properties of constituents are given in Table 2.5. While the presented method is obtained by analytical methods, for the sake of comparison, the critical buckling temperature difference of a beam with two piezoelectric layers is compared with the previous results of References [23, 24, 33]. A clamped beam made of Alumina with two bonded piezoelectric layers is assumed to be under uniform temperature rise loading. Piezoelectric layers are made of $G1195N$. Properties of the host layer are $E = 380\,\text{Gpa}$, $\alpha = 7.4 \times 10^{-6} K^{-1}$ and $\nu = 0.3$. Five cases of applied actuator voltages are studied. It is seen that the results of this study are less than those reported by

Table 2.5 Material properties for $SUS304$, Si_3N_4 and $G1195N$ [14, 33]

Material	Property	Magnitude
$SUS304$	$\alpha_m[\mathrm{K}^{-1}]$	15.3210×10^{-6}
	$E_m[\mathrm{Pa}]$	$207.79 \times 10^{+9}$
	ν	0.28
Si_3N_4	$\alpha_c[\mathrm{K}^{-1}]$	7.4746×10^{-6}
	$E_c[\mathrm{Pa}]$	$322.27 \times 10^{+9}$
	ν	0.28
$G1195N$	$\alpha_p[\mathrm{K}^{-1}]$	0.9×10^{-6}
	$E_p[\mathrm{Pa}]$	$63 \times 10^{+9}$
	$d_p[\mathrm{m/V}]$	2.54×10^{-10}
	ν_p	0.3

Table 2.6 A comparison on the effect of applied actuator voltage on the $\Delta T_{cr}[K]$ for an Alumina beam with two smart layers [34]. Geometry of the beam are $h_p = 0.001$ m, $h = 0.01$ m, $L = 0.25$ m

Source	$V_p = -500\,\mathrm{V}$	$V_p = -200\,\mathrm{V}$	$V_p = 0$	$V_p = +200\,\mathrm{V}$	$V_p = +500\,\mathrm{V}$
Kiani et al. [23]	797.744	797.403	797.175	796.948	796.606
Kiani et al. [24]	783.611	783.270	783.042	782.814	782.473
Fu et al. [33]	–	797.403	797.180	796.950	–
Present study	780.645	780.304	780.077	779.850	779.510

Kiani et al. [23] and Fu et al. [33], which is expected since their results are developed within the framework of Euler beam theory. Relative difference between these results and those of [23] and [33] is at most 2.5 percent. It is worth mentioning that results of this study has a smaller difference with the results of Kiani et al. [24] which is also developed based on the Timoshenko beam theory. The small deviation arises from the assumption considered in [24], where the effect of piezoelectric layer thickness in thermal force resultant calculation is neglected. As seen, the assumption of Kiani et al. [24] is valid and relative differences is at most 0.4 percent (Table 2.6).

Numerical results presented in Figs. 2.10, 2.11, 2.12, 2.13, 2.14, 2.15, 2.16 cover the case of an FGM beam without piezoelectric layers and Figs. 2.17 and 2.18 are associated with the case of hybrid FGM beams [34].

In Fig. 2.10 the critical buckling temperature difference of FGM beam without piezoelectric layers with respect to slenderness ratio and power law index for the $C-C$ case is presented. As expected, higher L/h ratio results into lower ΔT_{cr}, which is due to the lower flexural rigidity of the beam. For the constituents of this study, as the power law index increases the critical buckling temperature increases permanently, which is due to the less thermal expansion coefficient of ceramic constituent.

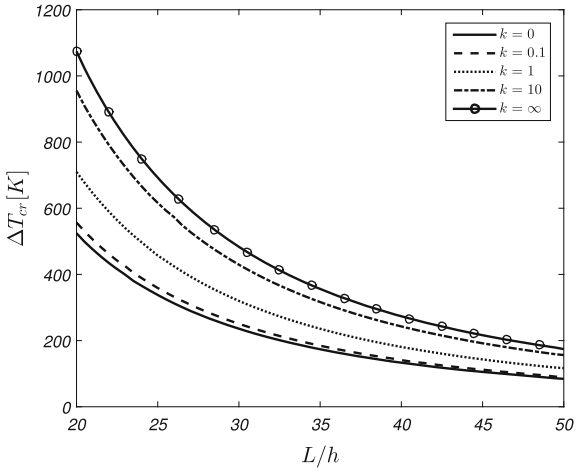

Fig. 2.10 Critical buckling temperature difference $\Delta T_{cr}[K]$ for an FGM beam with both edges clamped

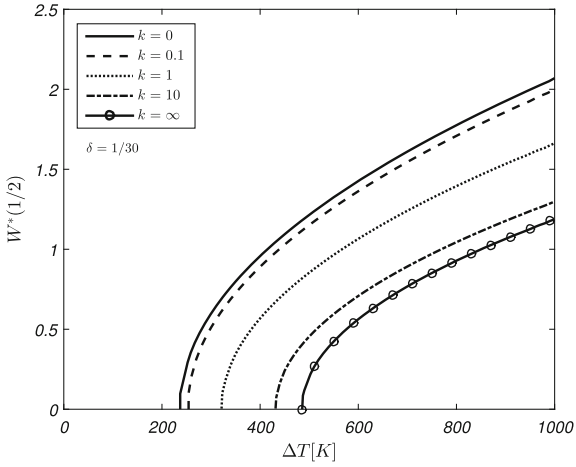

Fig. 2.11 Temperature-deflection equilibrium path of a $C - C$ FGM beam without piezoelectric layers with respect to various slenderness ratios

The effect of power law index on temperature-deflection equilibrium path of the FGM beams with various power law indices are given in Fig. 2.11. As the graphs exhibit, the load-deflection path of FGM beams for each value of power law index is of the bifurcation-type buckling. For the constituents of this study, behavior of the FGM beam stands between two associated homogeneous cases. For a prescribed temperature parameter, an increase in the power law index results in less deflection.

The effect of slenderness ratio for an FGM beam is plotted in Fig. 2.12. As expected, the thicker beams result into higher critical buckling temperatures. For a prescribed temperature parameter, the higher values of L/h ratio produce higher midpoint deflection of the beam.

For the studied cases of Fig. 2.12, the total in-plane load parameter as a function of temperature rise is plotted in Fig. 2.13. It is seen that similar to Fig. 2.12, the

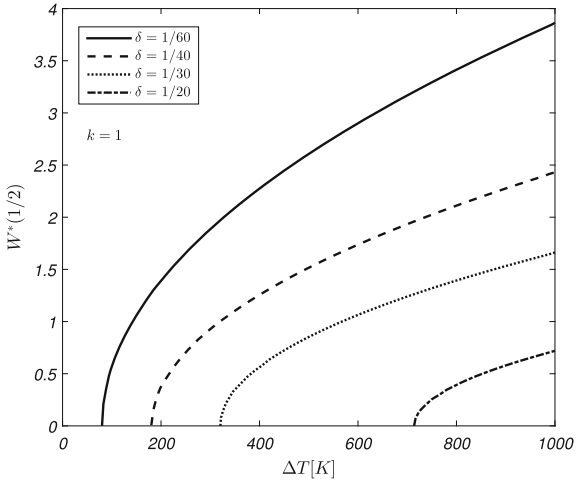

Fig. 2.12 Temperature-deflection equilibrium path of a $C - C$ FGM beam without piezoelectric layers with respect to various power law indices

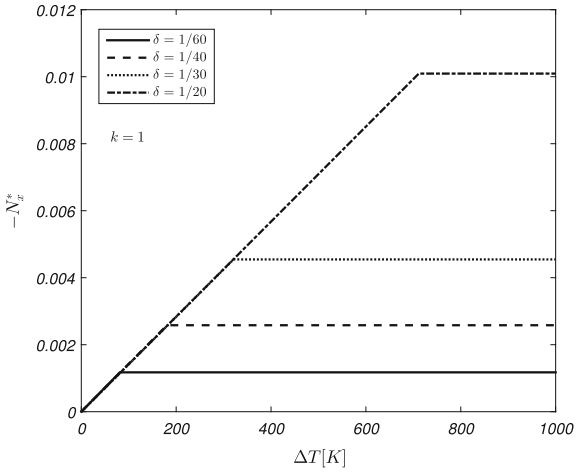

Fig. 2.13 In-plane force-temperature path of a $C - C$ FGM beam without piezoelectric layers

bifurcation temperatures are detectable from the force-deflection paths. As theoretically proved, in the pre-buckling state, the total in-plane force varies linearly with respect to the uniform temperature rise parameter, while it remains independent of temperature rise in post-buckling equilibrium path.

For the case of a linearly graded FGM beam with both edges simply-supported, the temperature-deflection equilibrium path for various slenderness ratios are plotted in Fig. 2.14. As it is seen, the temperature-deflection equilibrium path of FGM beams are not of the bifurcation-type buckling. Through the studied range, the load-deflection path of FGM beam with both ends simply-supported is unique and stable. A comparison of Figs. 2.12 and 2.14 reveals that the mid-plane deflection of the $S - S$ beams is larger than that of the $C - C$ beams, since in the latter case beam remains flat, while the $S - S$ beam initially starts lateral deflection. Besides, after

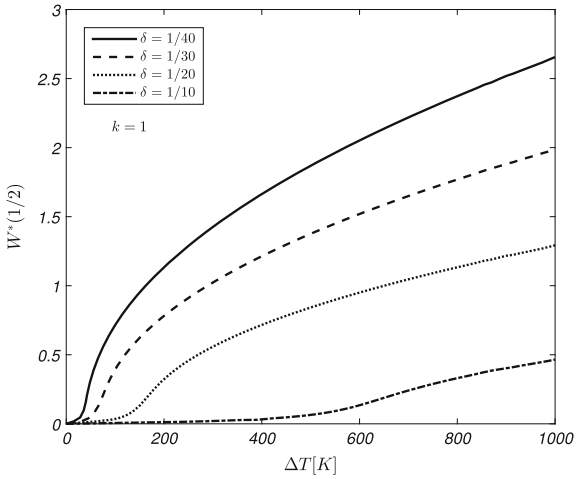

Fig. 2.14 Temperature-deflection equilibrium path of a $S - S$ FGM beam without piezoelectric layers with respect to various slenderness ratios

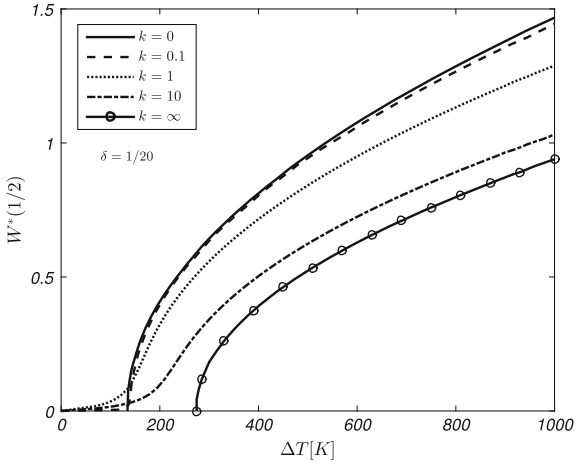

Fig. 2.15 Temperature-deflection equilibrium path of a $S - S$ FGM beam without piezoelectric layers with respect to various power law indices

the bifurcation point in which the $C - C$ beam starts to have lateral deflection, the ability of edges to sustain the moment at boundaries results in less lateral deflection in comparison with the $S - S$ case.

For various values of the power law index, the load-deflection equilibrium path of FGM beams with both edges simply-supported is presented in Fig. 2.15. It is worth mentioning that, except for the two especial cases of homogeneity i.e. $k = 0, \infty$, the load-deflection path of the beam is unique and stable. On the other hand, the response for $k = 0, \infty$ cases is of the primary-secondary equilibrium path. Due to the unsymmetrical distribution of properties with respect to the mid-plane of simply-supported FGM beam, lateral deflection occurs at the onset of thermal loading. It is interesting to note that, unlike the case of $C - C$ beams, the response of $S - S$ FGM beam does not stand between the two associated homogeneous cases.

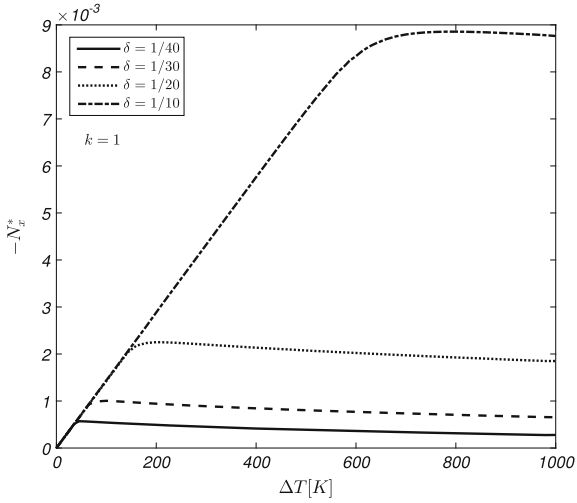

Fig. 2.16 In-plane force-temperature path of a $S - S$ FGM beam without piezoelectric layers

For the studied cases of Fig. 2.15, in Fig. 2.16 the total in-plane force is plotted as a function of uniform temperature rise parameter. As seen, unlike the $C - C$ case of boundary conditions, there is no branching point in the curves. The total force as a function of temperature rise is completely smooth.

To investigate the effect of applied actuator voltage on the post-buckling equilibrium path of $C - C$ and $S - S$ FGM beams, temperature-deflection curves are plotted in Figs. 2.17 and 2.18 for linearly graded $C - C$ and $S - S$ FGM beams, respectively. As seen, the effect of applied actuator voltage to the smart layers is negligible. For the piezoelectric layers used in this study, in comparison to the grounding case condition, applying the negative magnitude of V_p postpones the bifurcation point of the $C - C$ case. Consequently, within the post-buckling range, applying a prescribed temperature rise results in less deflection. The latter case is true for the $S - S$ case too. However, as pointed-out, the effect of the applied actuator voltage is hardly distinguishable.

2.8 Vibration of Thermo-Electrically Post-buckled FGPM Beams

2.8.1 Introduction

The ability of piezoelectric materials to surpass the vibrational motion, shape control, and delay the buckling is reported in literature. This ability is documented by some valuable books on the subject, such as Tzou's one [36], or those reported by Yang [37, 38].

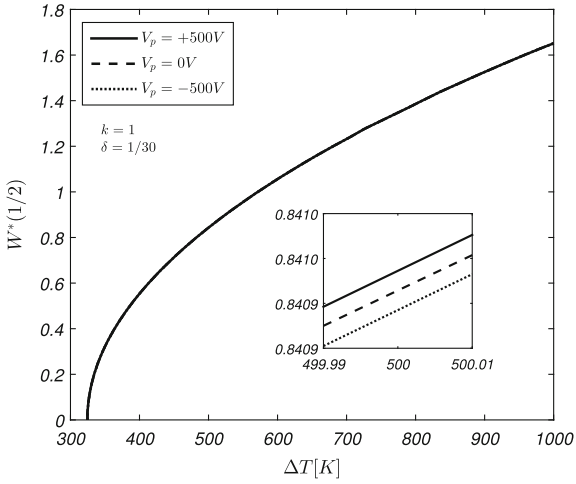

Fig. 2.17 Temperature-deflection equilibrium path of a hybrid $C - C$ FGM beam ($\mu = 0.01$)

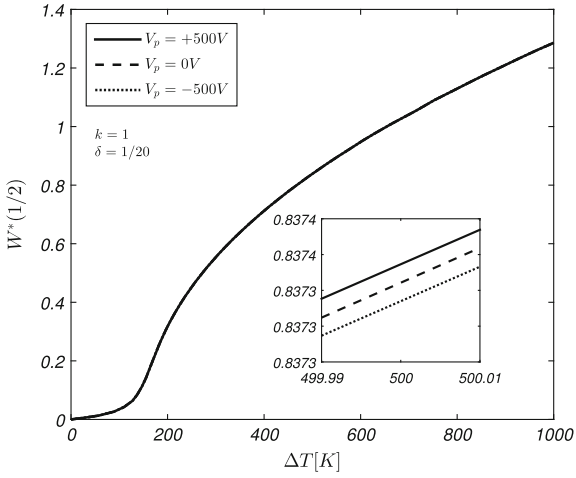

Fig. 2.18 Temperature-deflection equilibrium path of a hybrid $S - S$ FGM beam ($\mu = 0.01$)

For the case when beam has a rectangular cross-shape, Yang and his co-authors [39–41] have analyzed the three-dimensional behavior of electroelastic beams. In these works, extensional and transversal motions are studied. Double power-series solutions are developed in thickness and width directions. Wang and Queck [42, 43] analyzed the free vibration problem of a beam integrated with piezoelectric layer(s) based on the classical beam theory. Both open and closed-circuit electrical states are examined and the effect of electrical boundary conditions on free vibration motion is investigated. Most recently, Ke et al. [44] and Ke and Wang [45] analyzed the free vibration problem of a piezoelectric beam including Eringen's nonlocal effects in thermo-electro-mechanical field.

Pradhan and Murmu have analyzed the free vibration of FGM sandwich beam including thickness variations in thermal field [46]. Based on the first order shear deformation beam theory, Xiang and Yang [47] examined the transverse heat conduction effects on small free vibrations of symmetrically laminated FGM beams. Using an improved perturbation technique and based on a higher-order shear deformation theory, Xia and Shen [48] investigated the small and large-amplitude vibration analysis of compressively and thermally post-buckled sandwich plates with functionally graded material (FGM) face sheets in thermal environments. The results of this paper show that as the volume fraction index increases, the fundamental frequency increases in the pre-buckling region, while in the post-buckling regime the behavior is vice versa. The free vibration analysis of an elastic rod around its post-buckled equilibrium state is addressed in the work of Neukirch et al. [49]. They employed both analytical and numerical schemes to conclude the results, before and after the buckling point.

The FGM structures when are incorporated with the piezoelectric layers are called hybrid FGMs. Vibrations of a Timoshenko beam with surface bonded piezoelectric layers in both pre/post-buckling states is studied by Li et al. [22]. In this work shooting method is implemented to solve the post-buckling and free vibration problems of a hybrid FGM beam, clamped at both ends. Recently, the free vibration of a clamped hybrid FGM beam under in-plane thermal loading is investigated by Fu et al. [33]. In this work, a fully analytical method is developed to analyze the post-buckling equilibrium path and large amplitude vibrations of the beam.

Researches on the analysis of FGPM structures, FGM structures and piezoelectric smart layers combined together, under thermo-electro mechanical loadings are limited in number. Besides, among these investigations, most of them analyze the geometrically linear response of the graded actuators. In many studies, variation of material properties in a specific direction is assumed to follow a prescribed distributed function. Huang et al. [50] developed a solution based on the two-dimensional theory of elasticity for the response of an FGPM beam with arbitrary through-the-thickness distribution of material properties. Introducing a stress function and an electrical displacement function, the equilibrium and Maxwell electrical equations are satisfied. Solution of stress function and electrical displacement function, however, are assumed to be quadratic through the span. Shi [51], Shi and Chen [52], and Liu and Shi [53] performed a series of investigations on orthotropic FGPM beams. In reference [51], Shi reported various analytical solutions for a cantilever beam where density varies as a cubic polynomial across the thickness. Shi and Chen in [52] consider the case of quadratic and cubic variations of elastic property and density of the beam across the thickness. With consideration of linearly graded piezoelectric parameter through-the-thickness, Liu and Shi [53] obtained the response of an FGPM beam based on the definition of stress function.

Kruusing [54] obtained an analytical solution for a cantilever Euler–Bernoulli FGPM beam under the action of a shear force at the tip. When an FGPM beam is subjected to electrical or electro-thermal loading, Joshi et al. [55, 56] developed the bending response of the structure. It is concluded that the behavior of an FGPM beam is largely affected by the composition rule of the constituents. Based on a

layer-wise formulation, Lee [57, 58] developed a finite elements method to investigate the response of the FGPM beam subjected to the combined action of thermal and electrical loads. Yang and Xiang [59] performed a comprehensive study on the static, dynamic, and free vibration behavior of the FGPM Timoshenko beams under the action of thermal, mechanical, and electrical excitations. In this work, three mechanical equations and the Maxwell-type electrical equation are solved simultaneously, employing the differential quadrature (DQ) method. Employing the classical, first order, and third order shear deformation beam theories, Komeili et al. [60] developed the finite elements and finite Fourier formulations to study the bending response of a monomorph FGPM beam under various types of loading. Dynamic response of the beam employing the Galerkin-based finite elements formulation is reported by Doroushi et al. [61] based on the third order shear deformation theory.

The present section implements the Ritz finite elements method to discrete the governing equations associated with the post-buckling of FGPM beams [62]. Furthermore, the vibration behavior of the beam in pre- and post-buckling regimes is analyzed. The established equations are nonlinear due to the presence of von-Karman's geometrical non-linearity in strain components. The solution is divided into static and dynamic responses. Static response of the beam is the study of postbuckling equilibrium path under the in-plane thermoelectrical loading. The Newton–Raphson method is implemented to solve the nonlinear system of equations, iteratively. The dynamic response is the study of small free vibration in thermoelectrically pre/post-buckled states via the linear eigenvalue analysis. The variation of fundamental frequency in thermal field reveals that the behavior of a structure, depending on boundary conditions and the applied loads, may be of the bifurcation or critical point responses. It is shown that applying the appropriate external voltage, the buckling phenomenon of an FGPM structure is controlled and postponed within a noticeable range.

2.8.2 Governing Equations

Consider a beam made of functionally graded piezoelectric materials (FGPMs) of length L, width b, and thickness h. The beam is subjected to a mechanical distributed load q, temperature rise ΔT, and applied voltage V_0, as shown in Fig. 2.19.

It is considered that the material properties vary continuously across the thickness direction according to the power law distribution given by Eq. (2.2.8). In this section, the Timoshenko beam theory is used with the following displacement field

$$\begin{aligned} U(X, Z, t) &= U_0(X, t) + Z\Psi(X, t) \\ W(X, Z, t) &= W_0(X, t) \end{aligned} \tag{2.8.1}$$

where (U_0, W_0) are the displacement components of a point on the mid-plane of the beam along axial and thickness coordinates, respectively, and Ψ stands as the rotation of the cross-section.

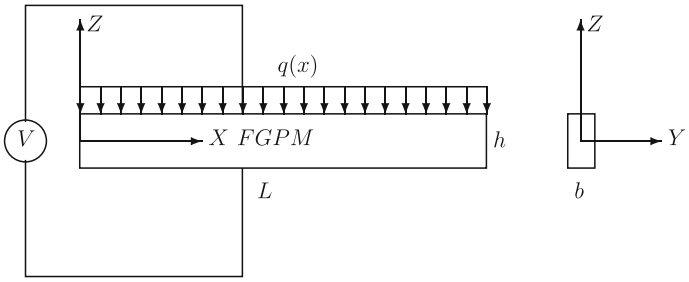

Fig. 2.19 Geometry and coordinate system of an FGPM beam

Wang and Queck [63] performed a two-dimensional elasticity solution to obtain the distribution of electrical potential across the thickness, when beam is subjected to a constant uniform mechanical load. Results of this study reveals that for the case where a simply-supported beam is closed circuit at both top and bottom surfaces, the analytical distribution of electrical potential is obtained in a parabolic form, where the peak point stands at the middle. This type of distribution, also, has been used for the other types of boundary conditions, loading, and material property distribution. Also, some authors used the trigonometric functions along the thickness direction to satisfy the closed-circuit electrical conditions at the top and bottom layers [59, 64, 65].

In this part, considering both reverse and direct effects of a piezoelectric layer, the electric potential V is assumed to obey the following distribution [44, 66]

$$V(X, Z, t) = \cos(\beta Z)\Phi(X, t) + \frac{V_0}{h}Z \tag{2.8.2}$$

where $\beta = \pi/h$ and $\Phi(X, t)$ is spatial function of the electric potential and the second term denotes the external electric voltage applied to beam's electrodes.

The constitutive equations for the FGPM beam under thermo-electro-mechanical loads may be expressed as follow [61]

$$\begin{aligned}
\sigma_X &= Q_{11}\varepsilon_X - Q_{11}\alpha_1\Delta T - e_{31}E_Z \\
\tau_{XZ} &= Q_{55}\gamma_{XZ} - e_{15}E_X \\
D_X &= e_{15}\gamma_{XZ} + k_{11}E_X \\
D_Z &= e_{31}\varepsilon_X + k_{33}E_Z + p_3\Delta T
\end{aligned} \tag{2.8.3}$$

where ε_X, γ_{XZ}, σ_X, τ_{XZ}, D_i, and E_i represent the axial strain, shear strain, axial stress, shear stress, dielectric displacements, and the corresponding electric field components, respectively. Here, e_{ij}, k_{ij}, α_1, p_3 are the piezoelectric, dielectric, thermal expansion, and pyroelectric coefficients, respectively, and Q_{11} and Q_{55} are the elastic stiffness coefficients.

The von-Karman type nonlinear strain-displacement relations can be obtained using Eq. (2.8.1) as

$$\begin{aligned}\varepsilon_X &= U_{0,X} + \frac{1}{2}W_{0,X}^2 + Z\Psi_{,X}\\ \gamma_{XZ} &= W_{0,X} + \Psi\end{aligned} \tag{2.8.4}$$

Since the electric field vector is negative gradient of the total potential function, using Eq. (2.8.2), the electric field components are

$$\begin{aligned}E_X &= -V_{,X} = -\cos(\beta Z)\Phi_{,X}\\ E_Z &= -V_{,Z} = \beta\sin(\beta Z)\Phi - E_0\end{aligned} \tag{2.8.5}$$

where we have set $E_0 = \dfrac{V_0}{h}$.

The governing equations may be derived on the basis of Hamilton's principle. According to this principle, equations of motion are obtained when the following equality holds

$$\delta\int_t (K - H + R)dt = 0 \tag{2.8.6}$$

where the variation of the electric enthalpy δH and the variation of the kinetic energy δK are, respectively [59]

$$\delta H = b\int_0^L \int_{-\frac{h}{2}}^{+\frac{h}{2}} (\sigma_X \delta\varepsilon_X + K_s\tau_{XZ}\delta\gamma_{XZ} - D_X\delta E_X - D_Z\delta E_Z)\, dZdX \tag{2.8.7}$$

$$\delta K = b\int_0^L \int_{-\frac{h}{2}}^{+\frac{h}{2}} \rho(U_{,t}\delta U_{,t} + W_{,t}\delta W_{,t})dZdX \tag{2.8.8}$$

In definition of δT, K_s is the shear correction factor and is taken as $K_s = \pi^2/12$.

The virtual work δR due to the out-of-plane mechanical load q is

$$\delta R = b\int_0^L q\delta W dX \tag{2.8.9}$$

Using Eqs. (2.8.3), (2.8.4), and (2.8.5), the stress resultants of the Timoshenko beam theory are

$$\begin{aligned}N_X &= A_{11}(U_{0,X} + \frac{1}{2}W_{0,X}^2) + B_{11}\Psi_{,X} - N_X^T - A_{31}^e\Phi + D_{31}^e E_0\\ M_X &= B_{11}(U_{0,X} + \frac{1}{2}W_{0,X}^2) + D_{11}\Psi_{,X} - M_X^T - B_{31}^e\Phi + E_{31}^e E_0\\ Q_X &= K_s A_{55}(W_{0,X} + \Psi) - K_s D_{15}^e\Phi_{,X}\end{aligned} \tag{2.8.10}$$

where N_X^T and M_X^T are the thermal force and moment resultants that are defined as

$$(N_X^T, M_X^T) = \int_{-\frac{h}{2}}^{+\frac{h}{2}} Q_{11}\alpha_1 \Delta T(1, Z)dZ \tag{2.8.11}$$

Other quantities that are not specified, are given in [61].

The inertia terms are defined as

$$(I_0, I_1, I_2) = \int_{-\frac{h}{2}}^{+\frac{h}{2}} \rho(1, Z, Z^2)dZ \tag{2.8.12}$$

For the sake of generality and simplicity, the following non-dimensional parameters [59] are introduced and used in the rest of this work

$$x = \frac{X}{L}, \quad \Phi_0 = \sqrt{\left(\frac{A_{11}}{F_{33}^e}\right)}, \quad u = \frac{U_0}{h}, \quad w = \frac{W_0}{h},$$

$$\psi = \Psi, \quad \phi = \frac{\Phi}{\Phi_0}, \quad \lambda_q = \frac{qL^2}{A_{11}h}, \quad \lambda_T = \frac{D_Z^T}{F_{33}^e\Phi_0},$$

$$\lambda_V = \frac{H_{33}^e E_0}{F_{33}^e\Phi_0}, \quad \lambda_{VT} = \frac{(D_{31}^e E_0 - N_X^T)L}{A_{11}h}, \quad \overline{\lambda}_{VT} = \frac{(E_{31}^e E_0 - M_X^T)L}{D_{11}} \tag{2.8.13}$$

where $D_Z^T = \int_{-\frac{h}{2}}^{+\frac{h}{2}} p_3\Delta T\beta\sin(\beta Z)dZ$, and the quantities that are not introduced are given in [61].

Substituting Eqs. (2.8.4) and (2.8.5) into Eq. (2.8.6), then integrating in thickness direction with consideration of Eq. (2.8.10), and applying the fundamental lemma of calculus, the weak-formulation of the governing equations in dimensionless form are obtained as [62]

$$\int_0^1 [u_{,x} + \frac{1}{2}\gamma_{12}w_{,x}^2 + \gamma_{13}\psi_{,x} - \gamma_{14}\phi + \lambda_{VT}]\delta u_{,x}dx =$$

$$-\int_0^1 \left[\eta_{11}u_{,tt} + \eta_{13}\psi_{,tt}\right]\delta u dx \tag{2.8.14}$$

$$\int_0^1 \left[\left\{u_{,x} + \frac{1}{2}\gamma_{12}w_{,x}^2 + \gamma_{13}\psi_{,x} - \gamma_{14}\phi + \lambda_{VT}\right\}\gamma_{12}w_{,x}\right.$$

$$\left.+\gamma_{22}w_{,x} + \frac{\gamma_{22}}{\gamma_{12}}\psi - \gamma_{24}\phi_{,x}\right]\delta w_{,x}dx - \int_0^1 \lambda_q\delta w dx =$$

$$-\int_0^1 \left[\eta_{22}w_{,tt}\right]\delta w dx \tag{2.8.15}$$

$$\int_0^1 \left[\left\{ \gamma_{31} \left(u_{,x} + \frac{1}{2}\gamma_{12} w_{,x}^2 \right) + \psi_{,x} - \overline{\gamma}_{34}\phi + \overline{\lambda}_{VT} \right\} \delta\psi_{,x} \right.$$

$$\left. + \left\{ \gamma_{32} w_{,x} + \frac{\gamma_{32}}{\gamma_{12}}\psi + \left(\gamma_{34} - \overline{\gamma}_{34}\right)\phi_{,x} \right\} \delta\psi \right] dx =$$

$$-\int_0^1 \left[\eta_{31} u_{,tt} + \eta_{33}\psi_{,tt} \right] \delta\psi dx \tag{2.8.16}$$

$$\int_0^1 \left[\left\{ \gamma_{42} w_{,x} + \overline{\gamma}_{43}\psi + \gamma_{44}\phi_{,x} \right\} \delta\phi_{,x} + \right.$$

$$\left. \left\{ \gamma_{41} \left(u_{,x} + \frac{1}{2}\gamma_{12} w_{,x}^2 \right) - \left(\gamma_{43} - \frac{\gamma_{42}}{\gamma_{12}} \right) \psi_{,x} + \phi + \lambda_T - \lambda_V \right\} \delta\phi \right] dx = 0 \tag{2.8.17}$$

where the constants appeared in the above equations are defined in [61].

Using integration by parts in Eqs. (2.8.14)–(2.8.17), the boundary conditions become

$$\begin{aligned} &N_X = 0 \quad \text{or} \quad u = 0, \\ &\gamma_{12} N_X w_{,x} + Q_X = 0 \quad \text{or} \quad w = 0, \\ &M_X = 0 \quad \text{or} \quad \psi = 0, \\ &\gamma_{42} w_{,x} + \overline{\gamma}_{43}\psi + \gamma_{44}\phi_{,x} = 0 \quad \text{or} \quad \phi = 0, \end{aligned} \tag{2.8.18}$$

where the latter one is the electrical boundary condition, and the first three are the mechanical ones. It is noted that in the solution process of this work, the natural electrical boundary condition is considered for each of the edge supports.

In the stability analysis of an FGPM beam, the boundary conditions may be assumed to be immovable simply supported or clamped. Mathematical expressions for each of these edges are

$$\begin{aligned} \text{Simply-supported} \quad (S): \quad & u = w = M_X = 0 \\ \text{Clamped} \quad (C): \quad & u = w = \psi = 0 \end{aligned} \tag{2.8.19}$$

2.8.3 Finite Elements Model

The Ritz-based finite element method is used to solve the weak forms of the governing equations. The variables are approximated as [62, 67]

$$u(x,t) = \sum_{j=1}^{l} u_j^e(t)\Psi_j^1(x)$$
$$w(x,t) = \sum_{j=1}^{m} w_j^e(t)\Psi_j^2(x)$$
$$\psi(x,t) = \sum_{j=1}^{n} \psi_j^e(t)\Psi_j^3(x)$$
$$\phi(x,t) = \sum_{j=1}^{p} \phi_j^e(t)\Psi_j^4(x) \tag{2.8.20}$$

where $\Psi_j^\alpha(x)(\alpha = 1,2,3,4)$ are the Lagrange interpolation functions of degree $(l-1)$, $(m-1)$, $(n-1)$, and $(p-1)$, respectively. Using Eq. (2.8.20), the virtual displacements are

$$\delta u = \Psi_i^1, \quad \delta w = \Psi_i^2, \quad \delta\psi = \Psi_i^3, \quad \delta\phi = \Psi_i^4 \tag{2.8.21}$$

In this work, the quadratic interpolation functions are used to approximate the variables in the elements. Substitution of Eqs. (2.8.20) and (2.8.21) into Eqs. (2.8.14)–(2.8.17), yield the following finite element model [62]

$$\sum_{j=1}^{l} M_{ij}^{11}(u_j^e)_{,tt} + \sum_{j=1}^{m} M_{ij}^{12}(w_j^e)_{,tt} + \sum_{j=1}^{n} M_{ij}^{13}(\psi_j^e)_{,tt} + \sum_{j=1}^{p} M_{ij}^{14}(\phi_j^e)_{,tt} +$$

$$\sum_{j=1}^{l} K_{ij}^{11}u_j^e + \sum_{j=1}^{m} K_{ij}^{12}w_j^e + \sum_{j=1}^{n} K_{ij}^{13}\psi_j^e + \sum_{j=1}^{p} K_{ij}^{14}\phi_j^e = F_i^1, (i = 1,\ldots,l) \tag{2.8.22}$$

$$\sum_{j=1}^{l} M_{ij}^{21}(u_j^e)_{,tt} + \sum_{j=1}^{m} M_{ij}^{22}(w_j^e)_{,tt} + \sum_{j=1}^{n} M_{ij}^{23}(\psi_j^e)_{,tt} + \sum_{j=1}^{p} M_{ij}^{24}(\phi_j^e)_{,tt} +$$

$$\sum_{j=1}^{l} K_{ij}^{21}u_j^e + \sum_{j=1}^{m} K_{ij}^{22}w_j^e + \sum_{j=1}^{n} K_{ij}^{23}\psi_j^e + \sum_{j=1}^{p} K_{ij}^{24}\phi_j^e = F_i^2, (i = 1,\ldots,m) \tag{2.8.23}$$

$$\sum_{j=1}^{l} M_{ij}^{31}(u_j^e)_{,tt} + \sum_{j=1}^{m} M_{ij}^{32}(w_j^e)_{,tt} + \sum_{j=1}^{n} M_{ij}^{33}(\psi_j^e)_{,tt} + \sum_{j=1}^{p} M_{ij}^{34}(\phi_j^e)_{,tt} +$$

$$\sum_{j=1}^{l} K_{ij}^{31}u_j^e + \sum_{j=1}^{m} K_{ij}^{32}w_j^e + \sum_{j=1}^{n} K_{ij}^{33}\psi_j^e + \sum_{j=1}^{p} K_{ij}^{34}\phi_j^e = F_i^3, (i = 1,\ldots,n) \tag{2.8.24}$$

$$\sum_{j=1}^{l} M_{ij}^{41}(u_j^e)_{,tt} + \sum_{j=1}^{m} M_{ij}^{42}(w_j^e)_{,tt} + \sum_{j=1}^{n} M_{ij}^{43}(\psi_j^e)_{,tt} + \sum_{j=1}^{p} M_{ij}^{44}(\phi_j^e)_{,tt} +$$

$$\sum_{j=1}^{l} K_{ij}^{41} u_j^e + \sum_{j=1}^{m} K_{ij}^{42} w_j^e + \sum_{j=1}^{n} K_{ij}^{43} \psi_j^e + \sum_{j=1}^{p} K_{ij}^{44} \phi_j^e = F_i^4, (i = 1, \ldots, p) \quad (2.8.25)$$

Definitions of the elements of M_{ij}, K_{ij}, and F_i are given in [61].

The element equations (2.8.22)–(2.8.25) can be expressed in a compact form as

$$[M]\left\{\ddot{\Delta}\right\} + ([K_L] + [K_{NL1}] + [K_{NL2}])\{\Delta\} = \{F_m\} + \{F_e\} + \{F_T\} \quad (2.8.26)$$

where $[M]$ is the matrix of inertia, and $[K_L]$, $[K_{NL1}]$, and $[K_{NL2}]$ are the linear, first order nonlinear, and second order nonlinear stiffness matrices, respectively, and $\{F_m\}$, $\{F_e\}$, and $\{F_T\}$ are the mechanical, electrical, and thermal force vectors, respectively. Besides $\{\Delta\} = \{\{u\}, \{\phi\}, \{w\}, \{\Psi\}\}^T$, is the matrix of nodal values.

To study the vibration of a beam in pre/post-buckling states, the solution of the governing equation (2.8.26) is assumed as [68]

$$\{\Delta\} = \{\Delta_s\} + \{\Delta_d\} \quad (2.8.27)$$

where $\{\Delta_s\}$ is the time-independent particular solution denoting the large displacements and is implemented to study the pre-buckling and post-buckling regimes of the beam. Besides, $\{\Delta_d\}$ is the time-dependent solution with small magnitude which is used to study the free vibration analysis of a beam in the pre/post-buckling configurations.

Substituting Eq. (2.8.27) into the finite element equation (2.8.26), results to the following set of equations [62]

$$([K_L] + [K_{NL1}] + [K_{NL2}])\{\Delta_s\} = \{F_m\} + \{F_e\} + \{F_T\} \quad (2.8.28)$$

$$[M]\left\{\ddot{\Delta}_d\right\} + ([K_L] + 2[K_{NL1}] + 3[K_{NL2}])\{\Delta_d\} = \{0\} \quad (2.8.29)$$

Equation (2.8.28) is for the post-buckling analysis, and Eq. (2.8.29) is associated with the vibration analysis of the buckled structure.

Due to the nonlinear effects in stiffness matrices of the above equations, an iterative method has to be used for each load step. Two commonly-used iterative schemes are the Picard iteration procedure and the Newton–Raphson method. The details of these methods are available in [69]. Both direct iteration and Newton–Raphson methods are examined to solve the nonlinear finite element equation (2.8.28). It is important to note that for the cases in which there exists a rapid change in the graph trend of load-deflection path, the direct iterative procedure (Picard method) does not converge within the reasonable iteration steps. This feature occurs due to dependency of the solutions to converged magnitudes of the previous load step in each load increment.

Table 2.7 Thermo-electro-mechanical properties of PZT-4 and PZT-5H [61]

P	$PZT-4$	$PZT-5H$
Q_{11}[GPa]	81.3	60.6
Q_{55}[GPa]	25.6	23.0
e_{31}[Cm^{-2}]	-10.0	-16.604
e_{15}[Cm^{-2}]	40.3248	44.9046
k_{11}[$\mathrm{C}^2\mathrm{m}^{-2}\mathrm{N}^{-1}$]	0.6712×10^{-8}	1.5027×10^{-8}
k_{33}[$\mathrm{C}^2\mathrm{m}^{-2}\mathrm{N}^{-1}$]	1.0275×10^{-8}	2.554×10^{-8}
α_1[K^{-1}]	2×10^{-6}	10×10^{-6}
p_3[$\mathrm{Cm}^{-2}\mathrm{K}^{-1}$]	2.5×10^{-5}	0.548×10^{-5}
ρ[$\mathrm{kg.m}^{-3}$]	7500	7500

The Newton–Raphson method, however, seems to be more rapid-convergent. In this section, therefore, only the Newton–Raphson method is considered to obtain the results. Using the converged magnitudes of the nodal parameters, obtained through the iterative procedure for each load step in Eq. (2.8.28), the free vibration response of the post-buckled actuator is analyzed using Eq. (2.8.29) as the updated static equilibrium position of each load increment.

2.8.4 *Result and Discussions*

To assess the nonlinear pre/post-buckling free vibration behavior of an FGPM beam, a monomorph FGPM beam made of PZT-4 and PZT-5H piezoelectric materials is considered. Top surface of the beam is PZT-4 rich, while the bottom one is PZT-5H rich. Table 2.7 represents the thermo-electro-mechanical properties of these constituents. In all the rest, thickness is assumed to be $h = 0.001$ m, unless otherwise stated. Here, the dimensionless natural frequency is assumed to be $\Omega = \omega h\sqrt{(\rho/Q_{11})_{PZT-4}}$.

The temperature-deflection path of FGPM beam with $L/h = 25$ is depicted in Fig. 2.20 [62]. It is seen that, due to the non-symmetrical distribution of material properties across the thickness, the behavior of an FGPM beam under in-plane thermal loading is not of the bifurcation-type buckling, except for the case where the FGPM beam is reduced to a fully homogeneous one ($k = 0$). On the other hand, the equilibrium path of monomorph $S-S$ FGPM beam is unique and stable. Furthermore, due to the higher coefficient of thermal expansion near the bottom surface, beam bends downward. The power law index of composition rule plays an important role on the magnitude of lateral deflection. For the constituents of this study, as the power law index decreases, structure becomes stiffer and experiences less deflection.

The end-shortening force of an FGPM beam with the $S-S$ boundary conditions is plotted in Fig. 2.21 for three different values of power law index when beam is subjected only to temperature rise. Apparently, for the case of $k = 0$, when beam is

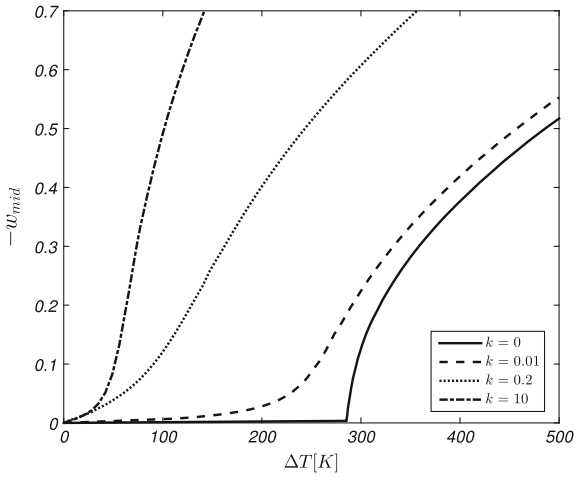

Fig. 2.20 Effect of the volume fraction index on the thermal post-buckling equilibrium paths of immovable $S - S$ FGPM beams ($V_0 = 0, L/h = 40$)

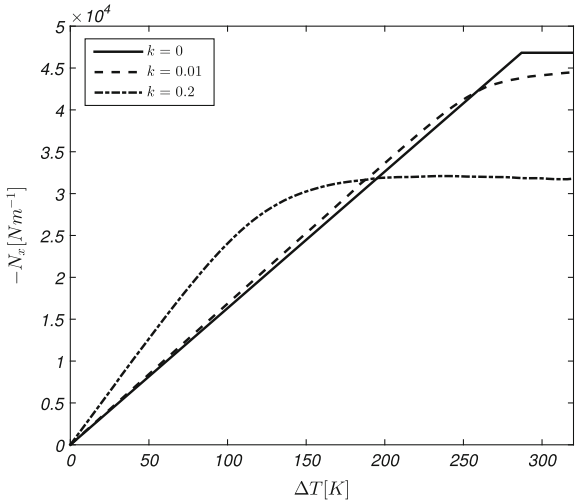

Fig. 2.21 The end-shortening force of an $S - S$ FGPM beam for different volume fraction indices ($V_0 = 0, L/h = 40$)

fully homogeneous, end-shortening force varies linearly up to the bifurcation-point. The reason is that in pre-buckling state beam does not undergo any rotation, axial displacement, lateral deflection, and electrical potential. For the case of non-zero power law indices, however, end-shortening force varies nonlinearly with respect to temperature during the thermal loading process.

The effect of slenderness on load-deflection path of isotropic/homogeneous beams is depicted in Fig. 2.22. Since beam is subjected to only uniform temperature rise loading, thermal load-deflection paths are of the symmetrical primary-secondary path, where the post-buckling branch is stable. As expected, the higher L/h ratio results in more magnitude of deflection. Consequently, the bifurcation temperatures

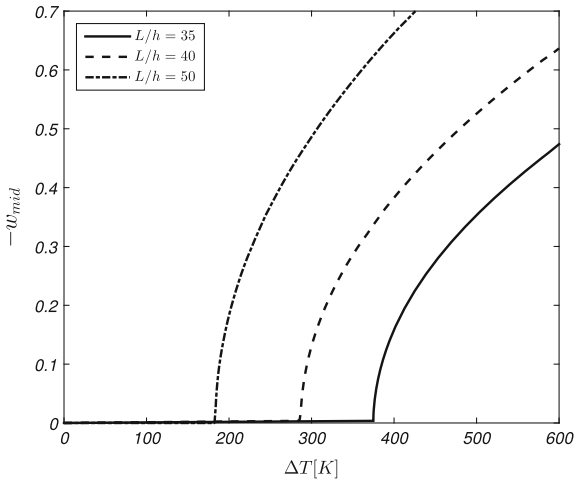

Fig. 2.22 Effect of slenderness ratio on the thermal post-buckling equilibrium paths of immovable $S-S$ FGPM beam ($V_0 = 0, k = 0$)

are postponed when beam becomes thicker. This is due to the stiffness loss caused by increasing the L/h ratio.

In Fig. 2.23 the temperature-deflection equilibrium paths of the FGPM beams are plotted for various power law indices. Similar to the case of $S-S$ beams, when $k = 0$, that is the reduction of an FGPM beam to a fully homogeneous one, the problem is posed as a bifurcation-type buckling. For the case when distribution of properties is described with a nonzero volume law index, problem is not of the bifurcation-type buckling. However, the behavior of the beam is totally different from those observed for the $S-S$ beams in Fig. 2.20. In the case of $C-C$ FGPM beams, thermal moments are handled by the edge supports while due to the pyroelectric effect, at the onset of thermal loading, beam experiences lateral deflection. The magnitude of this deflection in initial levels of loading, however, is very small. The load-deflection path of $C-C$ FGPM beams is unique and stable in the studied range. As seen in this figure, for each volume law index, there exist a unique temperature in which the deflection changes significantly with small amount of temperature increase. These points may be called the critical points, since they have high importance for design purposes.

The temperature-deflection path of $C-C$ FGPM beams for three values of slenderness ratio is given in Fig. 2.24, when beam is subjected to both external voltage and temperature rise loading. Due to the presence of both external voltage effect and pyroelectric effect in the Maxwell equation (denoted respectively by λ_V and λ_T), problem is not of the bifurcation-type buckling. However, in each load-deflection path there exist a critical temperature in which deflection changes significantly with a small amount of increase in temperature.

Boundary conditions effect the load-deflection path of the $S-S$, $C-S$, and $C-C$ FGPM beams and are shown in Fig. 2.25. Due to the inability of simply-supported edge in supplying the extra moment, the load-deflection paths of $S-S$ and $C-S$ are

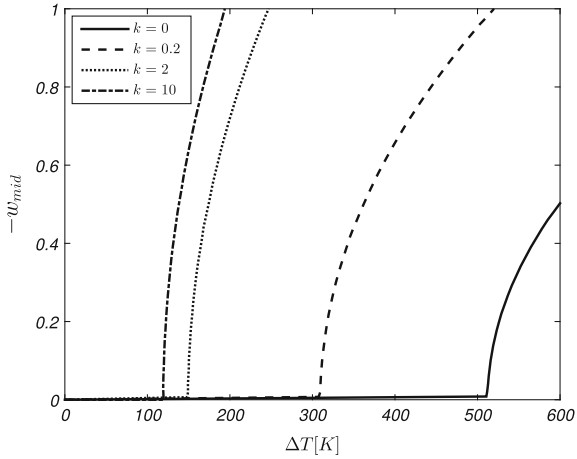

Fig. 2.23 Effect of the volume fraction index on the thermal post-buckling equilibrium paths of immovable $C - C$ FGPM beams ($V_0 = 0, L/h = 60$)

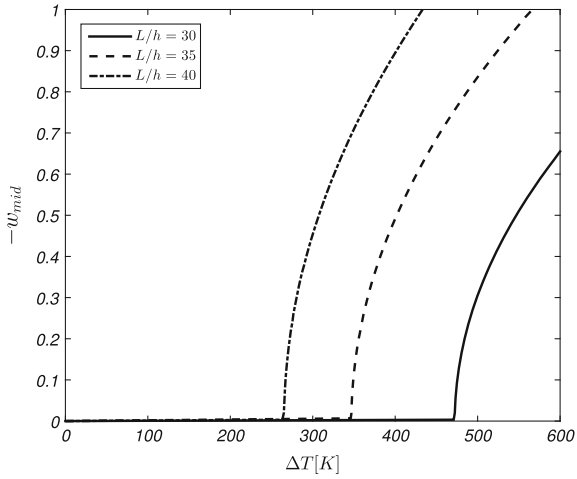

Fig. 2.24 Effect of slenderness ratio on the thermal post-buckling equilibrium paths of immovable $C - C$ FGPM beam ($V_0 = 100\,\mathrm{V}, k = 10$)

completely smooth, unique, and stable. For the $C - C$ case, however, critical point temperature is observed in load-deflection path. As expected, the $C - C$ is the most stiff case and $S - S$ is the least one.

The effect of external actuator voltage on load-deflection equilibrium path of the FGPM beams is revealed in Fig. 2.26. It is seen that applying the negative voltage to the actuator electrodes increases the critical point temperature. This feature is valid for the constituents of this study, since the induced in-plane force in the beam may be of the compressive or tensile type, depending on the signs of piezoelectric coefficients. The effect of applied external voltage is negligible in pre-critical state, while it is more pronounced in post-critical phase.

The curves of the fundamental frequency versus the applied temperature rise and the fundamental frequency versus the mid-point nonlinear deflection of the $S - S$

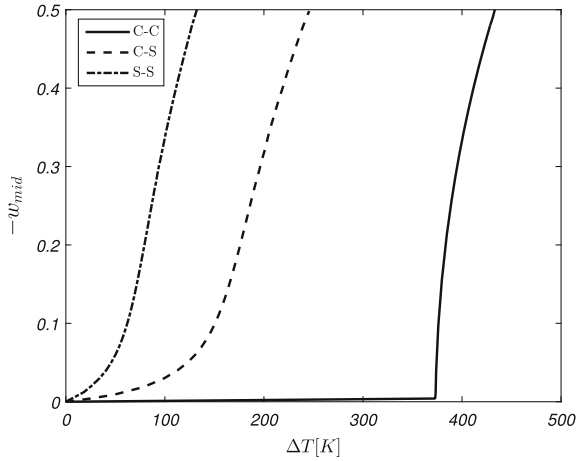

Fig. 2.25 A comparison on boundary conditions effect on thermal load-deflection path of a FGPM beam ($V_0 = 50\,\mathrm{V}$, $L/h = 35, k = 5$)

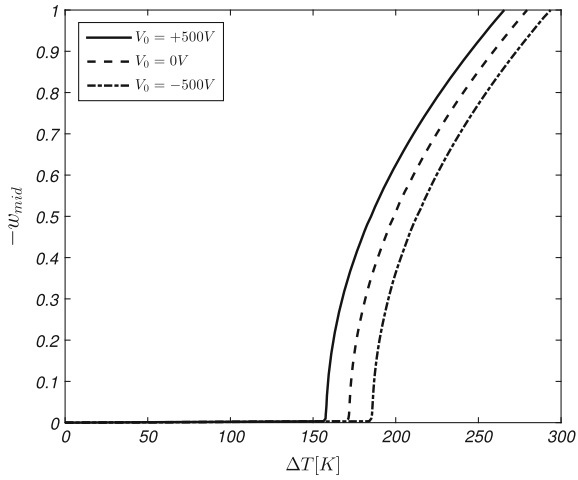

Fig. 2.26 The effect of the applied actuator voltage on the load-deflection path of a $C - C$ FGPM beam ($L/h = 50, k = 10$)

FGPM beams with ($L/h = 25$, $V_0 = 0\,\mathrm{V}$) in pre/post-buckling regimes, are depicted in Figs. 2.27 and 2.28, respectively, for different values of the volume fraction indices. As discussed previously, buckling temperature differences (bifurcation points) are distinguishable from the fundamental frequency-temperature curves. Since, for the structures of the present study the buckling phenomenon occurs in the first mode of instability, in the bifurcation temperature state the fundamental frequency of the beam has to be equal to zero. It is seen that, due to the non-symmetrical distribution of material properties across the thickness, the behavior of an FGPM beam under in-plane thermal loading is not of the bifurcation-type buckling, except for the case when the FGPM beam is reduced to a fully homogeneous one ($k = 0$) [70]. Apparently, volume fraction index of composition rule plays an important effect on the free

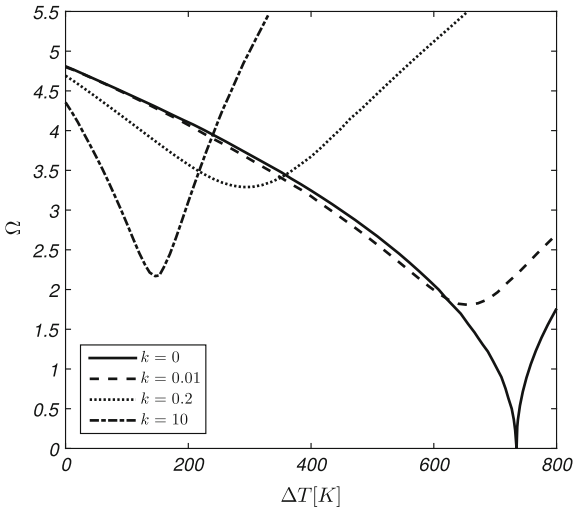

Fig. 2.27 Effect of the volume fraction index on the pre/post buckling fundamental frequency of immovable $S - S$ FGPM beams ($V_0 = 0, L/h = 25$)

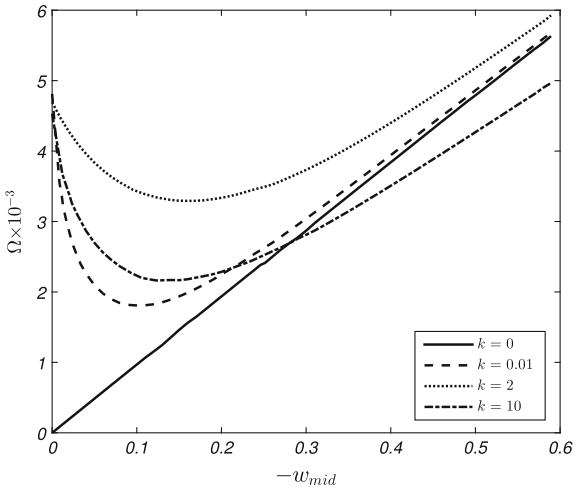

Fig. 2.28 The dimensionless fundamental frequency versus the mid-point dimensionless deflection of $S - S$ FGPM beam for different volume fraction indices ($V_0 = 0, L/h = 25$)

vibration behavior of the FGPM actuators. The associated load-deflection path for each case of positive power law index is unique and stable.

In Fig. 2.29 the temperature rise-fundamental frequency curves of the $C - C$ FGPM beams with $L/h = 60$, $V_0 = 0\,\mathrm{V}$ are plotted for various power law indices. Similar to the case of $S-S$ beams, when $k = 0$, that is the reduction of an FGPM beam to a fully homogeneous one, the problem is posed as a bifurcation-type buckling. For the case when distribution of properties is described with a non-zero volume law index, problem is not of the bifurcation-type buckling. However, the behavior of beam is totally different from those observed for the $S - S$ beams in Fig. 2.27. In the case of $C - C$ FGPM beams, thermal moments are handled by the edge

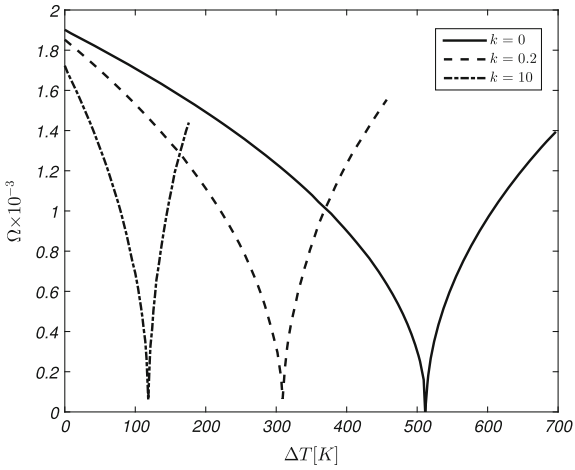

Fig. 2.29 Effect of the volume fraction index on the pre/post buckling fundamental frequency of immovable $C - C$ FGPM beams ($V_0 = 0, L/h = 60$)

supports, while due to the pyroelectric effect, at the onset of thermal loading beam experiences lateral deflection. The magnitude of this deflection in initial levels of loading, however, is so small but is not equal to zero. As seen in this figure, for each volume law index, there exist a unique temperature in which the magnitude of the fundamental frequency is very close to zero, and changes significantly with a small amount of temperature rise. These points may be called the critical points, since they have high importance for design purposes. However, the points can not be considered as the bifurcation points and the nonlinear behaviors of these structures are not of the primary-secondary equilibrium types.

2.9 Vibration of Thermally Post-buckled Beams on Elastic Foundation

2.9.1 Introduction

Thermal stability analysis of isotropic homogeneous beam-like structures and the vibration analysis in thermal field of beams with/without elastic foundation are conventional topics in structural mechanics. Li et al. [30] analyzed the buckling and postbuckling behavior of elastic rods subjected to thermal load. They achieved the results by solving the nonlinear equilibrium equations of the slender pinned-fixed Euler–Bernoulli beams via the shooting method. Li et al. [71] employed the shooting method for solving the equations related to buckling and postbuckling behavior of fixed-fixed elastic beam subjected to transversally non-uniform temperature loading. Li et al. [72] studied the natural frequency of slender Euler beams in thermal field with various boundary conditions. Thermal stability analysis of the Euler–Bernoulli

beams resting on a two-parameters nonlinear elastic foundation is studied by Song and Li [73] and Li and Batra [74]. In these studies ability of the Winkler foundation on mode alternation of buckling configuration of a pinned-fixed and pinned-pinned beams is examined. In all of the above-mentioned works, material properties are considered to be independent of temperature.

Stability analysis of the FGM beams that are in contact with an elastic foundation are limited in number. Sahraee and Saidi [75] applied the differential quadrature method and then analyzed the buckling and vibration of a deep FGM beam-columns resting on a Pasternak-type elastic foundation. Most recently, Fallah and Aghdam [76, 77] studied the nonlinear vibration and postbuckling behavior of functionally graded material beams resting on a nonlinear elastic foundation subjected to axial thermal [76] or mechanical [77] forces. Single mode Galerkin-based method is adopted to deduce the critical buckling and post-critical state of the beams. In this analysis, properties are assumed to be temperature independent and the response of the structure is confined to its first mode. However, as reported by Hetenyi [78], the Winkler elastic foundation largely affects the buckled shape of the beam, and therefore confining the buckled-shape of an in-contact beam similar to its contact-less shape causes the overestimation of both critical buckling temperature and post-buckling shape.

The problem of small amplitude vibration of beams under in-plane thermal or mechanical loadings is investigated employing various solution methods. Finite element formulation of Komijani et al. [62], shooting method solution of Li et al. [22], variational iteration method (VIM) solution of Fallah and Aghdam [77], single-term Galerkin solution of Wang et al. [33], differential quadrature solution of Pradhan and Murmu [46], and the analytical solution of Emam and Nayfeh [79] are some of the methods used to solve the resulting governing equations.

In this section, buckling, thermal post-buckling, and small amplitude free vibration of the FGM beams in thermal field are investigated [80]. The beam is analyzed under two types of thermal loads namely; uniform temperature rise and heat conduction across the thickness. Various combinations of clamped, simply-supported, and roller (sliding support) are considered as the edge supports of the structure. Properties of the graded medium are distributed across the thickness based on the power law model, where for each constituent they are functions of temperature. The general differential quadrature (GDQ) method is adopted to discretize the equation. The effects of various involved parameters are examined on the response of the structure.

2.9.2 Governing Equations

Consider a beam made of ceramic-metal FGMs with rectangular cross section $b \times h$ and length L resting on a hardening three-parameters nonlinear elastic foundation, as shown in Fig. 2.30 [80]

Thermo-mechanical properties are graded across the thickness based on the power law form Eq. (2.2.7). Effective thermo-mechanical properties of the beam are

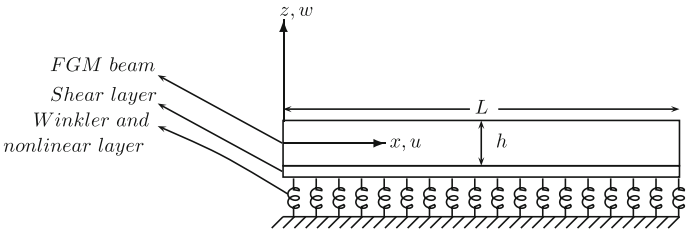

Fig. 2.30 Coordinate system and geometry of an FGM beam resting on a three-parameters elastic foundation

considered to follow the Voigt rule of mixture given by Eq. (2.2.8), except Poisson's ratio ν, that is assumed to be constant across the thickness since it varies in a small range.

The analysis in this section is based on the Timoshneko beam theory assumption. Therefore, basic equations are the same with those used in the second section through Eqs. (2.2.1)–(2.2.10).

The equations of motion of FGM beams may be derived by applying the principle of virtual displacements

$$\int_0^T \left(\delta U_s + \delta U_f - \delta T\right) dt = 0 \tag{2.9.1}$$

where the total virtual strain energy of the beam δU_s can be written as

$$\delta U_s = \int_0^L \int_{-\frac{h}{2}}^{\frac{h}{2}} \int_0^b \left(\sigma_{xx}\delta\varepsilon_{xx} + K_s\sigma_{xz}\delta\gamma_{xz}\right) dydzdx \tag{2.9.2}$$

The virtual strain energy of the nonlinear elastic foundation δU_f is expressed as

$$\delta U_f = \int_0^L \int_0^b \left(K_w w_0 \delta w_0 + K_g \frac{\partial w_0}{\partial x}\delta\left(\frac{\partial w_0}{\partial x}\right) + K_{NL}{w_0}^3\delta w_0\right) dydx \tag{2.9.3}$$

In which, the linear Winkler stiffness, the shear layer stiffness, and the nonlinear Winkler stiffness are indicated as K_w, K_g, and K_{NL}, respectively. Also, the kinetic energy δT is given by

$$\delta T = \int_0^L \int_0^b \left(I_1 \frac{\partial u_0}{\partial t}\frac{\partial \delta u_0}{\partial t} + I_2 \frac{\partial \varphi}{\partial t}\frac{\partial \delta u_0}{\partial t} + I_2 \frac{\partial u_0}{\partial t}\frac{\partial \delta \varphi}{\partial t} + I_3 \frac{\partial \varphi}{\partial t}\frac{\partial \delta \varphi}{\partial t}\right.$$

$$\left. + I_1 \frac{\partial w_0}{\partial t}\frac{\partial \delta w_0}{\partial t}\right) dydx \tag{2.9.4}$$

where I_1, I_2, and I_3 are constants to be derived by utilizing Eq. (2.2.8) as

$$I_1 = \int_{-\frac{h}{2}}^{\frac{h}{2}} \rho(z)dz = h\left(\rho_m + \frac{\rho_{cm}}{k+1}\right)$$
$$I_2 = \int_{-\frac{h}{2}}^{\frac{h}{2}} z\rho(z)dz = h^2\rho_{cm}\left(\frac{1}{k+1} - \frac{1}{2k+2}\right)$$
$$I_3 = \int_{-\frac{h}{2}}^{\frac{h}{2}} z^2\rho(z)dz = h^3\left(\frac{1}{12}\rho_m + \rho_{cm}\left(\frac{1}{k+1} - \frac{1}{k+2} + \frac{1}{4k+4}\right)\right) \quad (2.9.5)$$

The equations of motion of an in-contact FGM Timoshenko beam are obtained according to the virtual work principle [35]. Integrating Eq. (2.9.1) by part, with the consideration of Eqs. (2.7.4) and (2.7.5), results in the following equations of motion [80]

$$\delta u_0 : \frac{\partial N_x}{\partial x} = I_1\frac{\partial^2 u_0}{\partial t^2} + I_2\frac{\partial^2 \varphi}{\partial t^2}$$
$$\delta w_0 : \frac{\partial Q_{xz}}{\partial x} + \frac{\partial}{\partial x}\left(N_x\frac{\partial w_0}{\partial x}\right) - K_w w_0 + K_g\frac{\partial^2 w_0}{\partial x^2} - K_{NL}{w_0}^3 = I_1\frac{\partial^2 w_0}{\partial t^2}$$
$$\delta\varphi : Q_{xz} - \frac{\partial M_x}{\partial x} = I_2\frac{\partial^2 u_0}{\partial t^2} + I_3\frac{\partial^2 \varphi}{\partial t^2} \quad (2.9.6)$$

Due to the integration process, the natural and essential boundary conditions are obtained as

$$\begin{aligned} N_x &= 0 \text{ or } u_0 = \text{known} \\ Q_{xz} + (K_g + N_x)\frac{\partial w_0}{\partial x} &= 0 \text{ or } w_0 = \text{known} \\ M_x &= 0 \text{ or } \varphi = \text{known} \end{aligned} \quad (2.9.7)$$

For generalizing the subsequent results, the following non-dimensional variables are introduced and are used in the text

$$\xi = \frac{x}{L},\quad U^* = \frac{u}{L},\quad \delta = \frac{h}{L},\quad W^* = \frac{w}{h},\quad \kappa = \frac{K_s}{2(1+\nu)}$$

$$e_1 = \frac{E_1}{E_c^{ref}h},\quad e_2 = \frac{E_2}{E_c^{ref}h^2},\quad e_3 = \frac{E_3}{E_c^{ref}h^3}$$

$$K_w^* = \frac{K_w L^4}{E_c^{ref}I_0},\quad K_g^* = \frac{K_g L^2}{E_c^{ref}I_0},\quad K_{NL}^* = \frac{K_{NL}h^2L^4}{E_c^{ref}I_0}$$

$$N_x^* = \frac{NL^2}{E_c^{ref}I_0},\quad Q_{xz}^* = \frac{Q_{xz}L^2}{E_c^{ref}I_0},\quad M_x^* = \frac{M^T L}{E_c^{ref}I_0},\quad N^{T*} = \frac{N^T L^2}{E_c^{ref}I_0},\quad M^{T*} = \frac{M^T L}{E_c^{ref}I_0}$$

$$\omega^* = \omega h\sqrt{\frac{\rho_c^{ref}}{E_c^{ref}}},\quad \eta = \frac{t}{h}\sqrt{\frac{E_c^{ref}}{\rho_c^{ref}}},\quad \Lambda_1 = \frac{I_1}{h\rho_c^{ref}},\quad \Lambda_2 = \frac{I_2}{h^2\rho_c^{ref}},\quad \Lambda_3 = \frac{I_3}{h^3\rho_c^{ref}} \tag{2.9.8}$$

where I_0 is the moment of inertia of the cross section and E_c^{ref} and ρ_c^{ref} are the elasticity modulus and density of the ceramic constituent at reference temperature. Substitution of the above non-dimensional parameters into Eq. (2.7.7) and utilizing Eq. (2.7.4) give the governing equations of the beam in dimensionless forms as [80]

$$e_1\frac{\partial^2 U^*}{\partial\xi^2} + e_1\delta^2\,\frac{\partial W^*}{\partial\xi}\frac{\partial^2 W^*}{\partial\xi^2} + \delta\, e_2\,\frac{\partial^2\varphi}{\partial\xi^2} = \frac{\Lambda_1}{\delta^2}\frac{\partial^2 U^*}{\partial\eta^2} + \frac{\Lambda_2}{\delta}\frac{\partial^2\varphi}{\partial\eta^2}$$

$$\kappa e_1\left(\frac{\partial\varphi}{\partial\xi} + \delta\,\frac{\partial^2 W^*}{\partial\xi^2}\right) + \left[e_1\left(\frac{\partial U^*}{\partial\xi} + \frac{1}{2}\delta^2\left(\frac{\partial W^*}{\partial\xi}\right)^2\right) + \delta e_2\,\frac{\partial\varphi}{\partial\xi} - \frac{N^{T*}}{12}\delta^2\right]\delta\frac{\partial^2 W^*}{\partial\xi^2}$$
$$+\left[e_1\left(\frac{\partial^2 U^*}{\partial\xi^2} + \delta^2\frac{\partial W^*}{\partial\xi}\frac{\partial^2 W^*}{\partial\xi^2}\right) + e_2\delta\frac{\partial^2\varphi}{\partial\xi^2}\right]\delta\frac{\partial W^*}{\partial\xi}$$
$$-\frac{1}{12}K_w^*\,\delta^3 W^* + \frac{1}{12}K_g^*\,\delta^3\frac{\partial^2 W^*}{\partial\xi^2} - \frac{1}{12}\delta^3 K_{NL}^* W^{*3} = \frac{\Lambda_1}{\delta}\frac{\partial^2 W^*}{\partial\eta^2}$$

$$\kappa e_1\left(\varphi + \delta\frac{\partial W^*}{\partial\xi}\right) - e_2\left(\delta\,\frac{\partial^2 U^*}{\partial\xi^2} + \delta^3\frac{\partial W^*}{\partial\xi}\frac{\partial^2 W^*}{\partial\xi^2}\right) - \delta^2 e_3\frac{\partial^2\varphi}{\partial\xi^2} = \frac{\Lambda_2}{\delta}\frac{\partial^2 U^*}{\partial\eta^2} + \Lambda_3\frac{\partial^2\varphi}{\partial\eta^2} \tag{2.9.9}$$

Five possible types of boundary conditions as the combinations of the clamped, roller, and simply supported edges are considered. Mathematical expressions for these classes of edge supports are

$$\begin{aligned}\text{Clamped (C)} &: U^* = W^* = \varphi = 0\\ \text{Simply supported (S)} &: U^* = W^* = M_x^* = 0\\ \text{Roller (R)} &: U^* = \varphi = Q_{xz}^* + (K_g^* + N_x^*)\delta\frac{dW^*}{d\xi} = 0\end{aligned} \tag{2.9.10}$$

where

$$\begin{aligned}N_x^* &= \frac{12}{\delta^2}e_1\left(\frac{dU^*}{d\xi} + \frac{1}{2}\delta^2\left(\frac{dW^*}{d\xi}\right)^2\right) + \frac{12}{\delta}e_2\frac{d\varphi}{d\xi} - N^{T*}\\ M_x^* &= \frac{12}{\delta}e_2\left(\frac{dU^*}{d\xi} + \frac{1}{2}\delta^2\left(\frac{dW^*}{d\xi}\right)^2\right) + 12e_3\frac{d\varphi}{d\xi} - M^{T*}\\ Q_{xz}^* &= \frac{12}{\delta^2}\kappa e_1\left(\varphi + \delta\frac{dW^*}{d\xi}\right)\end{aligned} \tag{2.9.11}$$

Solution Procedures

The solution of equations of motion (2.9.9) is divided into two regimes. Part of the time-independent solution related to thermal post-buckling analysis with large magnitude and part of dynamic solution for free vibration with small magnitude that is time-dependent. Thus, the total solutions of Eq. (2.9.9) are [80]

$$\begin{aligned} U^*(\xi,\eta) &= U_s^*(\xi) + U_d^*(\xi,\eta) \\ W^*(\xi,\eta) &= W_s^*(\xi) + W_d^*(\xi,\eta) \\ \varphi(\xi,\eta) &= \varphi_s(\xi) + \varphi_d(\xi,\eta) \end{aligned} \tag{2.9.12}$$

Substituting Eq. (2.9.12) into (2.9.9) and collecting the static parts result in the following time-independent equations which describe the nonlinear stability behavior of a beam under in-plane thermal load

$$e_1 \frac{d^2U_s^*}{d\xi^2} + e_1\delta^2 \frac{dW_s^*}{d\xi}\frac{d^2W_s^*}{d\xi^2} + \delta\, e_2 \frac{d^2\varphi_s}{d\xi^2} = 0$$

$$\kappa e_1\left(\frac{d\varphi_s}{d\xi} + \delta \frac{d^2W_s^*}{d\xi^2}\right) + \left[e_1\left(\frac{dU_s^*}{d\xi} + \frac{1}{2}\delta^2\left(\frac{dW_s^*}{d\xi}\right)^2\right) + \delta e_2 \frac{d\varphi_s}{d\xi} - \frac{N^{T*}}{12}\delta^2\right]\delta\frac{d^2W_s^*}{d\xi^2}$$

$$-\frac{1}{12}K_w^*\,\delta^3 W_s^* + \frac{1}{12}K_g^*\,\delta^3\frac{d^2W_s^*}{d\xi^2} - \frac{1}{12}\delta^3 K_{NL}^* W_s^{*3} = 0$$

$$\kappa e_1\left(\varphi_s + \delta\frac{dW_s^*}{d\xi}\right) - e_2\left(\delta\,\frac{d^2U_s^*}{d\xi^2} + \delta^3\frac{dW_s^*}{d\xi}\frac{d^2W_s^*}{d\xi^2}\right) - \delta^2 e_3\frac{d^2\varphi_s}{d\xi^2} = 0 \tag{2.9.13}$$

and linearizing the remaining part about the static equilibrium position with a small amplitude dynamic response reaches us to

$$e_1\frac{\partial^2U_d^*}{\partial\xi^2} + e_1\delta^2\,\frac{\partial W_d^*}{\partial\xi}\frac{\partial^2W_s^*}{\partial\xi^2} + e_1\delta^2\,\frac{\partial W_s^*}{\partial\xi}\frac{\partial^2W_d^*}{\partial\xi^2} + \delta\, e_2\,\frac{\partial^2\varphi_d}{\partial\xi^2} = \frac{\Lambda_1}{\delta^2}\frac{\partial^2U_d^*}{\partial\eta^2} + \frac{\Lambda_2}{\delta}\frac{\partial^2\varphi_d}{\partial\eta^2}$$

$$\kappa e_1\left(\frac{\partial\varphi_d}{\partial\xi} + \delta\,\frac{\partial^2W_d^*}{\partial\xi^2}\right) + \left[e_1\left(\frac{\partial U_s^*}{\partial\xi} + \frac{1}{2}\delta^2\left(\frac{\partial W_s^*}{\partial\xi}\right)^2\right) + \delta e_2\,\frac{\partial\varphi_s}{\partial\xi} - \frac{N^{T*}}{12}\delta^2\right]\delta\frac{\partial^2W_d^*}{\partial\xi^2}$$
$$+\left[e_1\left(\frac{\partial U_d^*}{\partial\xi} + \delta^2\frac{\partial W_s^*}{\partial\xi}\frac{\partial W_d^*}{\partial\xi}\right) + e_2\delta\frac{\partial\varphi_d}{\partial\xi}\right]\delta\frac{\partial^2W_s^*}{\partial\xi^2} + \left[e_1\left(\frac{\partial^2U_d^*}{\partial\xi^2} + \delta^2\frac{\partial^2W_s^*}{\partial\xi^2}\frac{\partial W_d^*}{\partial\xi}\right.\right.$$
$$\left.\left.+\delta^2\frac{\partial W_s^*}{\partial\xi}\frac{\partial^2W_d^*}{\partial\xi^2}\right) + e_2\delta\frac{\partial^2\varphi_d}{\partial\xi^2}\right]\delta\frac{\partial W_s^*}{\partial\xi} + \left[e_1\frac{\partial^2U_s^*}{\partial\xi^2} + e_1\delta^2\frac{\partial W_s^*}{\partial\xi}\frac{\partial^2W_s^*}{\partial\xi^2} + e_2\delta\frac{\partial^2\varphi_s}{\partial\xi^2}\right]\delta\frac{\partial W_d^*}{\partial\xi}$$
$$-\frac{1}{12}K_w^*\,\delta^3 W_d^* + \frac{1}{12}K_g^*\,\delta^3\frac{\partial^2W_d^*}{\partial\xi^2} - \frac{1}{4}\delta^3 K_{NL}^* W_s^{*2} W_d^* = \frac{\Lambda_1}{\delta}\frac{\partial^2W^*}{\partial\eta^2}$$

$$\kappa e_1\left(\varphi_d+\delta\frac{\partial W_d^*}{\partial\xi}\right)-e_2\left(\delta\,\frac{\partial^2U_d^*}{\partial\xi^2}+\delta^3\frac{\partial W_d^*}{\partial\xi}\frac{\partial^2W_s^*}{\partial\xi^2}+\delta^3\frac{\partial W_s^*}{\partial\xi}\frac{\partial^2W_d^*}{\partial\xi^2}\right)-\delta^2e_3\frac{\partial^2\varphi_d}{\partial\xi^2}$$
$$=\frac{\Lambda_2}{\delta}\frac{\partial^2U_d^*}{\partial\eta^2}+\Lambda_3\frac{\partial^2\varphi_d}{\partial\eta^2} \tag{2.9.14}$$

The analytical solution of Eq. (2.9.13) is complicated, due to the strong nonlinearity and the included couplings in the partial differential equations. Therefore, to seek for a numerical solution to the problem, the GDQ method is employed. The ability of GDQ method to handle the nonlinear stability problems is exhibited by many authors [81]. A brief overview of the GDQ method is presented in Appendix A.

Utilizing the GDQ discretization to the dimensionless governing Eq. (2.9.13), one may reach to discretized form of the equations governing the pre/post-buckling equilibrium path of the beam. Equations and the associated boundary conditions are given in Appendix B.

The system of algebraic equations and associated boundary conditions presented in Appendix B may be written in the form

$$[K_s]_{3N\times3N}\,\{X_s\}_{3N\times1}=\{F\}_{3N\times1} \tag{2.9.15}$$

where $[K_s]_{3N\times3N}$ is the nonlinear stiffness matrix which depends on both unknown variable vector $\{X_s\}_{3N\times1}$ and temperature. It must be noted that the right hand side of Eq. (2.9.15) may be different for each set of boundary conditions. The force matrix $\{F\}_{3N\times1}$ is obtained through the thermally induced stress resultants and bending moments for the simply supported boundary conditions at the ends of the beam ($\xi=0,1$) and vanishes when the beam is clamped or roller at the ends (see the definition of thermal moment in Eq. 2.9.11). Thermal buckling, without consideration of the magnitude of the temperature difference, occurs only when $\{F\}_{3N\times1}=0$. Otherwise, lateral deflection occurs when $\{F\}_{3N\times1}\neq0$. The numerical algorithm to solve the postbuckling behavior in each case is given by Liew et al. [82]. The solution method of this section is the same with the process used by Komijani et al. [62]

When the solution of static phase is accomplished, small free vibration analysis is followed. The discrete form of the governing equations along with the associated boundary conditions are given in Appendix C. The presented equations are linear with respect to the dynamic variables denoted by a subscript d. Solution of this system is obtained as an eigenvalue problem. The eigenvalues of the established system of equations present the non-dimensional frequency of the beam defined as ω^*.

2.9.3 *Types of Thermal Loading*

Two distinct types of thermal loadings are considered for the beam. Uniform temperature rise (UTR) and nonlinear temperature across the thickness ($NLTD$). Details may be found in Sect. 2.6.

2.9.4 Results and Discussion

As stated earlier, for the FGM beams when thermal force or thermal moment resultants are absent in the force vector, problem may be posed as a bifurcation-type buckling. Conditions for an FGM beam to remain flat under in-plane thermal loadings with general boundary conditions are studied by Kiani et al. [23, 24] for various beam theories. Apparently, for isotropic homogeneous beams that are subjected to the UTR loading, bifurcation-type of instability occurs. In this section, an FGM beam made of $SUS304/Si_3N_4$ is considered. Properties of these constituents are highly temperature dependent based on the well-known Touloukian model. The dependency is demonstrated in Eq. (2.5.22). Desired constants for $SUS304$ and Si_3N_4 are given in Table 2.3.

In Table 2.8 the effects of temperature dependency, the Pasternak foundation, and the edge supports are examined on ΔT_{cr} [80]. As one may obtain from this Table, for beams without any foundation contact conditions, the critical buckling temperature of the $C-R$ and $S-S$ cases of edge supports are the same. Besides, in this case the TD condition under-estimates the critical buckling temperatures. As expected, the $S-R$ case of edge supports has the lowest buckling temperature and the $C-C$ has the highest. For beams that are in-contact with the Winkler elastic foundation $K_w^* = 100$, the $S-R$ presents a stiffer configuration compared to the $S-S$ boundary condition. It should be mentioned that, however, the critical buckling temperature differences of contact-less $C-R$ and $S-S$ beams are the same. In the case of in-contact beams, the $C-R$ exhibits a stiffer configuration compared to the $S-S$ beam. Furthermore, the ability of elastic foundation in postponing the bifurcation point of the structure is significant. For the foundations that are stiff enough, this ability may be accompanied with the increase of critical points. For instance, as indicated in Table 2.8, for the $C-C$ and $S-S$ beams that are resting on a stiff foundation, the critical buckling temperature difference is associated with an antisymmetric mode shape. The presented results for the Winkler and Pasternak foundations with $K_w^* = 500$ show that the TID case can not predict the correct buckling mode-shape of the beam. In this case, the buckling mode shape is predicted to be symmetric. The real state of the beam with TD properties predicts the antisymmetrical buckling state for the above-mentioned case.

In Tables 2.9 and 2.10 the critical buckling temperature differences of an FGM beam with two types of boundary conditions are examined. Beam is subjected to the UTR loading. As one may conclude, the $C-C$ type of boundary condition is stiffer than the $C-R$ type. Besides, for both types of edge supports, TD case reveals the more precise approximation of ΔT_{cr}, where in TID case the critical buckling temperature is over-estimated. The effect of temperature dependency is more pronounced when beam is in contact with stiffer foundations. Furthermore, a comparison between the results of two isotropic homogeneous cases, i.e. $k = 0$ and $k = \infty$, show that Si_3N_4 is more sensitive to temperature than the $SUS304$. Therefore, as the power law index increases, since the properties of FG media tends to a metallic beam, temperature dependency is less pronounced. Since each constant of elastic foundation

Table 2.8 $\Delta T_{cr}[K]$ for various boundary conditions of isotropic homogeneous ($SUS304$) Timoshenko beam with various parameters of elastic foundation subjected to UTR loading. The value of $\delta = 0.04$ is considered. Antisymmetrical buckled shapes are indicated with a superscript $*$ [80]

(K_w^*, K_g^*)		$C-C$	$C-R$	$S-S$	$S-R$	$C-S$
(0, 0)	TID	337.94	85.53	85.53	21.45	174.08
	TD	285.06	81.24	81.24	21.16	157.86
(100, 0)	TID	438.78	326.88	222.94	252.24	282.31
	TD	364.85	282.23	201.81	223.04	248.64
(100, 10)	TID	573.76	461.86	357.27	387.22	417.29
	TD	477.64	394.13	318.22	335.39	362.17
(200, 0)	TID	535.73	396.19	359.05	313.02	381.19
	TD	443.58	335.43	319.78	273.45	329.65
(200, 10)	TID	670.71	531.16	494.02	448.00	516.16
	TD	567.98	448.69	443.99	387.45	447.06
(500, 0)	TID	795.40	551.42	508.89*	495.37	580.88
	TD	621.54*	461.95	422.32*	429.60	478.15
(500, 10)	TID	930.37	686.40	643.86*	630.34	715.86
	TD	775.18*	593.91	543.52*	566.97	606.16

Table 2.9 $\Delta T_{cr}[K]$ for the $C-C$ FGM beams with $\delta = 0.04$, various power law indices and contact conditions subjected to UTR loading [80]

(K_w^*, K_g^*)		$k=0$	$k=0.5$	$k=1$	$k=2$	$k=5$	$k=10$	$k=\infty$
(0,0)	TID	692.70	509.89	458.68	423.53	394.39	376.14	337.94
	TD	508.17	399.50	367.32	345.15	326.40	313.58	285.06
(100,0)	TID	826.81	624.38	568.06	529.27	497.44	478.15	438.78
	TD	591.31	479.15	446.67	424.90	407.01	394.33	364.85
(100,10)	TID	1005.19	776.93	713.92	670.38	635.05	614.47	573.76
	TD	697.44	583.99	553.00	534.18	520.57	509.06	477.64
(200,0)	TID	957.82	735.73	674.21	631.71	597.07	576.63	535.73
	TD	669.32	555.15	523.17	502.87	487.22	474.94	443.58
(200,10)	TID	1136.20	888.27	820.07	772.82	734.68	712.96	670.71
	TD	772.44	660.03	631.69	617.62	611.54	602.65	507.98
(500,0)	TID	1328.21	1046.23	968.21	913.72	869.56	844.49	795.40
	TD	876.05	761.49	735.14	714.52	704.51	687.29	621.54
(500,10)	TID	1506.60	1198.78	1114.07	1054.83	1007.17	980.82	930.37
	TD	974.27	872.05	841.42	833.94	870.60	901.92	775.19

cause the elastic stiffness of the structure to be increased, an increase in the Winkler or shear constant of elastic foundation postpones the branching point of the beam.

In Tables 2.11 and 2.12 the critical buckling temperature differences of $C-C$ and $C-R$ types of boundary conditions are examined for various power law indices

Table 2.10 $\Delta T_{cr}[K]$ for $C-R$ FGM beams with various power law indices and contact conditions subjected to UTR loading [80]. The value of $\delta = 0.04$ is considered

(K_w^*, K_g^*)		$k=0$	$k=0.5$	$k=1$	$k=2$	$k=5$	$k=10$	$k=\infty$
(0, 0)	TID	175.32	129.02	116.07	107.21	99.88	95.26	85.53
	TD	157.58	119.30	108.19	100.46	93.98	89.88	81.24
(100, 0)	TID	578.09	449.94	413.32	387.57	366.28	353.46	326.88
	TD	450.88	369.07	344.52	327.27	312.78	303.29	282.24
(100, 10)	TID	756.47	602.49	559.18	528.68	503.90	489.79	461.86
	TD	567.21	480.33	455.38	438.77	425.63	416.40	394.13
(200, 0)	TID	719.12	551.24	504.21	471.60	444.85	428.82	396.19
	TD	533.87	435.78	407.10	387.53	371.37	360.36	335.43
(200, 10)	TID	897.50	703.79	650.07	612.71	582.47	565.15	531.16
	TD	644.08	543.46	515.65	498.19	485.17	475.05	448.69
(500, 0)	TID	948.27	738.35	680.33	640.10	607.49	588.64	551.42
	TD	669.57	562.99	533.66	515.48	502.04	491.13	461.95
(500, 10)	TID	1126.66	890.90	826.19	781.21	745.10	724.97	686.40
	TD	773.52	669.65	644.77	634.15	632.72	626.56	593.91

and contact conditions. Beam is assumed to be under the $NLTD$ case of thermal loading. To account for the temperature dependency of the constituents, the algorithm utilized by Shen [83] is studied herein. The bottom surface of the beam is kept at a constant temperature, i.e. $T_m = 305K$. Similar to the results of Shen [83] for the case of a clamped shell under heat conduction, both TD and TID cases of ΔT_{cr} are the same for $k = \infty$. In the case of $NLTD$ type of thermal loading, temperature dependency is more pronounced for lower values of the power law index. Due to the resistance of elastic foundation against deflection of the beam, as each constant of elastic foundation increases bifurcation point of the beam increases too.

For the $C-C$ and $S-S$ types of FGM beams, load-deflection path of a contact-less FGM beam is depicted in Figs. 2.31 and 2.32 [80]. Apparently, the response of the $C-C$ beams is of the bifurcation-type buckling for an arbitrary value of the power law index. For the FG beam with $S-S$ edge supports, except for the case of reduction of an FGM beam to an isotropic homogeneous one, problem can not be considered as a primary-secondary equilibrium path. The response of a $C-C$ beam is of the bifurcation-type buckling since edges are capable of supplying the arbitrary amount of the extra moment prior to buckling. The response of $S-S$ isotropic homogeneous beam is of the same type, since thermal moment vanishes through the beam for the isotropic homogeneous structure. For the case of an FGM beam with finite positive value of power law index, problem is not of the bifurcation-type and within the studied range, the load-deflection path is unique and stable. As one may conclude, temperature dependency is more pronounced in the post-buckling regime. In the post-buckling regime, since the $SUS304$ is less sensitive to temperature compared to Si_3N_4, as temperature rises the $SUS304/Si_3N_4$ beam bends downward. This is due

Table 2.11 $\Delta T_{cr}[K]$ for the $C-C$ FGM beams with various power law indices and contact conditions subjected to $NLTD$ loading [80]. The value of $\delta = 0.025$ is considered

(K_w^*, K_g^*)		$k=0$	$k=0.5$	$k=1$	$k=2$	$k=5$	$k=10$	$k=\infty$
(0, 0)	TID	536.62	422.18	379.47	345.22	312.64	292.87	255.81
	TD	412.24	377.96	357.94	337.03	310.12	291.35	255.81
(100, 0)	TID	641.48	518.55	471.73	433.29	396.27	374.34	334.47
	TD	481.57	458.95	442.45	422.72	393.88	373.11	334.47
(100, 10)	TID	780.84	646.84	594.65	550.70	507.84	483.08	439.62
	TD	570.00	563.80	552.87	535.85	505.48	482.34	439.62
(200, 0)	TID	744.10	612.47	561.48	518.83	477.37	453.22	410.33
	TD	546.83	535.83	523.15	505.15	474.92	452.27	410.33
(200, 10)	TID	883.46	741.76	684.40	636.24	588.93	561.96	515.48
	TD	632.56	638.24	631.59	617.00	586.08	561.35	515.48
(500, 0)	TID	1035.65	875.96	811.70	756.04	700.96	669.63	615.48
	TD	720.31	740.38	738.75	727.08	695.18	667.78	615.48
(500, 10)	TID	1175.01	1004.25	934.61	873.45	812.53	778.37	720.63
	TD	800.49	836.95	841.74	834.57	803.96	775.62	720.63

Table 2.12 $\Delta T_{cr}[K]$ for the $C-R$ FGM beams with various power law indices and contact conditions subjected to $NLTD$ loading [80]. The value of $\delta = 0.025$ is considered

(K_w^*, K_g^*)		$k=0$	$k=0.5$	$k=1$	$k=2$	$k=5$	$k=10$	$k=\infty$
(0, 0)	TID	127.32	97.97	87.23	78.74	70.77	65.92	56.77
	TD	116.74	94.88	85.85	78.23	70.60	65.81	56.77
(100, 0)	TID	443.85	369.63	339.44	313.70	288.41	273.49	246.23
	TD	360.23	339.58	325.49	309.45	287.95	273.28	246.23
(100, 10)	TID	583.21	497.92	462.36	431.11	399.98	382.24	351.38
	TD	457.04	449.94	439.80	424.81	400.38	382.88	351.38
(200, 0)	TID	555.66	455.87	416.90	384.77	352.77	334.19	300.64
	TD	431.51	410.32	395.12	377.14	351.61	333.66	300.64
(200, 10)	TID	695.02	584.16	539.82	501.78	464.34	442.93	405.79
	TD	523.28	517.51	507.27	491.34	463.67	443.11	405.79
(500, 0)	TID	735.44	613.76	565.80	525.02	485.06	462.09	421.96
	TD	545.56	539.61	529.06	512.62	483.66	461.87	421.96
(500, 10)	TID	874.80	742.05	688.71	642.43	596.63	570.83	527.11
	TD	631.88	642.35	637.71	624.63	594.95	571.07	527.11

to the higher coefficient of thermal expansion near the top surface in $SUS304/Si_3N_4$ beam.

The influence of three-parameters elastic foundation on the $S-S$ and $C-C$ beams subjected to UTR type of thermal loading is depicted in Figs. 2.33 and 2.34, respectively. Only TD case of material properties is considered. Linearly graded

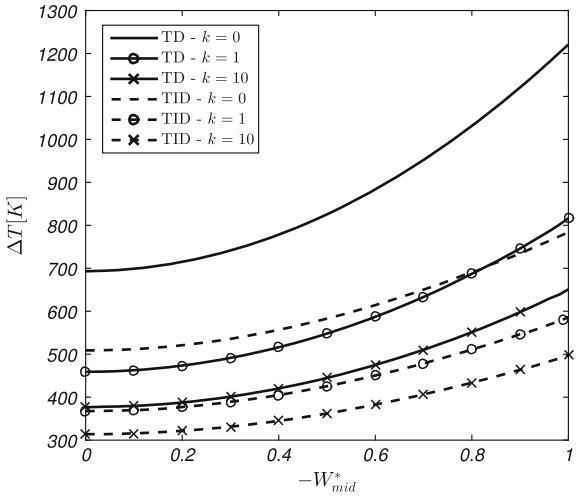

Fig. 2.31 Influences of the power law index and temperature dependency on load deflection path of contact-less $C - C$ FGM beams with $\delta = 0.04$ subjected to UTR loading

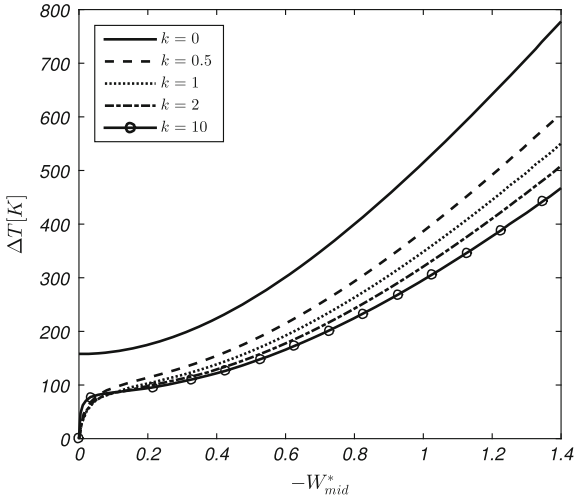

Fig. 2.32 Postbuckling equilibrium path of contact-less $S - S$ FGM beams with $\delta = 0.04$ subjected to UTR loading with various power law indices. Only TD case is addressed

properties of the constituents is assumed. The behavior of in-contact $C - C$ beams is of the bifurcation-type buckling. The nonlinear constant of elastic foundation has no effect on the critical buckling temperature difference, while it largely affects the post-buckling resistance of the beam. This effect is more pronounced in deep post-buckling regime. The Winkler and shear layer of the Pasternak elastic foundation deeply affect both critical buckling temperature and post-buckling equilibrium path of the beam. For the $S - S$ FGM beams, the load-deflection path is not of the bifurcation-type of instability. Apparently in this case beam initially starts to deflect laterally, since its material property is not symmetrical with respect to the mid-plane and edges can not supply the additional moment to retain the beam in its flat conditions. Each constant of

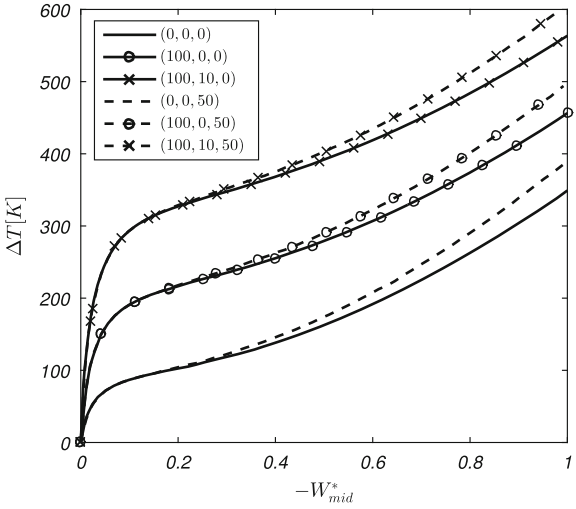

Fig. 2.33 Effect of three-parameters elastic foundation (K_g^*, K_w^*, K_{NL}^*) on load deflection path of a linearly graded $S-S$ FGM beams with $\delta = 0.04$ subjected to UTR loading

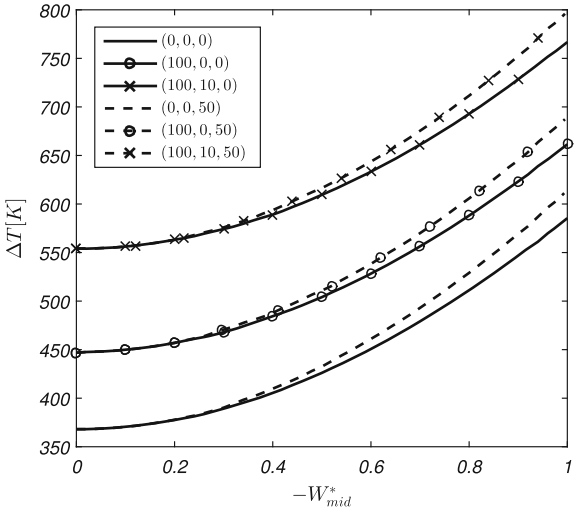

Fig. 2.34 Effect of three-parameters elastic foundation (K_g^*, K_w^*, K_{NL}^*) on load deflection path of a linearly graded $C-C$ FGM beams with $\delta = 0.04$ subjected to UTR loading

elastic foundation increases the elastic stiffness of the structure. Therefore in-contact beams has highly-raised post-buckling path when is compared with its contact-less state. Unlike the $C-C$ case, in the case of $S-S$ FGM beams the influence of nonlinear elastic foundation in load-deflection path initiates at the onset of thermal loading.

The end-shortening force of $C-C$ and $S-S$ FGM beams with various contact conditions is depicted in Figs. 2.35 and 2.36, respectively. Both TD and TID cases of material properties are addressed. As one may see, the bifurcation point for $C-C$ case of edge supports can be extracted from the force-temperature graph. Prior to stability loss, end-shortening force varies linearly with respect to temperature. This

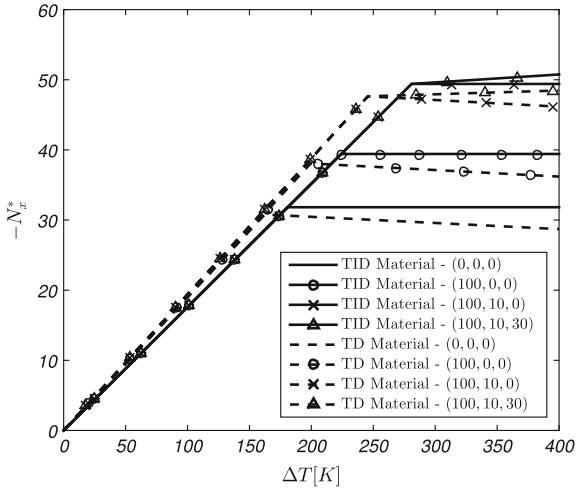

Fig. 2.35 Influences of three-parameters elastic foundation (K_w^*, K_g^*, K_{NL}^*) and temperature dependency on end-shortening force of a linearly graded $C - C$ FGM beam with $\delta = 0.025$ subjected to UTR loading

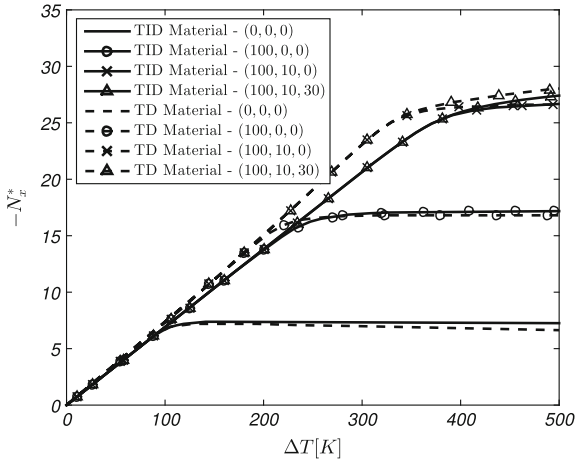

Fig. 2.36 Influences of three-parameters elastic foundation (K_w^*, K_g^*, K_{NL}^*) and temperature dependency on end-shortening force of a linearly graded $S - S$ FGM beam with $\delta = 0.04$ subjected to UTR loading

conclusion is also reported by Kiani et al. [24] based on the linear pre-buckling analysis. It is worth-mentioning that when properties are assumed to be TID, in post-buckling regime end-shortening force is constant and is equal to the buckling force. While in the TD case, as the real state of the structure, end-shortening force diminishes as a function of temperature in the thermal loading process. This is due to the fact that constituents are temperature dependent and as temperature rises, beam losses stiffness. For the case of $S - S$ edge supports, there is not a sharp change in force-temperature graph which accepts the uniqueness of a stable load-deflection path. From both of these figures, one may conclude that the stiffer the elastic foundation is, the more the axial end-shortening force is for a prescribed amount of temperature. Furthermore, since the load-deflection path of $C - C$ beams

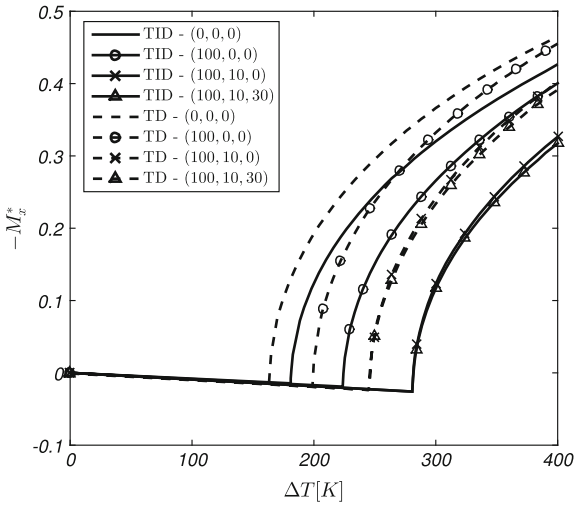

Fig. 2.37 Influences of three-parameters elastic foundation (K_w^*, K_g^*, K_{NL}^*) and temperature dependency on moment of a linearly graded $C-C$ FGM beam with $\delta = 0.025$ subjected to UTR loading

is of the bifurcation point, nonlinear constant of elastic foundation has no effect on pre-buckling axial end-shortening force.

The magnitude of moment at mid-point of the FGM beam is depicted for both $S-S$ and $C-C$ edge supports, when temperature distribution of the beam is raised uniformly through the beam. In Fig. 2.37, the bifurcation points are observed through the moment-temperature response of the $C-C$ beam. Prior to buckling, moment varies linearly with respect to temperature. This is formerly reported by Kiani et al. [24] based on the linear pre-buckling analysis of beams. In the post-buckling regime, however, moment changes significantly and alters nonlinearly with respect to temperature. Similar to the end-shortening force, nonlinear constant of elastic foundation has no influence on prebuckling moment at mid-point. For the $S-S$ beams, as seen in Fig. 2.38, however, there is no bifurcation point through the moment-temperature path of the beam. In both $C-C$ and $S-S$ cases, the effect of temperature dependency is more pronounced for stiffer elastic foundations.

The effect of elastic foundation on buckling and post-buckling resistance of both $C-C$ and $S-S$ beams is studied in Figs. 2.39 and 2.40, respectively. The $NLTD$ case of thermal loading is considered. Metal rich surface of the beam is kept at $T_m = 305\,\mathrm{K}$. Only TD case of material properties is addressed. The behavior of a simply-supported beam, even for the case of a homogeneous isotropic one, is not of the bifurcation-type buckling. It should be emphasized that, even for the case of fully isotropic homogeneous beams, the $S-S$ beams start gain lateral deflection at the onset of loading. This is due to the inability of edges to retain the beam flat at initial steps of thermal loading. Similar to the UTR loading, for the $NLTD$ case of temperature loading nonlinear constant of elastic foundation has no influence on critical-buckling temperature. Post-buckling resistance of the beam, however, is highly affected by this constant.

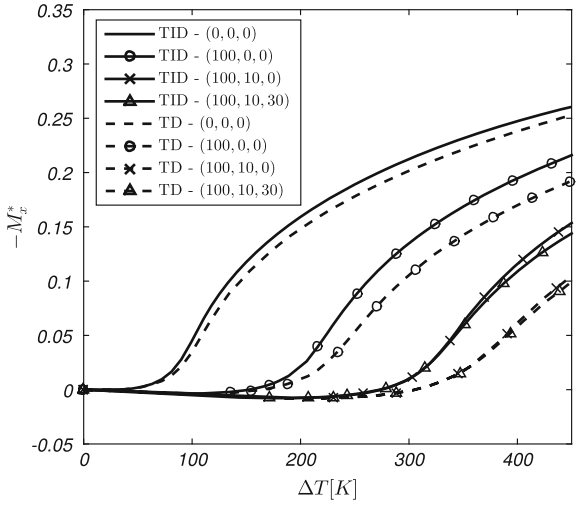

Fig. 2.38 Influences of three-parameters elastic foundation (K_w^*, K_g^*, K_{NL}^*) and temperature dependency on moment of a linearly graded $S-S$ FGM beam with $\delta = 0.04$ subjected to UTR loading

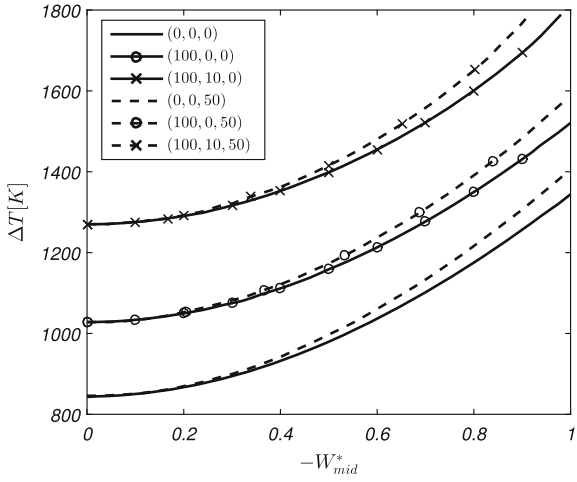

Fig. 2.39 Effect of three-parameters elastic foundation (K_g^*, K_w^*, K_{NL}^*) on load deflection path of a linearly graded $C-C$ FGM beams with $\delta = 0.04$ subjected to the $NLTD$ loading

As a benchmark study, the first three frequencies of the FGM beams with various boundary conditions are presented in Tables 2.13, 2.14, 2.15, 2.16 and 2.17. It is seen that for the constituents of this study, as the power law index increases, the natural frequency of the system decreases. For each case of edge supports, an increase in the Winkler or Pasternak constants of elastic foundation results in higher natural frequency. This is due to the higher elastic stiffness of the beam when is in-contact with foundation. As expected, for a prescribed contact condition and power law index, the $C-C$ beam has the highest natural frequency and $S-R$ has the least one.

For a contact-less beam, the fundamental frequency parameter as a function of temperature rise is depicted in Figs. 2.41 and 2.42 for the $S-S$ and $C-C$ cases of

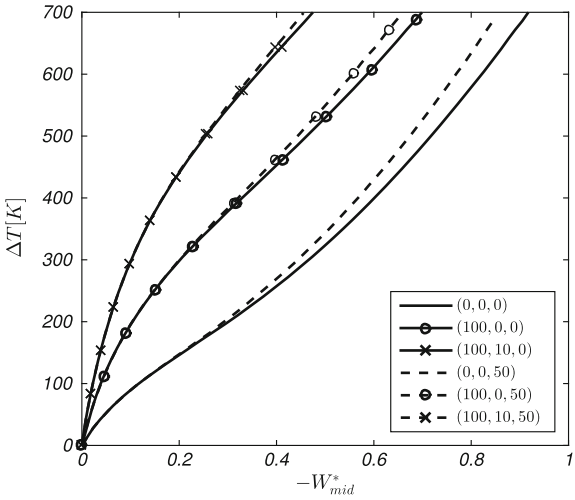

Fig. 2.40 Effect of three-parameters elastic foundation (K_g^*, K_w^*, K_{NL}^*) on load deflection path of a linearly graded $S-S$ FGM beams with $\delta = 0.04$ subjected to the $NLTD$ loading

boundary conditions, respectively. For the case of a beam with both edges clamped, it is seen that before a prescribed temperature, i.e. the bifurcation point temperature, as temperature increases the frequency parameter diminishes. This is due to the decrease in total stiffness of the beam, since geometrical stiffness diminishes as temperature rises. Near the bifurcation point, frequency approaches to zero. After the bifurcation point, an increase in temperature results in higher frequency. This feature refers to the higher elastic stiffness of the beam created from the von-Karman non-linearity [72]. It is seen that temperature dependency of the constituents leads to more accurate results, where with the assumption of constant material properties, bifurcation points are exaggerated. Besides, in pre-buckling range, with the assumption of temperature dependency, the predicted frequency is less than the one obtained with the temperature independent assumption. This is due to the lower elasticity modulus of the constituents in TD case. A comparison of Figs. 2.41 and 2.42 reveals that the behavior of an FGM beam with the $S-S$ boundary conditions is totally different from those with the $C-C$ boundary conditions. For the FGM beam with both edges simply-supported, frequency does not approaches to zero, which somehow proves the non-existence of bifurcation type buckling. This is expected since a simply supported edge does not handle the moment and the total bending moment is affected by the temperature loading. Since the statement of bending moment is non-homogeneous in terms of u, w, and φ, the resulting system of equations can not be posed as an eigen-value problem and the load-path of the beam within the studied range is unique and stable. It should be mentioned that, however, load-deflection path of the $S-S$ beams is free of bifurcation-point, but similar to the $C-C$ case, frequency decreases up to a definite temperature and then increases.

The influence of elastic foundation on fundamental frequency of an FGM beam for the $C-C$ and $S-S$ boundary conditions are depicted in Figs. 2.43 and 2.44, respectively. As previously discussed, the TD case results in more accurate conclusions

Table 2.13 The first three natural frequencies of lateral vibration for the $C-C$ FGM beams with $\delta = 0.04$, various power law indices, and contact conditions [80]

(K_w^*, K_g^*)		$k=0$	$k=0.5$	$k=1$	$k=2$	$k=5$	$k=10$	$k=\infty$
(0, 0)	First	22.1644	15.2640	13.3783	12.0136	10.9226	10.4046	9.5879
	Second	60.4948	41.6768	36.5201	32.7792	29.7880	28.3764	26.1690
	Third	117.1439	80.7439	70.7321	63.4475	57.6222	54.8942	50.6743
(100, 0)	First	24.3190	16.9750	14.9679	13.5055	12.3396	11.8036	10.9998
	Second	61.3204	42.3365	37.1344	33.3570	30.3383	28.9207	26.7208
	Third	117.5749	81.0884	71.0531	63.7496	57.9100	55.1791	50.9632
(100, 10)	First	26.7008	18.8431	16.6923	15.1163	13.8620	13.3008	12.4958
	Second	64.9355	45.2091	39.8021	35.8607	32.7161	31.2685	29.0911
	Third	121.6856	84.3659	74.1013	66.6141	60.6349	57.8726	53.6897
(200, 0)	First	26.2978	18.5298	16.4042	14.8483	13.6099	13.0535	12.2501
	Second	62.1350	42.9860	37.7386	33.9250	30.8787	29.4549	27.2615
	Third	118.0043	81.4316	71.3726	64.0502	58.1965	55.4624	51.2504
(200, 10)	First	28.5147	20.2545	17.9914	16.3270	15.0039	14.4215	13.6093
	Second	65.7053	45.8179	40.3664	36.3896	33.2179	31.7633	29.5885
	Third	122.1006	84.6958	74.4077	66.9019	60.9085	58.1428	53.9624
(500, 0)	First	31.4968	22.5587	20.1065	18.2945	16.8558	16.2358	15.4036
	Second	64.5172	44.8782	39.4959	35.5747	32.4460	31.0024	28.8228
	Third	119.2833	82.4524	72.3227	64.9439	59.0474	56.3040	52.1027
(500, 10)	First	33.2699	23.9955	21.4210	19.5138	18.0001	17.3547	16.5050
	Second	67.9624	47.5976	42.0139	37.9322	34.6796	33.2033	31.0329
	Third	123.3371	85.6777	75.3195	67.7579	61.7221	58.9461	54.7725

and therefore in the following discussion only this case is addressed. It is seen that an increase in the Winkler or Pasternak constants of elastic foundation results in higher stiffness and therefore fundamental frequency and critical buckling temperature are increased. For the case of $C-C$ beams, the nonlinear coefficient of elastic foundation has no effect on frequency parameter of the beam prior to buckling. This is expected since the pre-buckling deformation of the beam is linear. In contrast, in the $S-S$ beams nonlinear coefficient of elastic foundation affects the fundamental frequency with the initiation of temperature loading. This effect, however, is negligible.

The effects of various boundary conditions on frequency parameter of a beam subjected to uniform temperature rise loading is shown in Fig. 2.45. It is seen that responses of the $C-C$ and $C-R$ beams are totally different from the other three types. In the $C-C$ and $C-R$ cases, since edges are capable of supplying the extra moment, beam remains flat until a prescribed temperature in which frequency approaches to zero. After that, frequency increases monolithically as beam deflects more. For three other cases, however, the behavior is slightly different, since the beam initially starts lateral deflection at the onset of thermal loading.

Table 2.14 The first three natural frequencies of lateral vibration for the $C-R$ FGM beams with $\delta = 0.04$, various power law indices, and contact conditions [80]

(K_w^*, K_g^*)		$k=0$	$k=0.5$	$k=1$	$k=2$	$k=5$	$k=10$	$k=\infty$
(0, 0)	First	5.5801	3.8421	3.3678	3.0250	2.7510	2.6206	2.4138
	Second	29.9847	20.6501	18.0983	16.2514	14.7755	14.0751	12.9708
	Third	73.4283	50.5880	44.3260	39.7840	36.1545	34.4422	31.7637
(100, 0)	First	11.4533	8.3591	7.5665	6.8689	6.3637	6.1566	5.9043
	Second	31.6133	21.9477	19.3049	17.3850	15.8533	15.1402	14.0484
	Third	74.1116	51.1342	44.8374	40.2626	36.6101	34.8930	32.2210
(100, 10)	First	12.6982	9.2948	8.3558	7.6520	7.0945	6.8677	6.5960
	Second	35.2964	24.8485	21.9884	19.8956	18.2300	17.4806	16.3948
	Third	78.4420	54.5785	48.0346	43.2666	39.4646	37.7123	35.0695
(200, 0)	First	15.2059	11.1799	10.0675	9.2311	8.5688	8.3030	7.9935
	Second	33.1620	23.1728	20.4404	18.4490	16.8623	16.1350	15.0490
	Third	74.7887	51.6747	45.3377	40.7355	37.0602	35.3380	32.6720
(200, 10)	First	16.1642	11.8956	10.7157	9.8277	9.1247	8.8432	8.5171
	Second	36.6900	25.9369	22.9917	20.8318	19.1140	18.3490	17.2599
	Third	79.0821	55.0852	48.5044	43.7070	39.8825	38.1245	35.4842
(500, 0)	First	23.0508	17.0391	15.3745	14.1176	13.1229	12.7298	12.2881
	Second	37.4256	26.5104	23.5202	21.3250	19.5798	18.8065	17.7149
	Third	76.7843	53.2632	46.8142	42.1224	38.3788	38.6408	33.9888
(500, 10)	First	23.6939	17.5170	15.8064	14.5147	13.4924	13.0885	12.6350
	Second	40.5846	28.9576	25.7683	23.4168	21.5493	20.7371	19.6277
	Third	80.9718	56.5780	49.8872	45.0024	41.1106	39.3350	36.7003

In Figs. 2.46 and 2.47 the effect of heat conduction for the case of thermal loading on frequency parameter of contact-less FGM beams is depicted for the $C-C$ and $S-S$ cases of boundary conditions, respectively. The TD case of properties for the heat conduction case developed by Shen [83] is studied herein. It is seen that the behavior of $C-C$ beam in this case is also similar to the case of UTR loading, where the behavior is of the bifurcation type buckling. However, the behavior of a beam with simply-supported edges, even for the case of the reduction of an FGM beam to a fully homogeneous one, is not of the bifurcation type of instability. It is seen that for the constituents of this study, critical buckling temperature decreases as the power law index increases.

Appendix A

The basic concept of the GDQ method is to find the derivatives of a function at a sample point to be approximated as a weighted linear summation of the value of the function in the whole domain. The governing differential equations have been reduced to a set of algebraic equations by this approximation. The number of algebraic equations depend upon the number of grid points. The mth. order derivative

Table 2.15 The first three natural frequencies of lateral 0771 vibration for the $S-S$ FGM beams with $\delta = 0.04$, various power law indices, and contact conditions [80]

(K_w^*, K_g^*)		$k=0$	$k=0.5$	$k=1$	$k=2$	$k=5$	$k=10$	$k=\infty$
(0, 0)	First	9.8558	6.8104	5.9860	5.3809	4.8791	4.6370	4.2634
	Second	39.2590	27.0363	23.6933	21.2748	19.3439	18.4280	16.9827
	Third	87.7174	60.4548	52.9828	47.5561	43.2060	41.1515	37.9449
(100, 0)	First	14.0452	10.0771	8.9933	8.1864	7.5340	7.2501	6.8729
	Second	40.5189	28.0417	24.6289	22.1541	20.1805	19.2551	17.8209
	Third	88.2918	60.9140	53.4103	47.9581	43.5890	41.5306	38.3297
(100, 10)	First	17.2073	12.4898	11.1955	10.2267	9.4492	9.1225	8.7132
	Second	45.1507	31.7013	28.0189	25.3292	23.1901	22.2217	20.8026
	Third	93.2395	64.8502	57.0669	51.3916	46.8536	44.7566	41.5912
(200, 0)	First	17.2452	12.5052	11.2217	10.2509	9.4719	9.1447	8.7349
	Second	41.7408	29.0138	25.5302	22.9999	20.9837	20.0481	18.6214
	Third	88.8626	61.3698	53.8344	48.3568	43.9686	41.9062	38.7106
(200, 10)	First	19.9054	14.5314	13.0532	11.9436	11.0563	10.6903	10.2460
	Second	46.2504	32.5030	28.8143	26.0722	23.8923	22.9123	21.4923
	Third	93.7801	65.2584	57.0464	51.7639	47.2070	45.1054	41.9426
(500, 0)	First	24.4498	17.9503	16.1576	14.8079	13.7325	13.2940	12.7859
	Second	45.2089	31.7408	28.0609	25.3685	23.2272	22.2589	20.8391
	Third	90.5533	62.7171	55.0870	49.5337	45.0884	43.0061	39.8315
(500, 10)	First	26.3935	19.4077	17.4793	16.0262	14.8697	14.4037	13.8622
	Second	49.4028	35.0213	31.0787	28.1837	25.8849	24.8692	23.4400
	Third	95.3837	66.5467	58.6391	52.8650	48.2517	46.1358	42.9792

of a function $f(x)$ with respect to x at a sample point x_i is approximated by linear summation of all functional values at all grid points [84]. The mathematical expression is

$$\frac{d^m f(x)}{dx^m}\,|_{x_i} \approx \sum_{j=1}^{N} C_{ij}^{(m)} \times f(x_j)$$

where N is the number of grid points, x_i is the location of grid points, $f(x_j)$ is the function value at x_j, and $C_{ij}^{(m)}$'s are the weighting coefficients corresponding to the mth. order derivative. Quan et al. [85] suggested a Lagrangian interpolation polynomial to overcome the numerical ill-conditions in determining the weighting coefficients $C_{ij}^{(m)}$

$$f(x) = \sum_{i=1}^{N} \frac{M(x)}{(x - x_i)M^{(1)}(x_i)} f(x_i)$$

where

Table 2.16 The first three natural frequencies of lateral vibration for the $C-S$ FGM beams with $\delta = 0.04$, various power law indices, and contact conditions [80]

(K_w^*, K_g^*)		$k=0$	$k=0.5$	$k=1$	$k=2$	$k=5$	$k=10$	$k=\infty$
(0, 0)	First	15.3433	10.5716	9.2703	8.3268	7.5680	7.2064	6.6372
	Second	49.3767	34.0161	29.8129	26.7658	24.3268	23.1718	21.3595
	Third	102.0257	70.3097	61.5994	55.2714	50.2126	47.8345	44.1345
(100, 0)	First	18.3185	12.9204	11.4453	10.3637	9.4993	9.1104	8.5510
	Second	50.3846	34.8210	30.5620	27.4702	24.9974	23.8351	22.0320
	Third	102.5202	70.7051	61.9675	55.6178	50.5426	48.1610	44.4658
(100, 10)	First	21.2027	15.1545	13.4973	12.2732	11.2979	10.8741	10.2990
	Second	54.4712	37.0606	33.5672	30.2882	27.6720	26.4745	24.6921
	Third	107.0224	74.2916	65.3016	58.7499	53.5112	51.1050	47.4443
(200, 0)	First	20.8739	14.9035	13.2684	12.0614	11.0994	10.6802	10.1087
	Second	51.3727	35.6076	31.2932	28.1570	25.6504	24.4804	22.6845
	Third	103.0123	71.0982	62.3333	55.9621	50.8704	48.4854	44.7947
(200, 10)	First	23.4457	16.8770	15.0742	13.7368	12.6729	12.2193	11.6247
	Second	55.3864	38.7816	34.2343	30.9125	28.2633	27.0569	25.2761
	Third	107.4940	74.6658	65.6490	59.0759	53.8309	51.4108	47.7527
(500, 0)	First	27.1324	19.6887	17.6413	16.1148	14.9024	14.3968	13.7617
	Second	54.2290	37.8696	33.3908	30.1236	27.5167	26.3216	24.5384
	Third	104.4748	72.2648	63.4188	56.9824	51.8416	49.4456	45.7671
(500, 10)	First	29.1572	21.2217	19.0366	17.4042	16.1085	15.5728	14.9108
	Second	58.0456	40.8683	36.1617	32.7138	29.9673	28.7334	26.9522
	Third	108.8962	75.7775	66.6803	60.0433	54.7495	52.3173	48.6660

$$M(x) = \prod_{j=1}^{N}(x - x_j)$$

$$M^{(1)}(x_i) = \prod_{j=1}^{N}(x_i - x_j) \quad for \quad i = 1, 2, 3, \ldots, N$$

By combining the above equation, one may reach to

$$C_{ij}^{(1)} = \sum_{i=1}^{N} \frac{M^{(1)}(x_i)}{(x_j - x_i)M^{(1)}(x_j)} \quad for \;\; i, j = 1, 2, 3, \ldots, N \;\; and \;\; i \neq j$$

$$C_{ii}^{(1)} = -\sum_{j=1, j\neq i}^{N} C_{ij}^{(1)} \quad for \;\; i = 1, 2, 3, \ldots, N$$

Table 2.17 The first three natural frequencies of lateral vibration for the $S-R$ FGM beams with $\delta = 0.04$, various power law indices, and contact conditions [80]

(K_w^*, K_g^*)		$k=0$	$k=0.5$	$k=1$	$k=2$	$k=5$	$k=10$	$k=\infty$
(0, 0)	First	2.4666	1.7036	1.4972	1.3454	1.2107	1.1603	1.0672
	Second	22.1371	15.2505	13.3709	12.0094	10.9170	10.3967	9.5762
	Third	61.1498	42.1266	36.9185	33.1441	30.1256	28.6965	26.4524
(100, 0)	First	10.3013	7.6167	6.8736	6.3121	5.8666	5.6904	5.4928
	Second	24.2970	16.9649	14.9623	13.5026	12.3356	11.7978	10.9913
	Third	61.9684	42.7799	37.5264	33.7157	30.6700	29.2354	26.9995
(100, 10)	First	11.4367	8.4623	7.6388	7.0161	6.5224	6.3275	6.1101
	Second	28.5142	20.2612	18.0017	16.3391	15.0151	14.4314	13.6179
	Third	66.7966	46.6125	41.0838	37.0531	33.8395	32.3644	30.1564
(200, 0)	First	14.3579	10.6359	9.6047	8.8245	8.2063	7.9633	7.6943
	Second	26.2800	18.5220	16.4008	14.8472	13.6077	13.0497	12.2440
	Third	62.7763	43.4242	38.1256	34.2788	31.2057	29.7650	27.5359
(200, 10)	First	15.1931	11.2570	10.1663	9.3410	8.6872	8.4304	8.1465
	Second	30.2217	21.5818	19.2140	17.4667	16.0705	15.4717	14.6477
	Third	67.5469	47.2045	41.6318	37.5663	34.3257	32.8436	30.6376
(500, 0)	First	22.4999	16.6869	15.0751	13.8549	12.8889	12.5106	12.0954
	Second	31.4883	22.5574	20.1081	18.2973	16.8574	16.2363	15.4025
	Third	65.1401	45.3021	39.8694	35.9152	32.7002	31.3001	29.0857
(500, 10)	First	23.0419	17.0894	15.4390	14.1895	13.2003	12.8130	12.3880
	Second	34.8457	25.1306	22.4617	20.4802	18.9066	18.2399	17.3746
	Third	69.7491	48.9376	43.2344	39.0652	35.7448	34.2409	32.0377

The coefficients of the first order weighting matrix may be obtained using the above equations. Higher order coefficient matrices may be expressed as follow

$$C_{ij}^{(2)} = \sum_{k=1}^{N} C_{ik}^{(1)} C_{kj}^{(1)} \quad for \;\; i, j = 1, 2, 3, \ldots, N$$

$$C_{ij}^{(3)} = \sum_{k=1}^{N} C_{ik}^{(1)} C_{kj}^{(2)} \quad for \;\; i, j = 1, 2, 3, \ldots, N$$

$$C_{ij}^{(4)} = \sum_{k=1}^{N} C_{ik}^{(1)} C_{kj}^{(3)} \quad for \;\; i, j = 1, 2, 3, \ldots, N$$

Various types of grid distributions which provide acceptable results have been introduced. However, in this section we use the normalized Chebyshev–Gauss–Lobatto grid points that are

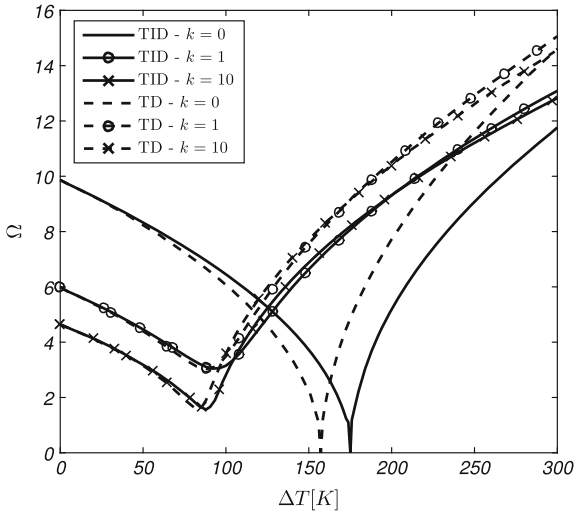

Fig. 2.41 Effect of temperature dependency and power law index on the first mode frequency of $S - S$ FGM beams with $\delta = 0.04$ subjected to UTR loading

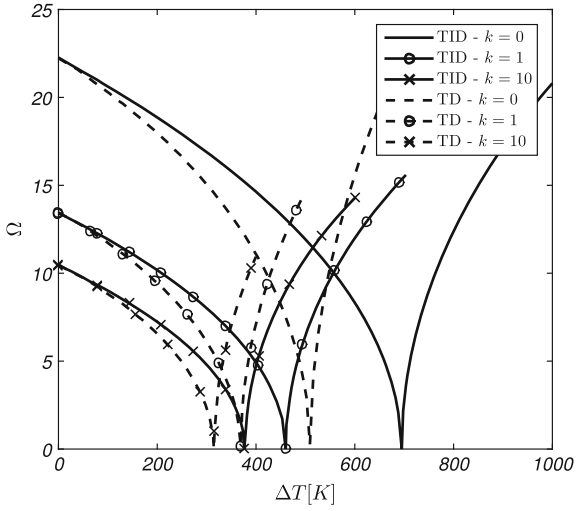

Fig. 2.42 Effect of temperature dependency and power law index on the first mode frequency of the $C - C$ FGM beams with $\delta = 0.04$ subjected to UTR loading

$$x_i = \frac{1}{2}\left[1 - \cos\left(\pi \times \frac{i-1}{N-1}\right)\right] \quad for \;\; i = 1, 2, 3, \ldots, N$$

For more details about the GDQ and method of distribution of grid points, one may refer to [86, 87].

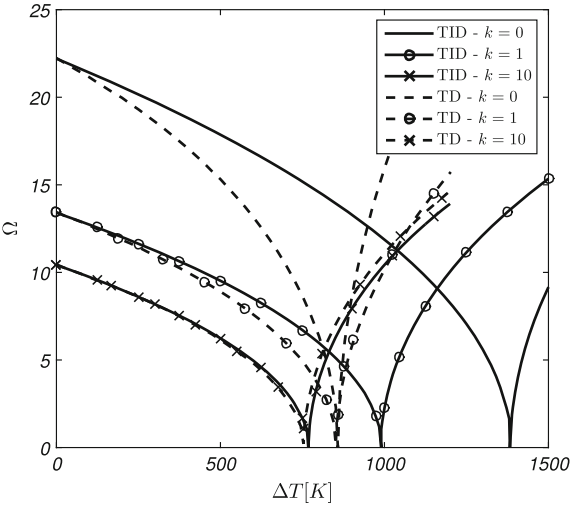

Fig. 2.43 Influences of three-parameters nonlinear elastic foundation (K_w^*, K_g^*, K_{NL}^*) on the first mode frequency of the linearly graded $C - C$ FGM beam with $\delta = 0.04$ subjected to UTR loading

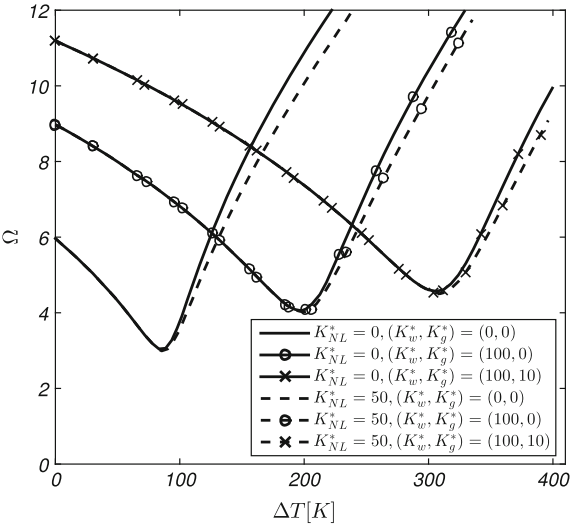

Fig. 2.44 Influences of three-parameters nonlinear elastic foundation (K_w^*, K_g^*, K_{NL}^*) on the first mode frequency of the linearly graded $S - S$ FGM beam with $\delta = 0.04$ subjected to UTR loading

Appendix B

The governing equations and the associated equations for the pre/post-buckling equilibrium states of the beam are

$$e_1 \sum_{j=1}^{N} C_{ij}^{(2)} U_{sj}^* + e_1 \delta^2 \left(\sum_{j=1}^{N} C_{ij}^{(1)} W_{sj}^* \right) \sum_{j=1}^{N} C_{ij}^{(2)} W_{sj}^* + \delta e_2 \sum_{j=1}^{N} C_{ij}^{(2)} \varphi_{sj} = 0$$

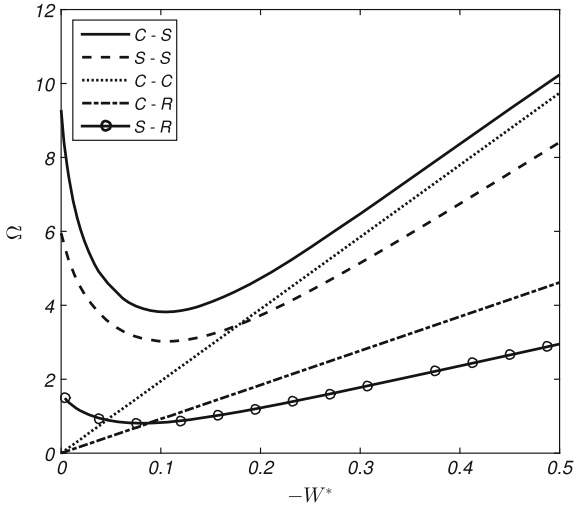

Fig. 2.45 Effect of various boundary conditions of linearly graded FGM beam on the dimensionless frequency and deflection with $\delta = 0.04$ subjected to UTR loading

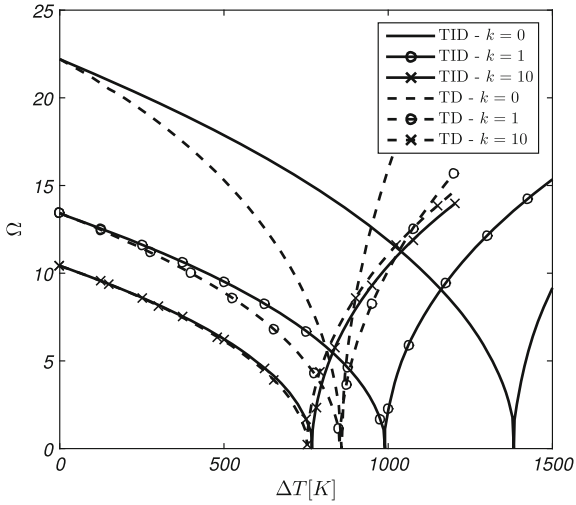

Fig. 2.46 Influences of various power law indices and temperature dependency on the first frequency of the $C - C$ FGM beam with $\delta = 0.04$ subjected to $NLTD$ loading

$$\kappa e_1 \left(\sum_{j=1}^{N} C_{ij}^{(1)} \varphi_{sj} + \delta \sum_{j=1}^{N} C_{ij}^{(2)} W_{sj}^* \right) + \left\{ e_1 \left[\sum_{j=1}^{N} C_{ij}^{(1)} U_{sj}^* + \frac{1}{2}\delta^2 \left(\sum_{j=1}^{N} C_{ij}^{(1)} W_{sj}^* \right)^2 \right] \right.$$

$$\left. + \delta e_2 \sum_{j=1}^{N} C_{ij}^{(1)} \varphi_{sj} - \frac{1}{12}\delta^2 \sum_{j=1}^{N} C_{ij}^{(0)} N_j^{T*} \right\} \delta \sum_{j=1}^{N} C_{ij}^{(2)} W_{sj}^* - \frac{1}{12} K_w^* \, \delta^3 \sum_{j=1}^{N} C_{ij}^{(0)} W_{sj}^*$$

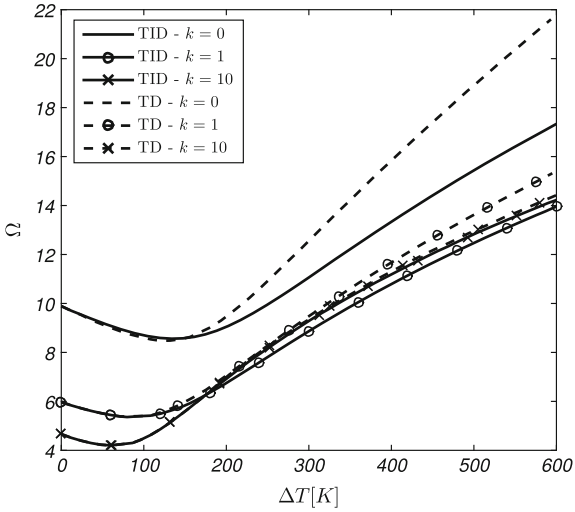

Fig. 2.47 Effect of various power law indices and temperature dependency on the $S-S$ FGM beams with $\delta = 0.04$ subjected to $NLTD$ loading

$$+\frac{1}{12}K_g^*\,\delta^3\sum_{j=1}^{N}C_{ij}^{(2)}W_{sj}^* - \frac{1}{12}\delta^3 K_{NL}^*\left(\sum_{j=1}^{N}C_{ij}^{(0)}W_{sj}^*\right)^3 = 0$$

$$\kappa e_1\left(\sum_{j=1}^{N}C_{ij}^{(0)}\varphi_{sj} + \delta\sum_{j=1}^{N}C_{ij}^{(1)}W_{sj}^*\right) - \delta^2 e_3\sum_{j=1}^{N}C_{ij}^{(2)}\varphi_{sj}$$

$$-\delta e_2\left[\sum_{j=1}^{N}C_{ij}^{(2)}U_{sj}^* + \delta^2\left(\sum_{j=1}^{N}C_{ij}^{(1)}W_{sj}^*\right)\sum_{j=1}^{N}C_{ij}^{(2)}W_{sj}^*\right] = 0 \quad i = 1, 2, 3, \ldots, N$$

Here, $C_{ij}^{(0)}$ is the Kronecker delta which is equal to one, when $i = j$, otherwise is equal to zero. Also, $C_{ij}^{(1)}$ and $C_{ij}^{(2)}$ are the weighting coefficient matrices of first and second order differentiations, respectively. Besides, subscript 's' indicates the static displacement. The beam is divided into N grid points which indicate the number of nodes in the ξ direction.

The boundary conditions at edge points ($i = 1, N$) may be written as

For the clamped end:

$$U_{si}^* = W_{si}^* = \varphi_{si} = 0$$

For the simply supported edge:

$$U_{si}^* = W_{si}^* = M_{x,si}^* = 0$$

For the roller edge:

$$U_{si}^{*} = \varphi_{si} = Q_{xz,si}^{*} + (K_g + N_{x,si})\delta \frac{dW_{si}^{*}}{dx} = 0$$

Appendix C

The governing equations and the associated boundary conditions for the small-scale vibrations of a beam in pre/post-buckling regimes are

$$e_1 \sum_{j=1}^{N} C_{ij}^{(2)} U_{dj}^{*} + e_1 \delta^2 \frac{\partial^2 W_{si}^{*}}{\partial \xi^2} \sum_{j=1}^{N} C_{ij}^{(1)} W_{dj}^{*} + e_1 \delta^2 \frac{\partial W_{si}^{*}}{\partial \xi} \sum_{j=1}^{N} C_{ij}^{(2)} W_{dj}^{*} + \delta e_2 \sum_{j=1}^{N} C_{ij}^{(2)} \varphi_{dj}$$

$$= \frac{\partial^2}{\partial \eta^2} \left(\frac{\Lambda_1}{\delta^2} \sum_{j=1}^{N} C_{ij}^{(0)} U_{dj}^{*} + \frac{\Lambda_2}{\delta} \sum_{j=1}^{N} C_{ij}^{(0)} \varphi_{dj} \right)$$

$$\kappa e_1 \left(\sum_{j=1}^{N} C_{ij}^{(1)} \varphi_{dj} + \delta \sum_{j=1}^{N} C_{ij}^{(2)} W_{dj}^{*} \right) + \left[e_1 \left(\frac{\partial U_{si}^{*}}{\partial \xi} + \frac{1}{2} \delta^2 \left(\frac{\partial W_{si}^{*}}{\partial \xi} \right)^2 \right) + \delta e_2 \frac{\partial \varphi_{si}}{\partial \xi} \right.$$

$$\left. - \frac{\delta^2}{12} N^{T*} \right] \delta \sum_{j=1}^{N} C_{ij}^{(2)} W_{dj}^{*} + \left[e_1 \left(\sum_{j=1}^{N} C_{ij}^{(1)} U_{dj}^{*} + \delta^2 \frac{\partial W_{si}^{*}}{\partial \xi} \sum_{j=1}^{N} C_{ij}^{(1)} W_{dj}^{*} \right) + e_2 \delta \sum_{j=1}^{N} C_{ij}^{(1)} \varphi_{dj} \right] \delta \frac{\partial^2 W_{si}^{*}}{\partial \xi^2}$$

$$+ \left[e_1 \left(\sum_{j=1}^{N} C_{ij}^{(2)} U_{dj}^{*} + \delta^2 \frac{\partial^2 W_{si}^{*}}{\partial \xi^2} \sum_{j=1}^{N} C_{ij}^{(1)} W_{dj}^{*} + \delta^2 \frac{\partial W_{si}^{*}}{\partial \xi} \sum_{j=1}^{N} C_{ij}^{(2)} W_{dj}^{*} \right) + e_2 \delta \sum_{j=1}^{N} C_{ij}^{(2)} \varphi_{dj} \right] \delta \frac{\partial W_{si}^{*}}{\partial \xi}$$

$$+ \left[e_1 \frac{\partial^2 U_{si}^{*}}{\partial \xi^2} + e_1 \delta^2 \frac{\partial W_{si}^{*}}{\partial \xi} \frac{\partial^2 W_{si}^{*}}{\partial \xi^2} + e_2 \delta \frac{\partial^2 \varphi_{si}}{\partial \xi^2} \right] \delta \sum_{j=1}^{N} C_{ij}^{(1)} W_{dj}^{*}$$

$$- \frac{1}{12} K_w^{*} \delta^3 \sum_{j=1}^{N} C_{ij}^{(0)} W_{dj}^{*} + \frac{1}{12} K_g^{*} \delta^3 \sum_{j=1}^{N} C_{ij}^{(2)} W_{dj}^{*} - \frac{1}{4} \delta^3 K_{NL}^{*} W_{si}^{*2} \sum_{j=1}^{N} C_{ij}^{(0)} W_{dj}^{*} = \frac{\Lambda_1}{\delta} \frac{\partial^2}{\partial \eta^2} \sum_{j=1}^{N} C_{ij}^{(0)} W_{dj}^{*}$$

$$\kappa e_1 \left(\sum_{j=1}^{N} C_{ij}^{(0)} \varphi_{dj} + \delta \sum_{j=1}^{N} C_{ij}^{(1)} W_{dj}^{*} \right) - e_2 \left(\delta \sum_{j=1}^{N} C_{ij}^{(2)} U_{dj}^{*} + \delta^3 \frac{\partial^2 W_{si}^{*}}{\partial \xi^2} \sum_{j=1}^{N} C_{ij}^{(1)} W_{dj}^{*} \right.$$

$$\left. + \delta^3 \frac{\partial W_{si}^{*}}{\partial \xi} \sum_{j=1}^{N} C_{ij}^{(2)} W_{dj}^{*} \right) - \delta^2 e_3 \sum_{j=1}^{N} C_{ij}^{(2)} \varphi_{dj} = \frac{\partial^2}{\partial \eta^2} \left(\frac{\Lambda_2}{\delta} \sum_{j=1}^{N} C_{ij}^{(0)} U_{dj}^{*} + \Lambda_3 \sum_{j=1}^{N} C_{ij}^{(0)} \varphi_{dj} \right)$$

For the small amplitude free vibration analysis one may write

$$\frac{\partial^2}{\partial \eta^2} < U_{dj}^{*}, W_{dj}^{*}, \varphi_{dj} > = -\omega^{*2} < U_{dj}^{*}, W_{dj}^{*}, \varphi_{dj} > .$$

The boundary conditions at edge points ($i = 1, N$) may be written as
For the clamped edge:

$$U_{di}^{*} = W_{di}^{*} = \varphi_{di} = 0$$

For the simply supported edge:

$$U_{di}^{*} = W_{di}^{*} = M_{x,di}^{*} = 0$$

For the roller edge:

$$U_{di}^{*} = \varphi_{di} = Q_{xz,di}^{*} + (K_g + N_{x,si})\delta\frac{dW_{di}^{*}}{d\xi} + N_{x,di}\delta\frac{dW_{si}^{*}}{d\xi} = 0$$

2.10 FGM Beams, Thermal Dynamic Buckling

Dynamic buckling is a complicated behavior which should be explored through the response of non-linear equations of motion of a structure. Definition of a dynamically buckled structure strongly depends upon the selected criterion. A wealth review on the concept of dynamic buckling and its applications to solid structures is reported in a review paper by Simitses [89] and also documented in a book by Simitses [90]. Among the most well-known and suitable criteria, the equation of motion criterion of Budiansky–Roth [91] (which is also known as the Budiansky–Hutchinson for initially imperfect structures [92]), the phase-plane approach of Hoff-Hsu [93], the modified total potential energy approach of Hoff-Simitses [94], displacement control approach of Volmir [95], quasi-bifurcation dynamic buckling of Kleiber et al. [96] and the criterion of Kubiak [97] or Kounadis [98] are the most frequently used ones. Each criterion has its own advantages and shortcomings. Meanwhile, the Budiansky–Roth criterion is the most popular one since is easy to be used in computer programming and has no limitation in structural analysis [89].

Referring to the thermal dynamic buckling, the Budiansky-Roth criterion is applied successfully to cylindrical shells [99–104], plates [105, 106] and spherical caps [107, 108]. However, thermal dynamic buckling of beams made of FGMs or even homogeneous materials based on the Budiansky–Roth criterion is not frequent in literature. The thermal dynamic buckling of FGM beams under rapid heating is reported recently in [88]. This research, however, is developed based on the Hoff–Simitses criterion. As known, the Hoff-Simitses criterion yields only the magnitude of critical temperature in which dynamic buckling phenomenon occurs and does not establish the dynamic sense of the structure prior or at the onset of buckling.

This section examines the thermal dynamic buckling and imperfection sensitivity of the FGM beams subjected to uniform rapid heating [111]. Temperature dependency, initial imperfections, and contact of a three-parameter conventional non-linear elastic foundation are also taken into account. The Timoshenko beam theory, geometrical non-linearity in the von-Karman sense, and uncoupled thermoelastic

constitutive law of a continuum medium are incorporated together to establish the Hamiltonian of the system. The conventional multi-term Ritz method is applied to the Hamiltonian of the system to establish the matrix representation of the non-linear equations of motion. To solve the highly coupled non-linear equations in time and space domains, a hybrid Newmark–Newton–Raphson method is applied to the governing equations which traces the temporal evolution of beam deformations. Solution method is general and may be used for arbitrary grading profile and edge supports. The Budiansky-Roth criterion is applied successively to the equations of motion. It is shown that the FGM beams do not undergo any type of thermal dynamic buckling in the Budiansky-Roth sense. However, a sufficiently stiff non-linear softening elastic foundation violates the response of the beam and results in the unbounded motion type of dynamic buckling.

2.10.1 Fundamental Equations of the FGM Beam

A beam with length L and thickness h is considered in the conventional Cartesian coordinate system (x, z), as shown in Fig. 2.30 [111]. Material properties are assumed to be temperature dependent obeying the power law distribution given by Eqs. (2.2.8) and (2.5.22).

In this study, it is assumed that the displacement field is expressed based on the first order shear deformation theory (FSDT) consistent with the Timoshenko assumptions. According to this theory, the displacement components of a generic point of the beam can be written in terms of the mid-plane displacement components (u_0, w_0) given by Eq. (2.2.1) such that [80]

$$\begin{aligned} u(x, z, t) &= u_0(x, t) + z\phi(x, t) \\ w(x, z, t) &= w_0(x, t) \end{aligned} \tag{2.10.1}$$

where in the above equation ϕ denotes the transverse normal rotation about x axis.

Considering the von-Karman type of geometrical non-linearity, consistent with the small strains and moderate rotations, the strain-displacement relations may be written in terms of the mid-plane displacement components as

$$\begin{aligned} \varepsilon_{xx} &= u_{0,x} + \frac{1}{2}w_{0,x}^2 + w_{0,x}w_{,x}^* + z\phi \\ \gamma_{xz} &= w_{0,x} + \phi \end{aligned} \tag{2.10.2}$$

In which a comma indicates the partial derivative with respect to x-direction. Besides, w^* is the initial imperfection function through the beam which demonstrates a deviation with respect to the flat condition.

Under the uncoupled thermoelastic assumptions, the constitutive law for the linear thermoelastic FGM beam exposed to thermal loadings will be

$$\sigma_{xx} = E(z,T)\varepsilon_{xx} - E(z,T)\alpha(z,T)(T - T_0)$$
$$\sigma_{xz} = G(z,T)\gamma_{xz} \tag{2.10.3}$$

In the above equation, σ_{xx} and σ_{xz} are the axial and through-the-thickness shear stresses, respectively, and $E(z)$ and $G(z)$ are the elastic and shear modules. Furthermore, T and T_0 denote the temperature distribution and the initial temperature, respectively.

2.10.2 Governing Equations

The governing equations of the FGM Timoshenko beam exposed to sudden uniform temperature rise may be obtained based on the concept of Hamilton's principle. This principle is the dynamic form of the virtual displacement principle and may be written as

$$\delta \int_{t_1}^{t_2} [T - (V + U)]\, dt = 0 \tag{2.10.4}$$

In which δT and $\delta(U + V)$ represent the virtual kinetic energy and the virtual total potential energy, respectively.

The virtual kinetic energy of the beam per width is equal to summation of the virtual kinetic energy in longitudinal and transversal directions. Accordingly, one may write

$$\int_{t_1}^{t_2} \delta T dt = \int_{t_1}^{t_2} \int_0^L \int_{-0.5h}^{+0.5h} \rho(z)\,(\dot{u}\delta\dot{u} + \dot{w}\delta\dot{w})\, dz dx dt \tag{2.10.5}$$

By substituting Eq. (2.10.1) into (2.10.5) and performing some proper mathematical operations, the virtual kinetic energy of beam per unit width in terms of the mid-plane displacement components for the FGM beam becomes

$$\int_{t_1}^{t_2} \delta T dt = -\int_{t_1}^{t_2} \int_0^L \left\{ I_1\,(\ddot{u}_0\delta u_0 + \ddot{w}_0\delta w_0) + I_2\left(\ddot{\phi}\delta u_0 + \ddot{u}_0\delta\phi\right) + I_3\ddot{\phi}\delta\phi \right\} dx dt \tag{2.10.6}$$

In which the inertia resultants I_1, I_2, and I_3 are defined by

$$(I_1, I_2, I_3) = \int_{-0.5h}^{+0.5h} \rho(z)(1, z, z^2) dz \tag{2.10.7}$$

The virtual total potential energy of the FG beam is equal to the sum of the virtual energy of external applied loads, which is absent in this study, the virtual strain energy of the beam, and the virtual energy of elastic foundation. Thus, the virtual potential

energy of the beam per unit width is equal to

$$\int_{t_1}^{t_2} \delta(U+V)dt = \int_{t_1}^{t_2} \left\{ \int_0^L \int_{-0.5h}^{+0.5h} (\sigma_{xx}\delta\varepsilon_{xx} + \sigma_{xz}\delta\gamma_{xz})\, dzdx + \int_0^L \left(K_w w\delta w + K_s w_{,x}\delta w_{,x} + K_{nl} w^3 \delta w\right) dx \right\} dt \quad (2.10.8)$$

where in the above equation, K_w, K_s, and K_{nl} are the Winkler, Pasternak, and nonlinear constants of elastic foundation, respectively. Positive values of K_{nl} indicate softening nonlinear elastic medium whereas the negative values of K_{nl} are associated with the softening non-linear elastic medium. By substituting Eq. (2.10.1) into (2.10.8) and accomplishing some mathematical operations, the virtual total potential energy per unit width in terms of the mid-plane displacement components for the FGM beam may be written in the following form [111]

$$\begin{aligned}\int_{t_1}^{t_2} \delta(U+V)dt = \int_{t_1}^{t_2} \Bigg[& \left\{ E_1 \left(u_{0,x} + \frac{1}{2}w_{0,x}^2 + w_{0,x}w_{,x}^* \right) + E_2\phi_{,x} - N^T \right\} \delta u_{0,x} \\ & + \left\{ E_2 \left(u_{0,x} + \frac{1}{2}w_{0,x}^2 + w_{0,x}w_{,x}^* \right) + E_3\phi_{,x} - M^T \right\} \delta\phi_{,x} + G_1 \left(\phi + w_{0,x}\right)\delta\phi \\ & + \left\{ E_1 \left(u_{0,x} + \frac{1}{2}w_{0,x}^2 + w_{0,x}w_{,x}^* \right) + E_2\phi_{,x} - N^T \right\} \left(w_{0,x} + w_{,x}^*\right)\delta w_{0,x} \\ & + \left(G_1 \left(\phi + w_{0,x}\right) + K_s w_{0,x}\right)\delta w_{0,x} + \left(K_w w_0 \pm K_{nl} w_0^3\right)\delta w_0 \Bigg] dxdt \end{aligned} \quad (2.10.9)$$

where in the above equation E_1, E_2, and E_3 are the stretching, coupling bending-stretching, and bending stiffness, respectively, and G_1 is the shear stiffness which are defined by

$$(E_1, E_2, E_3, G_1) = \int_{-0.5h}^{+0.5h} (E(z), zE(z), z^2E(z), G(z))dz \quad (2.10.10)$$

Besides, N^T and M^T are, respectively, the thermal force and moment resultants generated in derivation of Eq. (2.10.9) as

$$(N^T, M^T) = \int_{-0.5h}^{+0.5h} (1, z)E(z,T)\alpha(z,T)(T - T_0)dz \quad (2.10.11)$$

Solution Method

At this stage, to accomplish the spatial approximation, the displacement field is expressed in terms of the proper shape functions based on the well-known Ritz method as follows [111]

Table 2.18 Appropriate p-Ritz shape functions associated with the boundary conditions (2.10.13) [111]

p-Ritz functions	$C-C$	$S-C$	$S-S$
N_m^u	$\left(\frac{x}{L}\right)^m(1-\frac{x}{L})$	$\left(\frac{x}{L}\right)^m(1-\frac{x}{L})$	$\left(\frac{x}{L}\right)^m(1-\frac{x}{L})$
N_m^w	$\left(\frac{x}{L}\right)^m(1-\frac{x}{L})$	$\left(\frac{x}{L}\right)^m(1-\frac{x}{L})$	$\left(\frac{x}{L}\right)^m(1-\frac{x}{L})$
N_m^ϕ	$\left(\frac{x}{L}\right)^m(1-\frac{x}{L})$	$\left(\frac{x}{L}\right)^m$	$\left(\frac{x}{L}\right)^{m-1}$

$$\begin{Bmatrix} u_0(x,t) \\ w_0(x,t) \\ \phi(x,t) \end{Bmatrix} = \sum_{m=1}^{M} \begin{bmatrix} N_m^u(x) & 0 & 0 \\ 0 & N_m^w(x) & 0 \\ 0 & 0 & N_m^\phi(x) \end{bmatrix} \begin{Bmatrix} U_m(t) \\ W_m(t) \\ \Phi_m(t) \end{Bmatrix} \tag{2.10.12}$$

In Eq. (2.10.12) M is a required number to assure the convergence of the series. Besides, N_m^u, N_m^w, and N_m^ϕ are the Ritz approximation functions which should be chosen according to the essential type of boundary conditions. Two types of edge supports, including immovable simply-supported (S) and immovable clamped (C), are considered. Mathematical interpretation of these supports are

$$\begin{aligned} S &: u_0 = w_0 = M_{xx} = 0 \\ C &: u_0 = w_0 = \phi = 0 \end{aligned} \tag{2.10.13}$$

Since the adoption of shape functions depends only on the essential type of boundary conditions [35], various functions may be chosen as the shape functions. In this study, polynomial type of shape functions are considered as the Ritz approximation functions. Table 2.18 presents these admissible shape functions for three types of boundary conditions namely; simply supported-simply simply supported ($S-S$), clamped-simply supported ($C-S$), and clamped–clamped ($C-C$).

It is to be noticed that the expressed shape functions in Table 2.18 are adopted according to the boundary conditions which are described by Eq. (2.10.13).

Substitution of the series expansion (2.10.12) into the virtual energies (2.10.6) and (2.10.9) and subsequently substitution of the results into the Hamilton principle (2.10.4) leads to the matrix representation of the equations of motion as

$$\begin{bmatrix} [M^{uu}][M^{uw}][M^{u\phi}] \\ [M^{wu}][M^{ww}][M^{w\phi}] \\ [M^{\phi u}][M^{\phi w}][M^{\phi\phi}] \end{bmatrix} \begin{Bmatrix} \{\ddot{U}\} \\ \{\ddot{W}\} \\ \{\ddot{\Phi}\} \end{Bmatrix} + \begin{bmatrix} [K^{uu}][K^{uw}][K^{u\phi}] \\ [K^{wu}][K^{ww}][K^{w\phi}] \\ [K^{\phi u}][K^{\phi w}][K^{\phi\phi}] \end{bmatrix} \begin{Bmatrix} \{U\} \\ \{W\} \\ \{\Phi\} \end{Bmatrix} = \begin{Bmatrix} \{F^u\} \\ \{F^w\} \\ \{F^\phi\} \end{Bmatrix} \tag{2.10.14}$$

For the interest of brevity, elements of the generalized mass matrix, stiffness matrix, and force vector are given at the end of this section.

In a compact form, Eq. (2.10.14) may be written as

$$[\mathbf{M}(\mathbf{T})]\left\{\ddot{\mathbf{X}}\right\} + [\mathbf{K}(\mathbf{T},\mathbf{X})]\{\mathbf{X}\} = \{\mathbf{F}(\mathbf{T})\} \tag{2.10.15}$$

It is noticed that due to accountancy of the von-Karman type of geometrical non-linearity, the generalized stiffness matrix is a function of unknown time-dependent nodal vector $\{\mathbf{X}\}$.

There are several available numerical methods to approximate the second-order time derivatives and convert the differential equations into the algebraic equations. Among them, the constant acceleration method of time-approximation schemes is widely used in structural dynamics [69]. Subsequently, here, following the Newmark method, temporal approximation is done. By utilizing this method, Eq. (2.10.15) can be reduced to

$$\left[\widehat{\mathbf{K}}(\mathbf{T},\mathbf{X})\right]\{\mathbf{X}\}_{j+1} = \left\{\widehat{\mathbf{F}}(\mathbf{T})\right\}_{j,j+1} \tag{2.10.16}$$

where

$$\begin{aligned}\left[\widehat{\mathbf{K}}(\mathbf{T},\mathbf{X})\right] &= [\mathbf{K}(\mathbf{T},\mathbf{X})] + a_0\,[\mathbf{M}(\mathbf{T})]\\ \left\{\widehat{\mathbf{F}}(\mathbf{T})\right\} &= \{\mathbf{F}(\mathbf{T})\}_{j+1} + [\mathbf{M}(\mathbf{T})]\left(a_0\{\mathbf{X}\}_j + a_1\left\{\dot{\mathbf{X}}\right\}_j + a_2\left\{\ddot{\mathbf{X}}\right\}_j\right)\end{aligned} \tag{2.10.17}$$

and

$$a_0 = \frac{1}{\beta\Delta t^2},\quad a_1 = \frac{1}{\beta\Delta t},\quad a_2 = \frac{1-2\beta}{2\beta} \tag{2.10.18}$$

Once the solution $\{\mathbf{X}\}$ is known at $t_{j+1} = (j+1)\Delta t$, the first and second derivatives of $\{\mathbf{X}\}$ at t_{j+1} can be computed from

$$\begin{aligned}\left\{\ddot{\mathbf{X}}\right\}_{j+1} &= a_0\left(\{\mathbf{X}\}_{j+1} - \{\mathbf{X}\}_j\right) - a_1\left\{\dot{\mathbf{X}}\right\}_j - a_2\left\{\ddot{\mathbf{X}}\right\}_j\\ \left\{\dot{\mathbf{X}}\right\}_{j+1} &= \left\{\dot{\mathbf{X}}\right\}_j + a_3\left\{\ddot{\mathbf{X}}\right\}_j + a_4\left\{\ddot{\mathbf{X}}\right\}_{j+1}\end{aligned} \tag{2.10.19}$$

and

$$a_3 = (1-\alpha)\Delta t,\quad a_4 = \alpha\Delta t \tag{2.10.20}$$

The resulting equations are solved at each time step using the information known from the preceding time step solution. At time $t = 0$, the initial values of $\{\mathbf{X}\}$, $\left\{\dot{\mathbf{X}}\right\}$, and $\left\{\ddot{\mathbf{X}}\right\}$ are known or obtained by solving Eq. (2.10.15) at time $t = 0$ and are used to initiate the time marching procedure. Since the beam is initially at rest, the initial values of $\{\mathbf{X}\}$ and $\left\{\dot{\mathbf{X}}\right\}$ are assumed to be zero. An iterative scheme should be applied to Eq. (2.10.15) to solve the resulting highly non-linear algebraic equations. In this section, the well-known Newton–Raphson iterative scheme is used in which the tangent stiffness matrix is evaluated based on the developed method in [69].

2.10.3 Numerical Investigation

The procedure outlined in the previous section is used herein to study the dynamic unbounded motion and imperfection sensitivity of the FGM beams under sudden thermal loading. Beam is resting on an elastic foundation. Constants of elastic foundation are normalized as given bellow [111]

$$(k_w, k_s, k_{nl}) = \left(\frac{12K_w L^4}{E_c^{ref} h^3}, \frac{12K_s L^2}{E_c^{ref} h^3}, \frac{12K_{nl} L^4 h^2}{E_c^{ref} h^3} \right) \tag{2.10.21}$$

where E_c^{ref} represents the ceramic elasticity modulus at the reference temperature.

Since only the clamped and simply supported edges are taken into consideration, the initial imperfection function is assumed as

$$w^* = \mu h \sin\left(\frac{\pi x}{L}\right) \tag{2.10.22}$$

where μ indicates the out of plane amplitude of imperfection with respect to the flatness condition.

In all presented examples of this section, Stainless Steel ($SUS304$) and Silicon Nitride (Si_3N_4) are considered as the combination of FGM material constituents. Temperature dependent coefficients of these materials are given in Table 2.3. In order to effectively model the material properties, the temperature dependency of the material should be taken into account. In all examples, beam thickness and length are set equal to $h = 4\,\text{cm}$ and $L/h = 25$.

Comparison Studies

To demonstrate the validity and accuracy of the proposed solution method and the obtained formulations, comparison studies are provided. In the first one, dynamic critical buckling temperature differences of this study for the clamped FGM beam resting on an elastic foundation are compared with those reported in [88], which is performed based on the Hoff-Simitsis criterion. The beam is subjected to sudden uniform temperature rise. It should be emphasized that softening constant of elastic foundation is chosen a sufficiently large number to ensure that post-buckling equilibrium path becomes unstable [88]. Besides, analysis is performed for the TD case of material properties. Thus, the results for several power law index values are reported in Table 2.19 with considering $\mu = 0.01$. In each case, relative difference is also provided. The imperfection shape function of [88] differs with the one used in this section. However, for small amplitudes of imperfection, the imperfection shapes will be the same. As seen, the results of two studies are close with small differences. These differences may be due to the different criteria, different beam theories, and also different numerical solutions.

Table 2.19 Comparison of dynamic critical buckling temperature difference of the $C-C$ FGM beam with $\mu = 0.01$ resting on a softening elastic foundation $(k_w, k_s, k_{nl}) = (10, 10, -1000)$ subjected to sudden uniform temperature rise between the results of this section [111] and those reported by Ghiasian et al. [88]

	$k=0$	$k=0.5$	$k=1$	$k=2$	$k=5$	$k=\infty$
Present	589.2	478.1	446.1	424.6	406.9	366.3
Ghiasian et al. [88]	590.9	480.3	448.9	426.3	409.8	367.7
Difference (%)	0.288	0.458	0.624	0.399	0.708	0.381

Parametric Studies

Based on the Budiansky-Roth criterion, dynamic buckling analysis of an FGM Timoshenko beam with initial geometric imperfection resting on a tree-parameter elastic foundation is studied. Thermal load is considered as uniform temperature rise which is applied suddenly to the beam and its temporal dependency is chosen as a unit step function. In the present parametric studies, essential conditions for occurrence of dynamic buckling phenomena are studied. In addition, time history of midspan displacement and phase-plane curves of the FGM beams are investigated under various values of the applied sudden thermal loads. According to these curves, dynamic thermal buckling load level of the system is recognized for different conditions. Subsequently, influences of temperature-dependency, imperfection amplitude, power law index, and boundary conditions on thermal dynamic buckling phenomenon are studied.

Based on the Budiansky-Roth criterion, a large increase occurs in the deflection amplitude when the nonlinear equations of motion of the system are solved for different load levels [109]. According to the Budiansky-Roth criterion, in this study, dynamic buckling load is detected via trail and error scheme. Based on this method, the equations of motion of the beam are solved for several values of sudden thermal loads starting from a small value and being gradually increased. The dynamic buckling phenomenon for the FGM beam is studied for two cases; the FGM beams with and without elastic foundation.

For the first case, the maximum transverse midspan displacement of the $C-C$ FGM Timoshenko beams $(w(L/2, t))$ versus thermal load is represented in Fig. 2.48a [111]. The imperfection amplitude is chosen to be $\mu = 0.1$. Furthermore, the constant values of softening elastic foundation are chosen as $(k_w, k_s, k_{nl}) = (10, 10, -1000)$. It is seen that the maximum displacement increases smoothly with the exposed thermal loading until an unbounded motion which occurs at a higher level of temperature. According to the Budiansky-Roth criterion, this load is introduced as dynamic buckling load level of the system. It is to be mentioned that the correspondent post-buckling equilibrium path is unstable under this condition (with considering softening elastic foundation), as formerly discussed in [88]. For the second case, the maximum transverse midspan displacement of a $C-C$ FGM beam without elastic foundation

versus the applied thermal load is represented in Fig. 2.48b. As seen, no large jump is observed in the maximum displacement as the applied thermal load increases. It should be emphasized that the correspondent post-buckling equilibrium path for this case is stable as reported in [88, 110]. So, it can be concluded that the occurrence of dynamic buckling phenomenon is possible for the FGM beam, just by making the post-buckling equilibrium path unstable. As known, nonlinear equilibrium path of the FGM beams subjected to uniform temperature rise may be unique and stable or of the bifurcation type of buckling with stable post-buckling branch. Therefore, thermal dynamic buckling phenomenon in the Budiansky-Roth sense does not occur for the contact-less FGM beams under sudden uniform heating. Dynamic buckling indeed occurs when beam is resting on a sufficiently stiff softening elastic medium. The phrase *sufficiently stiff softening elastic medium* for the foundation means that foundation changes the static equilibrium path from stable to unstable.

Figure 2.48c, d, e and f reveal the same results for the FGM beams exposed to sudden thermal loads in two cases, with and without elastic foundation for the $C-S$ and $S-S$ cases of boundary conditions [111]. Discussions in these cases are the same with Fig. 2.48a, b.

In the next sections, only the FGM beams resting on sufficiently softening elastic foundation ($(k_w, k_s, k_{nl}) = (10, 10, -1000)$) in which the possibility of dynamic buckling occurrence exists, are studied.

Dynamic buckling load may be detected by tracing the transversal displacement of the structure during a time span under different magnitudes of the applied load levels. Subsequently, here, the transverse midspan displacement of the FGM beam under four levels of thermal loads for three types of boundary conditions including $(C-C)$, $(C-S)$, and $(S-S)$ are represented in Figs. 2.49a, c and 2.50e, respectively. It is observed that for each case of boundary condition, simple oscillations with finite amplitudes are occurred under the first three load levels. By increasing only 0.1 K in magnitude of thermal shock and applying the fourth level of the thermal loads, the beams undergo unbounded displacements. These loads are identified as thermal dynamic buckling load level of the beams since only 0.1 K increase in temperature results in severe change in displacement. It should be emphasized that the type of dynamic buckling is unbounded, since the associated post-buckling equilibrium path of the beam under the associated static load is of the upper limit load type of instability with completely softening post-limit load behavior.

The phase-plane curves corresponding to traverse midspan displacement of the FGM beam are also depicted in Fig. 2.49b, d, e, respectively, for the $(C-C)$, $(C-S)$, and $(S-S)$ types of boundary conditions. As seen, for each case of boundary condition, three stable dynamic solutions with related closed form curves exist and these curves are associated with three load levels less than the dynamic buckling temperature. However, a diverged curve is observed for dynamic buckling temperature.

It is to be noticed that the fluctuations in the phase-plane curves for the $C-S$ and $S-S$ cases exist because of the coupling between in-plane and out of plane vibrations in these cases. For the $C-C$ case of FGM beams, the induced bending moments due to thermal loading and geometrical non-linearity are compensated at the edge supports, whereas in the $S-C$ and $S-S$ cases, such feature does not exist and

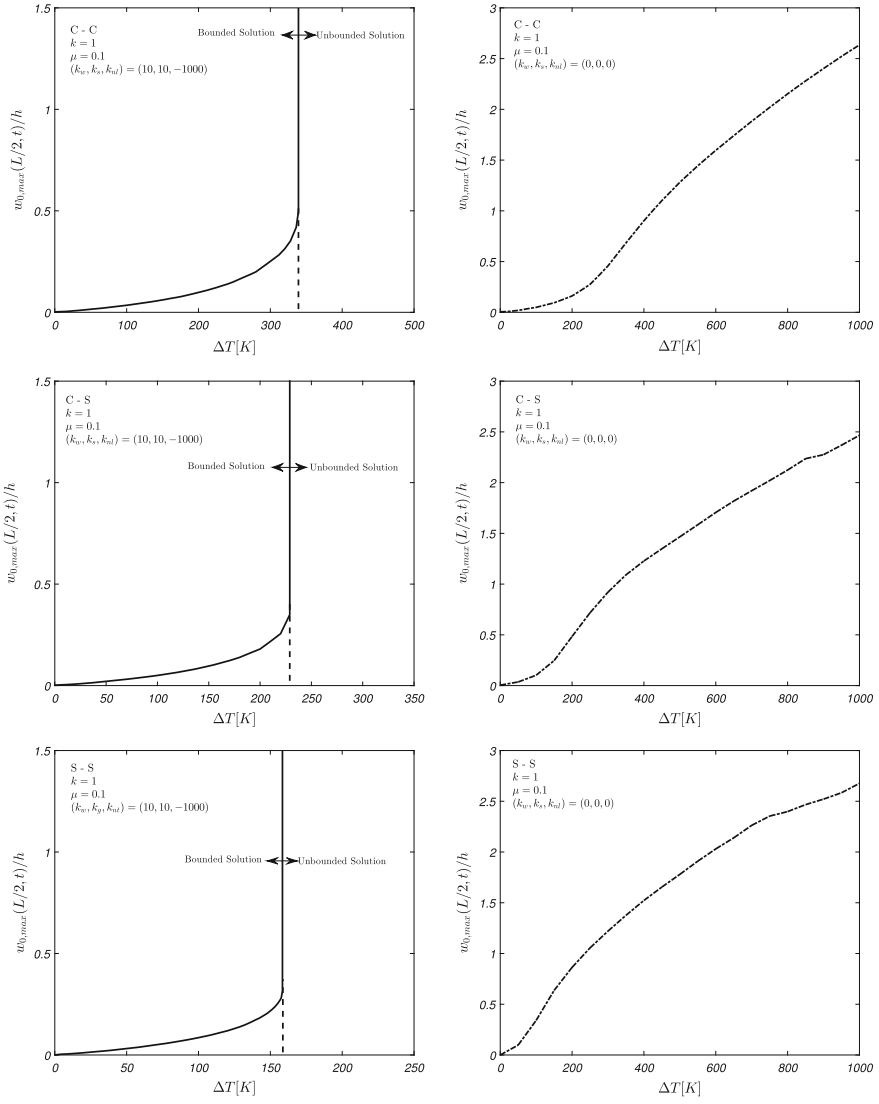

Fig. 2.48 Maximum non-dimensional deflection in temporal evolution of the midspan of the temperature dependent FGM beams for various edge supports

coupling between in-plane and out-of-plane motions results in such chaotic phase planes.

Figure 2.50 is known as the dynamic imperfection sensitivity curve in which the influence of amplitude imperfection is investigated on thermal dynamic buckling load. An FGM beam with $k = 1$ resting on a softening elastic foundation is considered. This investigation is done for three types of boundary conditions includ-

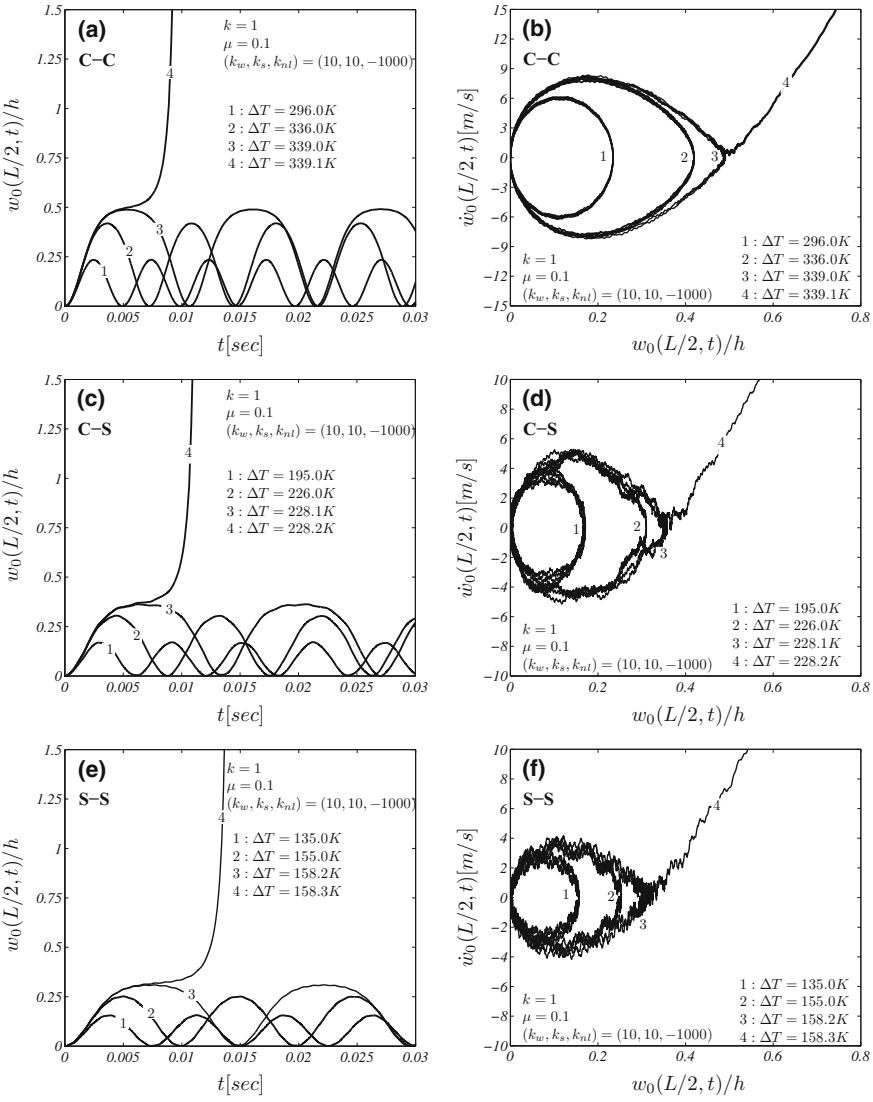

Fig. 2.49 Characteristics of temperature dependent FGM beams resting on softening elastic foundation and subjected to sudden heating. Right ones: Temporal evolution of non-dimensional mid-span lateral deflection for various rapid heating values, Left ones: The associated phase-planes

ing $C-C$, $C-S$, and $S-S$ and two model of material properties i.e. the TD and TID. As seen from Fig. 2.50, the dynamic buckling temperature difference is decreased with the increase of imperfection amplitude for each case of boundary condition. Besides, this decrease is much more noticeable for the lower values of imperfection amplitude. It should be mentioned that in this case the structure may be

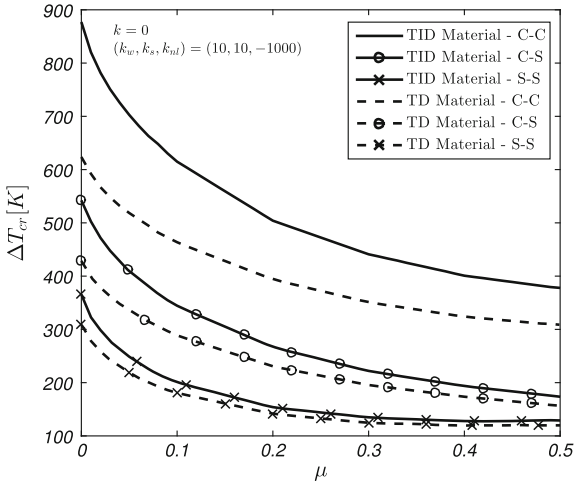

Fig. 2.50 Dynamic imperfection sensitivity of the FGM beam resting on softening elastic foundation

called imperfection sensitive in dynamic sense, since the dynamic limit load temperature decreases noticeably with the introduction of higher imperfection amplitude. Furthermore, considering temperature dependency leads to the underestimation of dynamic buckling temperature for all types of boundary conditions.

The comparison between the imperfection sensitivity curves associated with three types of boundary conditions reveals that for each value of imperfection parameter, the maximum dynamic buckling temperatures are obtained for the $C - C$ case of boundary condition and the minimum ones are related to the $S - S$ case.

The influence of power law index on dynamic buckling temperature difference for imperfect FGM beam resting on softening elastic foundation is exhibited in Fig. 2.51. The imperfection parameter of the beam is considered to be $\mu = 0.1$ and three types of boundary conditions, namely; $C - C$, $C - S$, and $S - S$ are investigated. Besides, results are presented for both TID and TD cases of material properties. As seen, for each type of boundary condition, dynamic buckling temperature differences are reduced by increasing the power law index. Specially, this reduction is much more profound for values of $k < 2$. In addition, results reveal the higher amount of ΔT_{cr} for the TID case of material properties. In other words, ΔT_{cr} under TID assumption stands as the upper bound for those obtained under the TD case of material properties for all types of boundary conditions.

Similar to the previous section, by comparing results obtained for the three types of boundary conditions, it could be understood that for each value of power law index, the maximum thermal dynamic buckling load is achieved for the $C - C$ boundary condition and the minimum ones are associated with the $S - S$ case.

The elements of the stiffness matrix of Eq. (2.10.14) are [111]

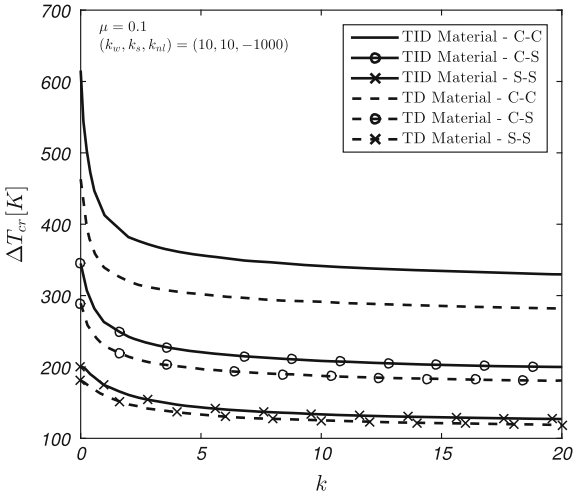

Fig. 2.51 Influence of power law index on dynamic buckling temperature difference of the FGM beams resting on softening elastic foundation

$$K_{nm}^{uu} = \int_0^L E_1 \frac{dN_m^u}{dx}\frac{dN_n^u}{dx}dx$$

$$K_{nm}^{uw} = \frac{1}{2}\int_0^L \left(E_1 \frac{dN_m^w}{dx}\frac{dw_0}{dx}\frac{dN_n^u}{dx} + 2E_1 \frac{dN_m^w}{dx}\frac{dw^*}{dx}\frac{dN_n^u}{dx}\right)dx$$

$$K_{nm}^{u\phi} = \int_0^L E_2 \frac{dN_m^\phi}{dx}\frac{dN_n^u}{dx}dx$$

$$K_{nm}^{wu} = \int_0^L \left(E_1 \frac{dN_m^u}{dx}\frac{dw_0}{dx}\frac{dN_n^w}{dx} + E_1 \frac{dN_m^u}{dx}\frac{dw^*}{dx}\frac{dN_n^w}{dx}\right)dx$$

$$\begin{aligned} K_{nm}^{ww} = \int_0^L \Bigg(&\frac{1}{2}E_1 \frac{dN_m^w}{dx}\left(\frac{dw_0}{dx}\right)^2 \frac{dN_n^w}{dx} + \frac{3}{2}E_1 \frac{dN_m^w}{dx}\frac{dw_0}{dx}\frac{dw^*}{dx}\frac{dN_n^w}{dx} \\ &+ E_1 \frac{dN_m^w}{dx}\left(\frac{dw^*}{dx}\right)^2 \frac{dN_n^w}{dx} - N^T \frac{dN_m^w}{dx}\frac{dN_n^w}{dx} + G_1 \frac{dN_m^w}{dx}\frac{dN_n^w}{dx} \\ &+ K_w N_m^w N_n^w + K_s \frac{dN_m^w}{dx}\frac{dN_n^w}{dx} + K_{nl} N_m^w w_0^2 N_n^w\Bigg)dx \end{aligned}$$

$$K_{nm}^{w\phi} = \int_0^L \left(E_2 \frac{dN_m^\phi}{dx}\frac{dw_0}{dx}\frac{dN_n^w}{dx} + E_2 \frac{dN_m^\phi}{dx}\frac{dw^*}{dx}\frac{dN_n^w}{dx} + G_1 N_m^\phi \frac{dN_n^w}{dx}\right)dx$$

$$K_{nm}^{\phi u} = \int_0^L E_2 \frac{dN_m^u}{dx}\frac{dN_n^\phi}{dx}dx$$

$$K_{nm}^{\phi w} = \frac{1}{2}\int_0^L \left(E_2 \frac{dN_m^w}{dx}\frac{dw_0}{dx}\frac{dN_n^\phi}{dx} + 2E_2 \frac{dN_m^w}{dx}\frac{dw^*}{dx}\frac{dN_n^\phi}{dx} + 2G_1 \frac{dN_m^w}{dx}N_n^\phi\right)dx$$

$$K_{nm}^{\phi\phi} = \int_0^L \left(E_3 \frac{dN_m^\phi}{dx}\frac{dN_n^\phi}{dx} + G_1 N_m^\phi N_n^\phi\right)dx$$

The elements of the mass matrix are

$$
\begin{aligned}
M_{nm}^{uu} &= \int_0^L I_1 N_m^u N_n^u dx \\
M_{nm}^{uw} &= 0 \\
M_{nm}^{u\phi} &= \int_0^L I_2 N_m^\phi N_n^u dx \\
M_{nm}^{wu} &= 0 \\
M_{nm}^{ww} &= \int_0^L I_1 N_m^w N_n^w dx \\
M_{nm}^{w\phi} &= 0 \\
M_{nm}^{\phi u} &= \int_0^L I_2 N_m^u N_n^\phi dx \\
M_{nm}^{\phi w} &= 0 \\
M_{nm}^{\phi\phi} &= \int_0^L I_3 N_m^\phi N_n^\phi dx
\end{aligned}
$$

and the elements of the force vector are

$$
\begin{aligned}
F_n^u &= \int_0^L N^T \frac{N_n^u}{dx} dx \\
F_n^w &= \int_0^L N^T \frac{dw^*}{dx} \frac{dN_n^w}{dx} dx \\
F_n^\phi &= \int_0^L M^T \frac{dN_n^\phi}{dx} dx
\end{aligned}
$$

2.11 Problems

1. Use Eqs. (2.2.5), (2.2.6), (2.2.9) and (2.3.1) to derive the equilibrium equations (2.3.2).
2. Derive the stability equations (2.4.3) using Eqs. (2.4.1), (2.4.2) and (2.3.2).
3. Employing the stability equations (2.4.3) and by eliminating u_1 and ϕ_1 arrive at (2.4.4).
4. Find the determinant of matrix equation (2.5.6) and prove that it yields Eq. (2.5.7).
5. Find the critical thermal force of a $C - S$ type of boundary condition of the Timoshenko beam with isotropic material property of length L and the modulus of elasticity E. Assume that the beam is under uniform temperature rise ΔT.

6. Obtain the parameter μ given by Eq. (2.6.11) for the piezo-FGM beams using Eq. (2.4.4).
7. What is the thermal buckling load for the same beam of Problem 6, when the beam is under uniform temperature rise ?
8. Find the thermal buckling load of Problem 7, when the beam material is made of an isotropic metal. Find the same buckling load when the material is pure 8 ceramic.
9. Reconsider Problem 8 and check the delay of thermal buckling load when a ± 500 Volts is applied to the beam.

References

1. Brush, D. O., & Almorth, B. O. (1975). *Buckling of bars, plates, and shells*. New York: McGraw-Hill.
2. Hetnarski, R. B., & Eslami, M. R. (2009). *Thermal stresses, advanced theory and applications*. Netherland: Springer.
3. Praveen, G. N., & Reddy, J. N. (1998). Nonlinear transient thermoelastic analysis of functionally graded ceramic-metal plates. *International Journal of Solids and Structures*, *35*(33), 4457–4476.
4. Suresh, S., & Mortensen, A. (1998). *Fundamentals of functionally graded materials*. London: IOM Communications Ltd.
5. Huang, Y., & Li, X. F. (2010). Buckling of functionally graded circular columns including shear deformation. *Materials and Design*, *31*(7), 3159–3166.
6. Zhao, F. Q., Wang, Z., & Liu, H. (2007). Thermal post-buckling analyses of functionally graded material rod. *Applied Mathematics and Mechanics*, *28*(1), 59–67.
7. Li, S., Zhang, J., & Zhao, Y. (2006). Thermal post-buckling of functionally graded material timoshenko beams. *Applied Mathematics and Mechanics*, *27*(6), 803–810.
8. Kiani, Y., & Eslami, M. R. (2010). Thermal buckling analysis of functionally graded material beams. *International Journal of Mechanics and Materials in Design*, *6*(3), 229–238.
9. Aydogdu, M. (2008). Semi-inverse method for vibration and buckling of axially functionally graded beams. *Journal of Reinforced Plastics and Composites*, *27*(7), 683–691.
10. Ke, L. L., Yang, J., & Kitipornchai, S. (2009). Postbuckling analysis of edge cracked functionally graded timoshenko beams under end-shortening. *Composite Structures*, *90*(2), 152–160.
11. Ke, L. L., Yang, J., Kitipornchai, S., & Xiang, Y. (2009). Flexural vibration and elastic buckling of a cracked Timoshenko beam made of functionally graded materials. *Mechanics of Advanced Materials and Structures*, *16*(6), 488–502.
12. Ma, L. S., & Lee, D. W. (2011). A further discussion of nonlinear mechanical behavior for FGM beams under in-plane thermal loading. *Composite Structures*, *93*(2), 831–842.
13. Anandrao, K. S., Gupta, R. K., Ramchandran, P., & Rao, G. V. (2010). Thermal post-buckling analysis of uniform slender functionally graded material beams. *Structural Engineering and Mechanics*, *36*(5), 545–560.
14. Ma, L. S., & Lee, D. W. (2011). Exact solutions for nonlinear static responses of a shear deformable FGM beam under an in-plane thermal loading. *European Journal of Mechanics A Solids*, *31*(1), 13–20.
15. Wang, C. M., Wang, C. Y., & Reddy, J. N. (2004). *Exact solutions for buckling of structural members*. Boca Raton: CRC Press.
16. Reddy, J. N., & Chin, C. D. (1998). Thermomechanical analysis of functionally graded cylinders and plates. *Journal of Thermal Stresses*, *21*(6), 593–626.

17. Kapuria, S., Ahmed, A., & Dumir, P. C. (2004). Static and dynamic thermo-electro-mechanical analysis of angle-ply hybrid piezoelectric beams using an efficient coupled zigzag theory. *Composite Science and Technology*, *64*(16), 2463–2475.
18. Chen, L. W., Lin, C. Y., & Wang, C. C. (2002). Dynamic stability analysis and control of a composite beam with piezoelectric layers. *Composite Structures*, *56*(1), 97–109.
19. Bian, Z. G., Lim, C. W., & Chen, W. Q. (2006). On functionally graded beams with integrated surface piezoelectric layers. *Composite Structures*, *72*(3), 339–351.
20. Alibeigloo, A. (2010). Thermoelasticity analysis of functionally graded beam with integrated surface piezoelectric layers. *Composite Structures*, *92*(6), 1535–1543.
21. Gharib, A., Salehi, M., & Fazeli, S. (2008). Deflection control of functionally graded material beams with bonded piezoelectric sensors and actuators. *Material Science and Engineering. A-Structures*, *498*(1–2), 110–114.
22. Li, S. R., Su, H. D., & Cheng, C. J. (2009). Free vibration of functionally graded material beams with surface-bonded piezoelectric layers in thermal environment. *Applied Mathematics and Mechanics*, *30*(8), 969–982.
23. Kiani, Y., Taheri, S., & Eslami, M. R. (2011). Thermal buckling of piezoelectric functionally graded material beams. *Journal of Thermal Stresses*, *34*(8), 835–850.
24. Kiani, Y., Rezaei, M., Taheri, S., & Eslami, M. R. (2011). Thermo-electrical buckling of piezoelectric functionally graded material Timoshenko beams. *International Journal of Mechanics and Materials in Design*, *7*(3), 185–197.
25. Liew, K. M., Yang, J., & Kitipornchai, S. (2003). Postbuckling of piezoelectric FGM plates subject to thermo-electro-mechanical loading. *International Journal of Solids and Structures*, *40*(15), 3869–3892.
26. Mirzavand, B., & Eslami, M. R. (2007). Thermal buckling of simply supported piezoelectric FGM cylindrical shells. *Journal of Thermal Stresses*, *30*(11), 1117–1135.
27. Shen, H. S. (2005). Postbuckling of FGM plates with piezoelectric actuators under thermo-electro-mechanical loadings. *International Journal of Solids and Structures*, *42*(23), 6101–6121.
28. Shen, H. S. (2005). Postbuckling of axially loaded FGM hybrid cylindrical shells in thermal environments. *Composite Science and Technology*, *65*(11–12), 1675–1690.
29. Shen, H. S., & Noda, N. (2007). Postbuckling of pressure-loaded FGM Hybrid cylindrical shells in thermal environments. *Composite Structures*, *77*(4), 546–560.
30. Li, S. R., Zhou, Y. H., & Zheng, X. (2002). Thermal post-buckling of a heated elastic rod with pinned-fixed ends. *Journal of Thermal Stresses*, *25*(1), 45–56.
31. Librescu, L., Oh, S. Y., & Song, O. (2005). Thin-walled beams made of functionally graded materials and operating in a high temperature environment: vibration and stability. *Journal of Thermal Stresses*, *28*(6–7), 649–712.
32. Bhangale, R. K., & Ganesan, N. (2006). Thermoelastic buckling and vibration behavior of a functionally graded sandwich beam with constrained viscoelastic core. *Journal of Sound and Vibration*, *295*(1–2), 294–316.
33. Fu, Y., Wang, J., & Mao, Y. (2012). Nonlinear analysis of buckling, free vibration and dynamic stability for the piezoelectric functionally graded beams in thermal environment. *Applied Mathematical Modelling*, *36*(8), 4324–4340.
34. Kargani, A., Kiani, Y., & Eslami, M. R. (2013). Exact solution for non-linear stability of piezoelectric FGM Timishenko beam under thermo-electrical loads. *Journal of Thermal Stresses*, *36*, 1056–1076.
35. Reddy, J. N. (2003). *Mechanics of laminated composite plates and shells, theory and application*. Cambridge: CRC Press.
36. Tzou, H. S. (1993). *Piezoelectric shells: distributed sensing and control of continua*. Dordrecht: Kluwer Academic Publisher.
37. Yang, J. S. (2005). *Introduction to the theory of piezoelectricity*. New York: Springer.
38. Yang, J. S. (2006). *The mechanics of piezoelectric structures*. Singapore: World Scientific Publishing.

39. Yang, J. S., & Zhang, W. (1999). A thickness-shear high voltage piezoelectric transformer. *International Journal of Applied Electromagnetics and Mechanics*, *21*(2), 131–141.
40. Yang, J. S., Fang, H. Y., & Jiang, Q. (1999). Analysis of a ceramic bimorph piezoelectric gyroscope. *International Journal of Applied Electromagnetics and Mechanics*, *10*(6), 459–473.
41. Yang, J. S. (1998). Equations for the extension and flexure of a piezoelectric beam with rectangular cross section and applications. *International Journal of Applied Electromagnetics and Mechanics*, *9*(4), 409–420.
42. Wang, Q., & Quek, S. T. (2012). Flexural vibration analysis of sandwich beam coupled with piezoelectric actuator. *Smart Materials and Structures*, *9*(1), 103–109.
43. Wang, Q., & Quek, S. T. (2002). A model for the analysis of beams with embedded piezoelectric layers. *Journal of Intelligent Materials Systems and Structures*, *13*(1), 61–70.
44. Ke, L. L., Wang, Y. S., & Wang, Z. D. (2012). Nonlinear vibration of the piezoelectric nanobeams based on the nonlocal theory. *Composite Structures*, *94*(6), 2038–2047.
45. Ke L. L., & Wang Y. S. (2012). Thermoelectric-mechanical vibration of piezoelectric nanobeams based on the nonlocal theory. *Smart Materials and Structures*, *21*(2), Article No. 025018.
46. Pradhan, S. C., & Murmu, T. (2009). Thermo-mechanical vibration of FGM sandwich bam under variable elastic foundations using differential quadrature. *Journal of Sound and Vibration*, *321*(1–2), 342–362.
47. Xiang, H. J., & Yang, J. (2008). Free and forced vibration of a laminated FGM Timoshenko beam of variable thickness under heat conduction. *Composites Part B : Engineering*, *39*(2), 292–303.
48. Xia, X. K., & Shen, H. S. (2008). Vibration of post-buckled sandwich plates with FGM face sheets in a thermal environment. *Journal of Sound and Vibration*, *314*(1–2), 254–274.
49. Neukirch, S., Frelat, J., Goriely, A., & Maurini, C. (2012). Vibrations of post-buckled rods: the singular inextensible limit. *Journal of Sound and Vibration*, *331*(3), 704–720.
50. Huang, D. J., Ding, H. J., & Chen, W. Q. (2007). Piezoelasticity solutions for functionally graded piezoelectric beams. *Smart Materials and Structures*, *16*(3), 687–695.
51. Shi, Z. F. (2002). General solution of a density functionally gradient piezoelectric cantilever and its applications. *Smart Materials and Structures*, *11*(1), 122–129.
52. Shi, Z. F., & Chen, Y. (2004). Functionally graded piezoelectric cantilever beam under load. *Archive of Applied Mechanics*, *74*(3–4), 237–247.
53. Liu, T. T., & Shi, Z. F. (2004). Bending behavior of functionally gradient piezoelectric cantilever. *Ferroelectrics*, *308*(1), 43–51.
54. Kruusing, A. (2006). Analytical and optimization of loaded cantilever beam microactuators. *Smart Materials and Structures*, *9*(2), 186–196.
55. Joshi, S., Mukherjee, A., & Schmauder, S. (2003). Exact solutions for characterization of electro-elastically materials. *Computational Material Science*, *28*(3–4), 548–555.
56. Joshi, S., Mukherjee, A., & Schmauder, S. (2003). Numerical characterization of functionally graded active materials under electrical and thermal fields. *Smart Materials and Structures*, *12*(4), 571–579.
57. Lee, H. J. (2005). Layerwise laminate analysis of functionally graded piezoelectric Bimorph beams. *Journal of Intelligent Material Systems and Structures*, *16*(2), 365–371.
58. Lee H. J. (2003). Layerwise analysis of thermal shape control in graded piezoelectric beams. *ASME 2003 International Mechanical Engineering Congress and Exposition*, Paper No. IMECE2003-41902, *68*(2), 79–87.
59. Yang, J., & Xiang, H. J. (2007). Thermo-electro-mechanical characteristics of functionally graded piezoelectric actuators. *Smart Materials and Structures*, *16*(3), 784–797.
60. Komeili A., Akbarzadeh A. H., Doroushi A., & Eslami M. R. (2001). Static analysis of functionally graded piezoelectric beams under Thermo-electro-mechanical Loads. *Advances in Mechanical Engineering*, Article No. 153731.
61. Doroushi, A., Eslami, M. R., & Komeili, A. (2011). Vibration analysis and transient response of an FGPM beam under thermo-electro-mechanical loads using higher-order shear deformation theory. *Journal of Intelligent Material Systems and Structures*, *22*(3), 231–243.

62. Komijani, M., Kiani, Y., Esfahani, S. E., & Eslami, M. R. (2013). Vibration of thermo-electrically post-buckled rectangular functionally graded piezoelectric beams. *Composite Structures*, *98*, 143–152. https://dx.doi.org/10.1016/j.compstruct.2012.10.047.
63. Liu, X., Wang, Q., Queck, S. T., Sun, C. T., & Liu, X. (2001). Analysis of piezoelectric coupled circular plate. *Smart Materials and Structures*, *10*(2), 229–239.
64. Parashar, S. K., Wagner, U. V., & Hagedorn, P. (2004). A modified Timoshenko beam theory for nonlinear shear-induced flexural vibrations of piezoelectric continua. *Nonlinear Dynamics*, *37*(3), 181–205.
65. Lee, P. C. Y., & Lin, W. S. (1998). Piezoelectrically forced vibrations of rectangular SC-cut quartz plates. *Journal of Applied Physics*, *83*(12), 7822–7833.
66. Liu, X., Wang, Q., & Queck, S. T. (2002). Analytical solution for free vibration of piezoelectric coupled moderately thick circular plates. *International Journal of Solids and Structures*, *39*(8), 2129–2151.
67. Eslami, M. R. (2014). *Finite elements methods in mechanics*. Netherlands: Springer.
68. Park, J. S., Kim, J. H., & Moon, S. H. (2004). Vibration of thermally post-buckled composite plates embedded with shape memory alloy fibers. *Composite Structures*, *63*(2), 179–188.
69. Reddy, J. N. (2004). *An introduction to nonlinear finite element analysis*. Oxford: Oxford University Press.
70. Komijani, M., Kiani, Y., & Eslami, M. R. (2012). Nonlinear thermoelectrical stability analysis of functionally graded piezoelectric material beams. *Journal of Intelligent Material Systems and Structures*, *29*(9), 399–410.
71. Li, S. R., Cheng, C. J., & Zhou, Y. H. (2003). Thermal post-buckling of an elastic beams subjected to a transversely non-uniform temperature rising. *Applied Mathematics and Mechanics, English Edition*, *24*(5), 514–520.
72. Li, S. R., Teng, Z. C., & Zhou, Y. H. (2004). Free vibration of heated, Euler-Bernoulli beams with thermal post-buckling deformations, *Journal of Thermal Stresses*, *27*(9), 843–856.
73. Song, X., & Li, S. R. (2007). Thermal buckling and post-buckling of pinned-fixed Euler-Bernoulli beams on an elastic foundation. *Mechanics Research Communications*, *34*(2), 164–171.
74. Li, S. R., & Batra, R. C. (2007). Thermal buckling and postbuckling of Euler Bernoulli beams supported on nonlinear elastic foundations. *AIAA Journal*, *45*(3), 712–720.
75. Sahraee, S., & Saidi, A. R. (2008). Free vibration and buckling analysis of functionally graded deep beam-columns on two-parameter elastic foundations using the differential quadrature method. *Proceedings of the Institution of Mechanical Engineers, Part C: Journal of Mechanical Engineering Science*, *223*(6), 1273–1284.
76. Fallah, A., & Aghdam, M. M. (2012). Thermo-mechanical buckling and nonlinear free vibration analysis of functionally graded beams on nonlinear elastic foundation. *Composites Part B: Engineering*, *43*(3), 1523–1530.
77. Fallah, A., & Aghdam, M. M. (2011). Nonlinear free vibration and post-buckling analysis of functionally graded beams on nonlinear elastic foundation. *European Journal of Mechanics A/Solids*, *30*(4), 571–583.
78. Hetenyi, M. (1948). *Beams on elastic foundation*. Ann Arbor, MI: University of Michigan Press.
79. Emam, S. A., & Nayfeh, A. H. (2009). Postbuckling and free vibrations of composite beams. *Composites Part B: Engineering*, *88*(4), 636–642.
80. Esfahani, S.E., Kiani, Y., & Eslami, M.R. (2014). Vibration of a temperature-dependent thermally pre/post-buckled FGM beam over a non-linear hardening elastic foundations. *ASME, Journal of Applied Mechanics*, *81*. https://dx.doi.org/10.1115/1.4023975.
81. Vosoughi A. R., Malekzadeh P., Banan Ma. R., Banan Mo. R. (2012). Thermal buckling and postbuckling of laminated composite beams with temperature-dependent properties. *International Journal of nonlinear Mechanics*, *47*(3), 96–102.
82. Liew, K. M., Yang, J., & Kitipornchai, S. (2004). Thermal post-buckling of laminated plates comprising functionally graded materials with temperature-dependent properties. *Journal of Applied Mechanics*, *71*(6), 839–850.

83. Shen, H. S. (2007). Thermal postbuckling of shear deformable FGM cylindrical shells with temperature-dependent properties. *Mechanics of Advanced Materials and Structures*, *14*(6), 439–452.
84. Bellman, R. E., Kashef, B. G., & Casti, J. (1972). Differential quadrature: a technique for the rapid solution of nonlinear partial differential equations. *Journal of Computational Physics*, *10*(1), 40–52.
85. Quan, J. R., & Chang, C. T. (1989). New insights in solving distributed system equations by the quadrature methods. *Computers in Chemical Engineering*, *13*(9), 779–788.
86. Wu, T. Y., & Liu, G. R. (1999). A differential quadrature as a numerical method to solve differential equations. *Computational Mechanics*, *24*(3), 197–205.
87. Shu, C. (2000). *Differential quadrature and its application in engineering*. London Limited: Springer.
88. Ghiasian, S. E., Kiani, Y., & Eslami, Y. (2013). Dynamic buckling of suddenly heated or compressed FGM beams resting on nonlinear elastic foundation. *Composite Structures*, *106*, 225–234.
89. Simitses, G. J. (1987). Instability of dynamically loaded structures. *Applied Mechanics Review*, *40*(10), 1403–1408.
90. Simitses, G. J. (1990). *Dynamic stability of suddenly loaded structures*. New-York: Springer.
91. Budiansky B., & Roth R. S. Axisymmetric dynamic buckling of clamped shallow spherical shells. *Thecnical Note NASA*, TN D-1510.
92. Hutchinson, J. W., & Budiansky, B. (1966). Dynamic buckling estimates. *AIAA Journal*, *4*(3), 525–530.
93. Hsu, C. S. (1967). The effect of various parameters on the dynamic stability of a shallow arch. *Journal of Applied Mechanics*, *34*(2), 349–358.
94. Simitses, J. G. (1967). Axiymmetric dynamic snap-through buckling of shallow spherical caps. *AIAA Journal*, *5*(5), 1019–1021.
95. Volmir S.A. (1972).*Nonlinear dynamics of plates and shells*. Moscow Science.
96. Kleiber, M., Kotula, W., & Saran, M. (1987). Numerical analysis of dynamic quasi-bifurcation. *Engineering Computations*, *4*(1), 48–52.
97. Kubiak, T. (2007). Criteria of dynamic buckling estimation of thin-walled structures. *Thin-Walled Structures*, *45*(10–11), 888–892.
98. Kounadis, A. N., Gantes, C., & Simitses, G. J. (1997). Nonlinear dynamic buckling of multi D.O.F structural dissipative system under impact loading. *International Journal of Impact Engineering*, *19*(1), 63–80.
99. Shariyat, M. (2008). Dynamic buckling of suddenly loaded imperfect hybrid FGM cylindrical shells with temperature-dependent material properties under thermo-electro-mechanical loads. *International Journal of Mechanical Sciences*, *50*(12), 1561–1571.
100. Shariyat, M. (2008). Dynamic thermal buckling of suddenly heated temperature-dependent FGM cylindrical shells, under combined axial compression and external pressure. *International Journal of Solids and Structures*, *45*(9), 2598–2612.
101. Mirzavand, B., Eslami, M. R., & Shakrei, M. (2010). Dynamic thermal postbuckling analysis of piezoelectric functionally graded cylindrical shells. *Journal of Thermal Stresses*, *33*(7), 646–660.
102. Mirzavand, B., Eslami, M. R., & Reddy, J. N. (2013). Dynamic thermal postbuckling analysis of shear deformable piezoelectric-FGM cylindrical shells. *Journal of Thermal Stresses*, *36*(3), 189–206.
103. Shariyat, M., & Eslami, M. R. (2000). On thermal dynamic buckling analysis of imperfect laminated cylindrical shells. *ZAMM*, *80*(3), 171–182.
104. Shariyat, M., & Eslami, M. R. (2002). Dynamic buckling and post-buckling of imperfect orthotropic cylindrical shells under mechanical and thermal loads. *Journal of Applied Mechanics*, *66*(2), 476–484.
105. Shuka, K. K., & Nath, Y. (2002). Buckling of laminated composite rectangular plates under transient thermal loading. *Journal of Applied Mechanics*, *69*(5), 684–692.

106. Shariyat, M. (2009). Vibration and dynamic buckling control of imperfect hybrid FGM plates with temperature-dependent material properties subjected to thermo-electro-mechanical loading conditions. *Composite Structures*, *88*(2), 240–252.
107. Prakash, T., Singha, M. K., & Ganapathi, M. (2007). Nonlinear dynamic thermal buckling of functionally graded spherical caps. *AIAA Journal*, *45*(2), 505–508.
108. Sundararajan, N., & Ganapathi, M. (2008). Dynamic thermal buckling of FG spherical caps. *Journal of Engineering Mechanics*, *134*(2), 206–209.
109. Jabareen, M., & Sheinmann, I. (2007). Buckling and sensitivity to imperfection of conical shells under dynamic step-loading. *Journal of Applied Mechanics*, *74*(6), 74–80.
110. Esfahani, S. E., Kiani, Y., & Eslami, M. R. (2013). Non-linear thermal stability analysis of temperature dependent FGM beams supported on non-linear hardening elastic foundations. *International Journal of Mechanical Sciences*, *69*, 1020. https://dx.doi.org/10.1016/j.ijmecsci.2013.01.007.
111. Ghiasian, S. E., Kiani, Y., & Eslami, M. R. (2015). Nonlinear thermal dynamic buckling of FGM beams. *European Journal of Mechanics, A/Solids*, *54*, 232–242. https://dx.doi.org/10.1016/j.euromechsol.2015.07.004

http://www.springer.com/978-3-319-62367-2

Buckling and Postbuckling of Beams, Plates, and Shells

Eslami, M.R.

2018, XVII, 588 p. 249 illus., 29 illus. in color.,
Hardcover
ISBN: 978-3-319-62367-2